

Measurement-induced phases of matter require adaptive dynamics

Aaron J. Friedman, Oliver Hart, and Rahul Nandkishore
*Department of Physics and Center for Theory of Quantum Matter,
 University of Colorado, Boulder CO 80309, USA*
 (Dated: October 17, 2022)

We investigate quantum dynamics with projective measurements using the Stinespring formalism, which affords significant technical advantages and conceptual insight into hybrid dynamics. We consider spectral properties as well as commonly used and experimentally tractable probes of phase structure and universality, finding that *all* of these probes are blind to the effects of measurement in nonadaptive hybrid protocols. Essentially, if the outcomes of measurements are not utilized, their effect is no different than chaotic time evolution, on average, precluding measurement-induced phases of matter. We therefore consider *adaptive* circuits, in which gates depend on the outcomes of prior measurements via active feedback, finding nontrivial examples of order related to symmetry and topology with connections to quantum computing. However, transitions as a function of measurement rate do not appear possible with maximally chaotic time evolution; we identify nonrandom adaptive hybrid protocols as the leading candidate for genuine, measurement-induced transitions between distinct phases of matter.

CONTENTS

1. Introduction	7.2. Enriched adaptive protocols	24
2. The Stinespring formalism	8. Conclusion	28
2.1. Stinespring dilation and isometric measurement	2	29
2.2. Unitary measurement	3	29
2.3. Measurement outcomes	3	30
2.4. Comment on particular trajectories	4	30
5	4.4. Projectors and other useful relations	31
3. Hybrid circuit models	5	31
3.1. The spacetime lattice	6	31
3.2. Measurement unitaries	6	32
3.3. Time evolution	7	32
3.4. Symmetries, constraints, and block structure	7	33
3.5. Floquet circuits	8	33
9	D. Details of the spectral form factor	33
4. Observables and correlations	10	33
4.1. Quantities of interest	10	33
4.2. Transfer matrix formulation	10	33
4.3. Time evolution transfer matrix	11	34
4.4. Measurement transfer matrix	11	34
4.5. Measurements have no effect in generic circuits	12	34
4.6. Measuring charge operators has no effect	12	35
4.7. Measuring other operators only “undoes” symmetries	13	35
5. Spectral form factors	16	35
5.1. Chaos and spectral rigidity	16	35
5.2. Extension to hybrid circuits	17	35
5.3. Ensemble averaging	18	35
5.4. Generic circuits	20	35
5.5. Charge measurements	20	35
6. What is a phase of matter?	21	35
7. Adaptive protocols	22	35
7.1. Generic adaptive protocols	23	35
1. INTRODUCTION		
<p>Understanding the possible phases of nonequilibrium quantum matter is a key frontier in quantum science. While most work has focused on well-isolated systems undergoing unitary time evolution [1–12], the most general quantum dynamics also includes <i>measurements</i>. It was recently observed that increasing the frequency of measurements can drive an <i>entanglement transition</i> [13–18] between area- and volume-law scaling of the entanglement entropy of the system’s state. Interest in the landscape of quantum dynamics—and transitions—that depend on the rate γ of measurements has since exploded (see [19] for a review). In this work, we investigate whether the transitions nominally induced by measurements amount to transitions between distinct phases of matter in any reasonable understanding of the term.</p>		
<p>A key ingredient to our analysis is the use of the Stinespring Dilation Theorem [20] to represent generic</p>		

quantum operations—including projective measurements—*unitarily* [21]. While formally equivalent to the Kraus formalism [22], we find that the Stinespring representation [20, 21] has significant technical and conceptual advantages. Owing to its scarcity in the literature, in Sec. 2 we provide a “textbook” exposition of the Stinespring formalism. In Sec. 3 we detail the “unitary-projective circuits” of interest in the Stinespring representation. We first consider nonadaptive hybrid circuits (which are not conditioned on prior measurement outcomes) both with and without block structure (adaptive protocols are considered in Sec. 7). Readers familiar with this formalism, or uninterested therein, may skip directly to Sec. 4. The remainder of our work considers whether and when measurements can give rise to new phases of matter or universal dynamics, compared to purely unitary circuits.

We consider standard diagnostics of phase structure and universality in “generic” hybrid quantum circuits [5–8], as well as those “enriched” by conservation laws [9–12, 23–25] and/or kinetic constraints [12, 26–31]. In Sec. 4 we consider experimentally tractable probes common to condensed matter and atomic, molecular, and optical (AMO) physics, corresponding to expectation values, correlation functions, and response functions; in Sec. 5 we consider the spectral form factor (SFF) [8, 11, 12, 32–39]. We show that *none* of these probes see a “transition” due to measurements¹. In the cases most relevant to experiment, measurements have no visible effect whatsoever, on average, compared to time evolution alone.

We do not consider a class of *postselected* probes, which have been reported to show a transition as a function of measurement rate. Essentially, the probes (4.1) of Sec. 4 see no transition in nonadaptive protocols because the measurement outcomes are not *utilized*. As a result, the system behaves as though measured by the environment, which is equivalent to ensemble-averaged time-evolution alone in chaotic systems, so the late-time density matrix is the featureless, maximally mixed state $\rho_\infty \propto \mathbb{1}$ (possibly within each symmetry or Krylov sector) [21]. Postselection provides a means by which to “use” the measurement outcomes—at least on paper. Generally, these quantities can be grouped into two categories: measures of entanglement [13–18, 23–25, 40–42] and variances of two-point functions [23–25, 43]. We refer the reader to the foregoing references for further detail; in Sec. 6 we discuss the well-known practical issue with postselection [19], as well as a conceptual issue that does not appear to be widely recognized, and cannot be sidestepped by any protocol, as far as we are aware. We argue that nonadaptive circuits cannot realize genuine phases of matter due to projective measurements, which requires the use of *active feedback*.

In Sec. 7, we consider *adaptive* hybrid protocols, in which measurement outcomes determine future gates [21, 44–46]. While postselected probes also “use” the

measurement outcomes, they do so in a manner that is incompatible with the definition of a phase of matter. By comparison, adaptive protocols are compatible with experimentally tractable probes (4.1). Their ability to produce nontrivial states is captured, e.g., by the Stinespring representation of quantum error correction [21]. When performing quantum teleportation, the target qubit realizes the maximally mixed state ρ_∞ unless until an error-correction gate is applied (based on the outcomes of “syndrome” measurements, which are communicated classically), realizing the desired state on the target qubit.

Adaptive protocols admit order parameters $\langle \mathcal{O}(t) \rangle \neq 0$ that vanish in *any* nonadaptive (or measurement-free) protocol. However, we find that adaptive protocols with chaotic random unitaries are not compatible with measurement-induced transitions between distinct phases of matter. In generic circuits [13], Haar-random time evolution instantly scrambles the system’s state so that adaptive gates act trivially; even if one fine tunes to preclude intervening time evolution, one expects $\langle \mathcal{O}(t) \rangle \sim \gamma$, which precludes a sharp feature as a function of γ . Models with global discrete symmetries admit nontrivial order parameters \mathcal{O} corresponding to the symmetry generators; these nonlocal string order parameters [47] relate to these protocols’ connection to symmetry-protected topological orders (SPTs) [47–50] and quantum teleportation [51–53]. However, one must measure every site of the system or else $\langle \mathcal{O}(t) \rangle = 0$, precluding a transition with γ . We also consider $U(1)$ -symmetric circuits, whose *local* order parameters $\langle Z_j(t) \rangle = c(\gamma, t)$ do not require measuring all sites. While $\langle Z_j(t) \rangle$ is more robust, discontinuities as a function of γ again appear impossible, precluding a transition between distinct phases of matter. However, we note that this appears to be—at least in part—an artifact of the maximally chaotic Haar ensemble.

We conclude that measurement-induced phase transitions cannot be realized in any physically meaningful sense in nonadaptive circuits, nor those evolved in time under highly chaotic ensembles [54], which trivialize $\rho(t)$. However, our results are compatible with such protocols being *useful* (e.g., for teleportation [21, 52]). The remaining candidates for realizing new, measurement-induced phases of matter in quantum systems correspond to adaptive protocols with particular time-evolution protocols, which may be nonrandom or simply not fast scramblers (see [44–46] for recent examples). In the absence of such an ensemble, care must be taken to establish any putative phase’s robustness to perturbations (guided by the most likely sources of experimental error [41]). In general, such adaptive protocols represent the most promising avenue for future research into measurement-induced phases.

2. THE STINESPRING FORMALISM

The Stinespring Dilution Theorem [20] provides an alternative representation of measurement channels that is technically better suited to the scrutiny of hybrid circuits

¹ For correlation functions of local observables in *generic* hybrid circuits, this is well known [13].

FIG. 1. Cartoon depiction of measurement of A (2.2) in the Stinespring formulation. The wave function only *appears* to collapse upon measurement—in reality, the observer and system become entangled, and the post-measurement state is a superposition of states where outcome m obtains and the observer records outcome m . The dilated Hilbert space encodes this entanglement using an “outcome register”.

and conceptually more revealing. Because it is not widely used, we introduce the formalism in detail herein.

2.1. Stinespring dilation and isometric measurement

The Stinespring Dilation Theorem [20] states that all quantum operations (or “quantum channels”) can be represented via isometries and [partial] traces acting on the density matrix. By Choi’s theorem [22], Stinespring’s isometric channels are equivalent to both the Kraus and Completely Positive Trace-Preserving (CPTP) map formulations of quantum channels. However, we find that the Stinespring formalism is more convenient and intuitive in the context of measurements².

An isometry is a norm-preserving map from a given Hilbert space \mathcal{H}_A to a “dilated” Hilbert space \mathcal{H}_B . The dimensions $\mathcal{D}_{A,B} = \dim(\mathcal{H}_{A,B})$ give the number of many-body states in each space, and must obey $\mathcal{D}_B \geq \mathcal{D}_A$. The isometry $\mathbb{V} : \mathcal{H}_A \mapsto \mathcal{H}_B$ satisfies $\|\mathbb{V}|u\rangle\| = \|u\|$ for all vectors $|u\rangle \in \mathcal{D}_A$; equivalently, we have that $\mathbb{V}^\dagger \mathbb{V} = \mathbb{1}_A$, while $\mathbb{V} \mathbb{V}^\dagger$ projects onto the subspace $\mathcal{H}_A \subset \mathcal{H}_B$. When $\mathcal{D}_A = \mathcal{D}_B$, \mathbb{V} is then *unitary* (i.e., $\mathbb{V} \mathbb{V}^\dagger = \mathbb{1}$). Hence, unitary channels—e.g., corresponding to time evolution—are a proper subset of isometric channels.

The rationale for dilating the Hilbert space in the context of measurement is that the act of measurement entangles the state of the physical system with that of the apparatus or observer (which reflects the *outcome*), as depicted in Fig. 1. The dilated Hilbert space,

$$\mathcal{H}_{\text{dil}} = \mathcal{H}_{\text{ph}} \otimes \mathcal{H}_{\text{ss}}, \quad (2.1)$$

includes an “outcome” (or “Stinespring”) register that records the measurement outcome quantumly.

An observable A has the spectral decomposition

$$A = \sum_{m=1}^M a_m \mathbb{P}^{(m)}, \quad (2.2)$$

where $\{a_m\}$ are the M *unique* eigenvalues of A (which are also the possible measurement outcomes), and $\mathbb{P}^{(m)}$ is a projector onto the eigenstate (or set of eigenstates) of A with eigenvalue a_m . That is, $A \mathbb{P}^{(m)} = a_m \mathbb{P}^{(m)}$; when the spectrum of A is nondegenerate, $\mathbb{P}^{(m)} = |m\rangle\langle m|$ projects onto a single eigenstate of A . The projectors are self adjoint and idempotent,

$$\mathbb{P}^{(m)} = (\mathbb{P}^{(m)})^\dagger = (\mathbb{P}^{(m)})^2, \quad (2.3)$$

as well as orthogonal and complete,

$$\mathbb{P}^{(m)} \mathbb{P}^{(n)} = \delta_{m,n} \mathbb{P}^{(n)} \quad \text{and} \quad \sum_m \mathbb{P}^{(m)} = \mathbb{1}. \quad (2.4)$$

The isometry corresponding to measurement of A (2.2) is captured pictorially in Fig. 1. The initial state of the system is $|\psi\rangle$, while the initial state of the observer is trivial (i.e., prior to measurement, the observer’s state is one dimensional). Measuring A (2.2) leads to

$$|\psi\rangle \rightarrow |\psi'\rangle = \sum_{m=1}^M (\mathbb{P}^{(m)} |\psi\rangle) \otimes |m\rangle_{\text{ss}}, \quad (2.5)$$

where the “ss” subscript labels the M -dimensional “Stinespring” or “outcome” register, where M is the number of *unique* eigenvalues of A (2.2). The Stinespring states are orthonormal and complete,

$$\langle m|n\rangle_{\text{ss}} = \delta_{m,n} \quad 1 \leq m, n \leq M, \quad (2.6)$$

and the Stinespring state $|m\rangle_{\text{ss}}$ encodes the fact that outcome a_m was observed upon measurement.

The post-measurement state is a superposition of states wherein the “collapsed” physical wavefunction for the system (which is proportional to $\mathbb{P}^{(m)} |\psi\rangle$) is entangled with the observer recording outcome m (reflected in the Stinespring register in (2.5) and Fig. 1).

Because (2.5) is isometric, there is no further need to normalize the wavefunction. Explicitly, we have

$$\begin{aligned} \langle \psi'|\psi'\rangle &= \sum_{m,n=1}^M \langle \psi|\mathbb{P}^{(m)} \mathbb{P}^{(n)}|\psi\rangle \otimes \langle m|n\rangle \\ &= \sum_{m=1}^M \langle \psi|\mathbb{P}^{(m)}|\psi\rangle = \langle \psi|\psi\rangle = 1, \end{aligned} \quad (2.7)$$

where we used completeness of the projectors to resolve the identity. Note that the explicit renormalization of the wavefunction required in the Copenhagen description of measurement is cancelled by normalization of the Stinespring part of (2.5).

2.2. Unitary measurement

The isometric dilation of the Hilbert space with each measurement can be sidestepped by including the Stinespring registers from the outset. Consider a (possibly

² See also [21] for another example of hybrid quantum dynamics in the Stinespring picture.

adaptive) hybrid protocol \mathcal{W} consisting of both unitary time evolution and projective measurements, where the choice and location of gates of both types may depend on the outcomes of prior measurements. Because the protocol \mathcal{W} is known, we know in advance the set of all observables we might measure while applying \mathcal{W} . We define the set $\{A_i \mid 1 \leq i \leq \mathcal{N}\}$ containing the \mathcal{N} “protocol observables” that may be measured in the application of \mathcal{W} . Correspondingly, we create \mathcal{N} Stinespring (or “outcome”) registers, where the i th Stinespring register has M_i states corresponding to the M_i unique eigenstates of the probe observable A_i .

We now work in the “dilated Hilbert space” (2.1), corresponding to all physical and Stinespring registers. By convention, we initialize all Stinespring registers in the “default” state $|0\rangle_{ss,i}$; the initial *dilated* density matrix is

$$\varrho = \rho_{ph} \otimes \left[\bigotimes_{i=1}^{\mathcal{N}} |0\rangle\langle 0|_{ss,i} \right], \quad (2.8)$$

where ρ_{ph} is the initial density matrix for the *physical* degrees of freedom at $t = 0$.

For convenience, we define the shorthand “vector” notation for all Stinespring registers,

$$|\mathbf{n}\rangle\langle\mathbf{n}|_{ss} \equiv \bigotimes_{i=1}^{\mathcal{N}} |n_i\rangle\langle n_i|_{ss,i}, \quad (2.9)$$

where the vector \mathbf{n} contains the \mathcal{N} outcomes $\{n_i\}$.

The motivation for including the outcome registers throughout the calculation is threefold: First, this avoids explicit dilation with each measurement; second, this allows us to represent measurement channels *unitarily* (an isometry from a vector space onto itself is always unitary); and third, the advantage of the Stinespring formulation itself over, say, the Kraus representation is to eschew explicit renormalization.

The unitary operator that implements measurement of observable A_i (2.2) is

$$\mathcal{V}_i = \mathcal{V}_{[A_i]} = \sum_{m=0}^{M_i-1} \mathbb{P}_{ph}^{(m)} \otimes \tilde{X}_{M_i;i}^m, \quad (2.10)$$

where $\tilde{X}_{M_i;i}$ is the M_i -state Weyl X operator³ acting on Stinespring register i (A.13a). The Weyl operators X and Z are defined in App. A, and unitarily extend the Pauli X and Z operators to $M > 2$. Specifically, $\tilde{X}_{M_i;i}$ shifts the state of the i th Stinespring register by one modulo M_i , so that $\tilde{X}_{M_i;i}^m$ takes the “default” state $|0\rangle_{ss,i}$ to the state $|m\rangle_{ss,i}$ corresponding to the m th outcome of A_i . Orthogonality of the projectors (2.4) ensures that $\mathbb{1} = \mathcal{V}_{[A]} \mathcal{V}_{[A]}^\dagger = \mathcal{V}_{[A]}^\dagger \mathcal{V}_{[A]}$.

³ We use tildes throughout to further distinguish Stinespring operators from their physical counterparts.

2.3. Measurement outcomes

The Stinespring formulation simplifies recovering various results related to the outcomes of measurements. For example, consider the Stinespring description of the measurement of a single observable A (2.2), where the state of the physical system is initially given by the density matrix ρ_{ph} as in (2.8).

Independent of the formalism used to describe measurement, considering only the physical Hilbert space, the expectation value of \mathcal{O} is given by

$$\langle A \rangle_\rho = \text{tr} [A \rho] = \sum_{m=1}^M a_m p_m, \quad (2.11)$$

where the probability to obtain outcome m depends on the density matrix ρ_{ph} according to

$$p_m = \text{tr} [\mathbb{P}_m \rho_{ph}], \quad (2.12)$$

and the normalized post-measurement wavefunction after obtaining outcome m is given by

$$|\psi_m\rangle = \frac{\mathbb{P}^{(m)}|\psi\rangle}{\langle\psi|\mathbb{P}^{(m)}|\psi\rangle^{1/2}}, \quad (2.13)$$

with the corresponding density matrix given by

$$\rho_m = \frac{\mathbb{P}^{(m)} \rho \mathbb{P}^{(m)}}{\text{tr} [\mathbb{P}^{(m)} \rho_{ph}]}, \quad (2.14)$$

which is also correctly normalized, with $\rho_m = |\psi_m\rangle\langle\psi_m|$.

In the *dilated* Hilbert space (2.1), using the notation (2.9), the dilated density matrix ϱ is given by

$$\varrho = \rho_{ph} \otimes |0\rangle\langle 0|_{ss}, \quad (2.8)$$

and we define expectation values in the dilated Hilbert space \mathcal{H}_{dil} according to

$$\langle A \otimes \tilde{A} \rangle_\varrho = \text{tr} [(A_{ph} \otimes \tilde{A}_{ss}) \varrho]. \quad (2.15)$$

For example, the probability p_m to obtain outcome m is given in terms of a dilated expectation value (2.15) as

$$\begin{aligned} p_m &= \langle \mathbb{1}_{ph} \otimes |n\rangle\langle n|_{ss} \rangle_\varrho \\ &= \text{tr} [(\mathbb{1}_{ph} \otimes |n\rangle\langle n|_{ss}) \varrho], \end{aligned} \quad (2.16)$$

and the expectation value for a Stinespring-measured observable A (2.2) can similarly be written as

$$\begin{aligned} \langle A \rangle_\varrho &= \langle \mathbb{1}_{ph} \otimes \sum_{m=1}^M a_m |m\rangle\langle m|_{ss} \rangle_\varrho = \sum_{m=1}^M a_m p_m \\ &= \text{tr} [(\mathbb{1}_{ph} \otimes \sum_{m=1}^M a_m |m\rangle\langle m|_{ss}) \varrho], \end{aligned} \quad (2.17)$$

and we note that all information about the measurement outcome is stored in the Stinespring register.

The preceding formulae for p_n (2.16) and $\langle A \rangle_\rho$ (2.17) generalize straightforwardly to the case of multiple measurements by including multiple Stinespring registers. The N outcomes of measuring the observables $\{A_i\}$ are stored in the outcome vector $\mathbf{n} = \{n_1, \dots, n_N\}$ (2.9). After any number of measurements, the dilated density matrix ρ is a sum over terms of the form $|\mathbf{n}\rangle\langle\mathbf{n}|$, which maps the outcome states $\{m_i\}$ to the outcome states $\{n_i\}$. In the foregoing formulae, one simply replaces $|n\rangle\langle n|$ with $|\mathbf{n}\rangle\langle\mathbf{n}|$ (2.9). For concreteness, the joint probability to obtain outcomes \mathbf{n} is given by

$$\begin{aligned} p_{\mathbf{n}} &= \langle \mathbf{1}_{\text{ph}} \otimes |\mathbf{n}\rangle\langle\mathbf{n}|_{\text{ss}} \rangle_\rho \\ &= \text{tr} [(\mathbf{1}_{\text{ph}} \otimes |\mathbf{n}\rangle\langle\mathbf{n}|_{\text{ss}}) \rho(t)], \end{aligned} \quad (2.18)$$

and all other joint and conditional expectation values follow straightforwardly from the various definitions above.

With multiple rounds of measurements, it may be useful to restrict various quantities to particular outcome *trajectories* (or alternatively, average over all outcomes) of a subset Ω of Stinespring registers, while leaving the rest of the density matrix (or some operator) intact. The density matrix (or any operator) is projected onto a particular outcome trajectory \mathbf{n} by the operator

$$\tilde{\mathbb{P}}_{\text{ss}}^{(\mathbf{n})} = \mathbf{1}_{\text{ph}} \otimes |\mathbf{n}\rangle\langle\mathbf{n}|_{\text{ss}}, \quad (2.19)$$

which may correspond to a subset Ω of outcomes. The normalized density matrix following (2.19) is then

$$\rho_{\mathbf{n}} = \frac{\text{tr} [\rho(t) |\mathbf{n}\rangle\langle\mathbf{n}|]}{\text{tr} [\rho(t) |\mathbf{n}\rangle\langle\mathbf{n}|]_{\text{dil}}}, \quad (2.20)$$

where the denominator is simply $p_{\mathbf{n}}$ (2.18). The trace in the numerator runs over Ω (where the corresponding measurements have already occurred). Note that (2.20) reproduces (2.14) for a single measurement, while (2.20) gives the post-measurement density matrix following a particular sequence of outcomes.

We can also compute the probability-weighted average over all outcomes. This involves summing (2.20) over all \mathbf{n} , weighted by $p_{\mathbf{n}}$, which cancels the denominator in (2.20). Summing the numerator over \mathbf{n} leads to $\sum_{\mathbf{n}} |\mathbf{n}\rangle\langle\mathbf{n}| = \mathbf{1}$ by completeness. The average over the subset of outcomes Ω is then

$$\rho_{\Omega}(t) = \mathbb{E}[\rho(t)]_{\Omega} = \sum_{\vec{n}} p_{\vec{n}} \rho_{\vec{n}} = \text{tr}_{\Omega} [\rho(t)], \quad (2.21)$$

where the “arrow” vector symbol indicates that the set $\vec{n} \subset \mathbf{n}$ is a subset of all the Stinespring registers. In general, (2.21) gives the reduced density matrix for the physical degrees of freedom and any remaining Stinespring registers over whose outcomes we do not [yet] wish to average. If Ω includes all outcome registers, then $\rho_{\Omega} \rightarrow \rho_{\text{ph}}$ is the density matrix for the physical system averaged over all measurement outcomes.

2.4. Comment on particular trajectories

Considering calculations involving monitored quantum systems in the Stinespring formalism, the two options presented so far for treating the Stinespring (outcome) degrees of freedom are to (i) project this object onto a particular outcome trajectory, via (2.19) or (ii) average over all possible outcomes via (2.21). We now motivate our restriction to the latter case in the remainder.

Importantly, because the recorded outcome of generic quantum measurements performed in some state $|\Psi\rangle$ are always random (as seen in Fig. 1), models of quantum systems are generally unable to make deterministic predictions about the outcome of any particular experimental “shot”. However, the probability p_m to obtain the m th outcome (2.12) can be determined from the initial state $|\Psi\rangle$; accordingly, one can make predictions about *expectation values* of measurements, and statistics associated with higher moments (or cumulants).

These statistics depend on the particular details of the many-body wavefunction $|\Psi\rangle$, which cannot be determined in a single experiment. Recovering statistics for measurement outcomes therefore generically requires many experimental “shots” to synthesize. Importantly, for the statistics to be meaningful, each shot should use the same many-body state $|\Psi\rangle$. However, measuring the state to extract statistics inherently disturbs (i.e., changes) it. Since the wavefunction cannot be accessed in its entirety (nor could that information be stored classical in the thermodynamic limit), and because the no-cloning theorem precludes copying the many-body state prior to a measurement, the same state $|\Psi\rangle$ must be prepared from scratch in each experimental shot.

Additionally, in performing the experiment, one has no control over the outcome of a given measurement. Thus, realizing a particular measurement trajectory \mathbf{n} multiple times requires a number of experimental shots that scales as $\mathcal{O}(q^{\gamma N T})$, where γ is the measurement rate, $N \sim L^D$ is the number of sites (in D spatial dimensions with linear size L), and NT is the total spacetime volume of the circuit, which becomes infinite in the thermodynamic limit of interest. This is also known as the “postselection problem” [19], which we discuss in Sec. 6 when we discuss the salient features of genuine phases of matter.

However, more familiar phases of matter (e.g., in the context of condensed matter or AMO systems) do not seem to require preparing multiple identical versions of the same state across a divergent number of experimental shots. This is due in part to the fact that, in a stable phase of matter, while measuring the system disturbs its state, it does not take the state out of the phase. Hence, one can still extract universal features—which are by definition insensitive to microscopic variations in particular samples and derive from a coarse-grained description of any sample in the phase—without reconstructing the state from scratch. Importantly, the universal probes have low variance from sample-to-sample, providing a notion of *typicality*, which allows one to extract statistics without

performing infinitely many shots.

The quantities we consider in Sec. 4 (and later in Sec. 7) have this property. One can quickly check that the variances of generic observables under Haar-random evolution is exponentially small in the system size. Thus, the observables measured in the application of the circuit—as well as the probe observables used to diagnose phase structure—enjoy a notion of typicality. Hence, the statistics for some quantity averaged over the Haar ensemble and measurement outcomes is well approximated by the statistics of a finite number of independent shots spanning a vanishing fraction of all possible realizations.

However, the same is not possible along a particular trajectory \mathbf{n} , where even two shots may require infinite time, and typicality cannot be invoked. After all, there is no notion of “approximate postselection”. For example, low-temperature equilibrium states are well captured by ground-state properties, as the low-temperature state has an exponentially large probability of sampling ground-state properties. In contrast, the probability that a random shot successfully produces the desired trajectory \mathbf{n} is exponentially small. We conclude that quantities evaluated with respect to (2.19) are not experimentally viable, while quantities evaluated with respect to (2.21) are.

3. HYBRID CIRCUIT MODELS

We now detail the treatment of random quantum circuit protocols including measurements in the Stinespring formalism, both with and without symmetries. In keeping with the spirit of standard quantum circuits, we restrict our measurements to *local* observables—i.e., measurements should act on finitely many neighboring sites.

3.1. The spacetime lattice

We begin by constructing the “spacetime lattice”, which defines the dilated Hilbert space \mathcal{H}_{dil} (2.1) for a given hybrid circuit. We consider systems with N total q -state qudits (with on-site Hilbert space $\mathcal{H}_j = \mathbb{C}^q$), so that

$$\mathcal{H}_{\text{ph}} = \bigotimes_{j=1}^N \mathcal{H}_j = (\mathbb{C}^q)^{\otimes N}, \quad (3.1)$$

where, in D spatial dimensions, $N \sim L^D$.

We now consider the Stinespring degrees of freedom. For the *isometric* representation of measurement discussed in Sec. 2.1, the additional Stinespring registers are “spawned” in real time as needed, and there is no need to codify the spacetime lattice. However, the *unitary* implementation of measurement discussed in Sec. 2.2 requires that all outcome registers be specified from the outset, and prepared in the initial state $|\mathbf{0}\rangle\langle\mathbf{0}|_{\text{ss}}$ (2.8). The prescription below for forming the spacetime lattice in some cases generates more Stinespring sites than are actually “used” by the circuit, to allow for the possibility

that the choice of measurements at a given time depend on prior measurement outcomes. However, we note that tracing over any unused outcome registers (still in the state $|\mathbf{0}\rangle\langle\mathbf{0}|$) gives the same result as not having included the register to begin with. Thus, the spacetime lattice contains all the degrees of freedom that one *might* need for a particular calculation involving measurements, providing a convenient means of labelling outcome registers and implementing unitary measurement.

We first suppose that the hybrid protocol involves T total time steps, where we may take $T \rightarrow \infty$. We next require that each time step contain at most \mathcal{S} “rounds” of measurements, labeled σ , where a “round” corresponds to a layer of nonoverlapping measurement gates. The number \mathcal{S}_t of measurement rounds may vary between time steps, and the total number of rounds is

$$\mathcal{S}_{\text{tot}} = \sum_{t'=1}^T \mathcal{S}_{t'}, \quad (3.2)$$

where \mathcal{S}_t the number of layers in time step t' .

The measurement layer t, σ of the circuit involves the measurement of some set $\Omega_{t,\sigma}$ of observables labeled $A_{t,\sigma,r}$, which may have different numbers of unique eigenvalues ($M_{t,\sigma,r}$), and act nontrivially on clusters r containing any finite number of neighboring sites. In general, the spacetime lattice is compatible with *adaptive* protocols, in which the composition of the circuit at time t may be conditioned on the outcomes of prior measurements.

The definition of the layers in terms of nonoverlapping measurements implies that each physical site j encounters *at most one* measurement per round (i.e. at most N observables per round). If a protocol naïvely requires two or more consecutive measurements involving site j , one simply splits these measurements into two separate rounds, without loss of generality. Consequently, it is possible to label each observable $A_{t,\sigma,j}$ unambiguously by one of the sites j upon which they act (e.g., identifying measurements by their left weight [6, 9, 10]); however, we also use the label r when convenient.

We further assume that the observables $A_{t,\sigma,j}$ have at most q unique eigenvalues. This assumption holds for all string-like observables that can be measured directly in experiment—in general, operators that have more than q unique outcomes correspond to superpositions of observables that can be measured directly (e.g., a local Hamiltonian term in a spin chain). Such expectation values are formed by making numerous individual measurements, each with at most q unique eigenvalues a piece. However, such a procedure is not possible midway through a hybrid circuit protocol. Thus, the assumption that $M_{t,\sigma,r} \leq q$ is fully compatible with the allowed circuit observables.

Hence, because there are at most q outcomes per measured observable, at most N observables per round, and at most \mathcal{S} rounds per time step, we can store the outcomes of measuring the circuit observables $A_{t,\sigma,j}$ using a total of $N \cdot \mathcal{S} \cdot T$ Stinespring sites with q internal states each. If $A_{t,\sigma,j}$ has $M_{t,\sigma,j} < q$ unique outcomes, we use only the

lowest $M_{t,\sigma,j}$ levels of the Stinespring register.

The composition of the *spacetime lattice* follows from the discrete-time nature of the circuit along with the foregoing considerations. The result is a $D+1$ -dimensional lattice with $L^D \times (\mathcal{S}_{\text{tot}} + 1)$ vertices labeled “ j, τ ”, where j runs over physical sites. The last axis of the lattice correspond to time: The temporal “slices” τ contain N q -state qudits. The D -dimensional slice $\tau = 0$ corresponds to the q -state *physical* degrees of freedom in \mathcal{H}_{ph} . The slice τ corresponds to measurement layer σ of time step t :

$$\tau(t, \sigma) = \sum_{t'=1}^{t-1} \mathcal{S}_{t'} + \sigma, \quad (3.3)$$

and contains N qudits to encode all possible measurement outcomes. The Stinespring site j, τ stores the outcome of measuring $\{A_{t,\sigma,j}\}$ in layer σ of time step t , and requires $M_{t,\sigma,j}$ internal states (the number of unique eigenvalues of $A_{t,\sigma,j}$). In principle, the result is recorded either in the first $M_{\varsigma,j}$ states $0, 1, \dots, M_{\varsigma,j} - 1$ of an q -state qudit, or equivalently, in an $M_{\varsigma,j}$ -state qudit at ς, j . In practice, this distinction is unimportant.

The Stinespring Hilbert space is given in terms of the $\tau > 0$ slices of the spacetime lattice as

$$\mathcal{H}_{\text{ss}} = \bigotimes_{\tau=1}^T \bigotimes_{\sigma=1}^{\mathcal{S}_t} \bigotimes_{j=1}^N \mathbb{C}^{M_{\tau,\sigma,j}}, \quad (3.4)$$

where $M_{j,\tau}$ is the number of unique eigenvalues of the corresponding observable $\mathcal{O}_{j,\tau}$ (and defaults to unity if no measurement is performed—i.e., a trivial outcome register). For convenience, we embed (3.4) in

$$\mathcal{H}_{\text{ss}}^{(q)} \equiv \mathbb{C}^{q \otimes N \mathcal{S}_{\text{tot}}}, \quad (3.5)$$

so that all degrees of freedom in \mathcal{H}_{dil} are q -state qudits.

3.2. Measurement unitaries

Hybrid circuits evolve a quantum system using a combination of time-evolution and projective measurements. The former are generated by local unitary gates acting on the physical degrees of freedom (3.1); the latter are represented via unitary (or isometric) gates according to the Stinespring formulation outlined in Sec. 2. The measurement gates in layer σ of time step t act on—and most importantly, entangle—the physical qudits in the slice $\tau = 0$ (3.1) and the Stinespring qudits in the slice $\tau = t, \sigma$ (3.5) of the spacetime lattice (discussed in Sec. 3.1). Their Hilbert space is given by (3.4), and may be embedded in the simplified spacetime lattice (3.5) for convenience.

Following the literature [13–18], we generally restrict to *nonadaptive* circuits, where the outcomes of measurements do not affect the selection of future gates. We discuss the new possibilities afforded by adaptive circuitry in Sec. 7. The primary effect of projective measurements in nonadaptive hybrid circuits is to purify the state, destroying

entanglement generated via unitary time evolution. Accordingly, the hybrid circuits of interest [13–18] typically alternate between time-evolution gates and single- and two-site measurements. The measurements are generally probabilistic: An observable $A_{t,\sigma,j}$ is measured on site j in layer σ of time step t with probability γ , while no measurement is made with probability $1 - \gamma$, independent of all other sites and prior time steps. One then looks for a sharp feature in the expectation value of some quantity as the parameter γ is tuned from zero to unity.

In this work we consider more generic hybrid protocols, which may have multiple rounds of measurement per time step, with observables of various bases, ranges, and degeneracies in each round. We require that each physical site j be measured at most once per round, reflecting the constraints of actual experiments. We restrict the circuit observables A to those that can be measured in a single shot (e.g., precluding the measurement of sums of operators). We also assume that the number of unique outcomes $M_{t,\sigma,r}$ for each observable is at most q .

We now consider projective measurements in the context of the circuit. The measurement of $A_{t,\sigma,r}$ on cluster r in layer σ of time step t is represented by the unitary,

$$\mathcal{V}_{t,\sigma,r} \equiv \sum_{m=0}^{M-1} \mathbb{P}_{r,0}^{(m)} \otimes \tilde{X}_{M;r,t}^m, \quad (3.6)$$

where the “ t, σ, r ” indices on M have been omitted for visual convenience and $\mathbb{P}_{r,0}^{(m)}$ projects the *physical* cluster $r, 0$ onto the m th eigenspace of $A_{t,\sigma,r}$ (2.2). The shift operator $\tilde{X}_{M;j,t}$ (A.13a) acts on the first $M_{t,\sigma,r} \leq q$ states of the *outcome* register at t, σ, r .

The measurement layer t, σ of the circuit is given by

$$\mathcal{V}_{t,\sigma} = \bigotimes_{r \in \Omega_{t,\sigma}} \mathcal{V}_{t,\sigma,r}, \quad (3.7)$$

where $\Omega_{t,\sigma}$ is the set of sites that participate in measurement layer σ of time step t . The measurement layers may be placed at any point in the single-time-step circuit relative the time-evolution layers.

3.3. Time evolution

Time evolution gates act solely on the physical Hilbert space (i.e., the $\tau = 0$ slice of the spacetime lattice). Locality of the dynamics is captured by evolving the system using a “circuit” of ℓ -site unitary “gates”. A local 1D circuit with the default $\ell = 2$ is depicted in Fig. 2.

The unitary gates are *local* in that the gate $\mathcal{U}_{t,\lambda,j}$ (in layer λ of time step t) acts on a cluster r comprising a contiguous region of ℓ neighboring qudits. We then arrange these gates into ℓ layers per time step, so that each site j realizes each of the ℓ positions in the various gates in each time step. In 1D, gates are uniquely labeled by the leftmost qubit $j \in r$, and in layer λ , the label j

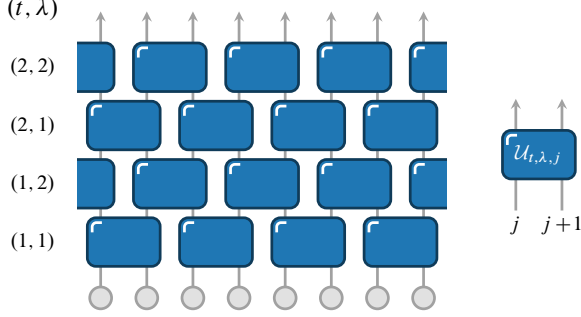


FIG. 2. Depiction of a 1D brickwork quantum circuit comprising two-site gates (left) and a single two-site unitary gate corresponding to time step t , unitary layer λ , and site j (right). Each time step t consists of $\ell = 2$ layers labeled λ , corresponding to even and odd bonds, as indicated by the labels (t, λ) . The two-site gates are drawn independently—in both space j and time t —from the Haar ensemble [54].

for the gate $\mathcal{U}_{t,\lambda,j}$ satisfies $j \bmod \ell = \lambda$. In this way, the ℓ layers of time-evolution gates tile the system in a brickwork geometry in every time step of the circuit. Fig. 2 depicts the $\ell = 2$ case, where the two layers alternate between even and odd bonds. Note that extension to higher dimensions is relatively straightforward: The 2D analogue of the brickwork circuit involves four layers of four-site gates acting on plaquettes of the square lattice.

The state $|\psi\rangle$ of the physical system is evolved from time t to time $t+1$ according to

$$|\psi(t+1)\rangle = \mathcal{W}_t |\psi(t)\rangle, \quad (3.8)$$

where \mathcal{W}_t is a circuit given by the *time-ordered* product

$$\mathcal{W}_t = \prod_{\lambda=1}^{\ell} \mathcal{W}_{t,\lambda}, \quad (3.9)$$

where $\mathcal{W}_{t,\lambda}$ is a *layer* of the circuit comprising mutually commuting ℓ -site unitary gates,

$$\mathcal{W}_{t,\lambda} \equiv \bigotimes_{r \in \lambda} \mathcal{U}_{t,\lambda,r}, \quad (3.10)$$

where $\mathcal{U}_{t,\lambda,r}$ is the gate that acts on the physical sites ($\tau = 0$) in cluster r . Absent any symmetries or constraints, we draw the gates $\mathcal{U}_{t,\lambda,r}$ independently for each cluster r in each layer λ of the circuit from the unitary group $U(q^\ell)$ with uniform measure (i.e., the gates are Haar-random $q^\ell \times q^\ell$ unitaries). We also define the full evolution from the initial state to time t via

$$|\psi(t)\rangle = \mathcal{W}(t) |\psi(0)\rangle, \quad \mathcal{W}(t) \equiv \prod_{s=1}^{t-1} \mathcal{W}_s, \quad (3.11)$$

where the product is time ordered.

Generally speaking, minimal brickwork circuits (e.g., as depicted in Fig. 2 for the 1D case) are sufficient to reproduce the maximally chaotic physics realized by a $q^N \times q^N$ many-body random unitary [7–12, 54].

$$\mathcal{U}_{j,j+1} = \begin{pmatrix} U_1 & 0 & 0 & 0 \\ 0 & U_2 & 0 & 0 \\ 0 & 0 & U_3 & 0 \\ 0 & 0 & 0 & U_4 \end{pmatrix} \begin{pmatrix} |00\rangle \\ |01\rangle \\ |10\rangle \\ |11\rangle \end{pmatrix}$$

FIG. 3. Block-diagonal gate for a 1D circuit with $U(1)$ conservation of Z (or “charge”), for $q = \ell = 2$. Blocks with different charges cannot mix under dynamics; consequently, the unitary gate acts nontrivially only within blocks of fixed charge, and the unitaries in different blocks are independently drawn.

3.4. Symmetries, constraints, and block structure

The circuits of Sec. 3.3 are designed to be fully generic, and therefore lack many ingredients present in typical systems—namely, *symmetries*. We now extend these generic circuits (3.10) to capture arbitrary Abelian symmetries [9–12] and/or kinetic constraints [12, 26–31].

We note that the generators of Abelian symmetries can always be represented using a common basis. In general, we take this to be the eigenbasis of the Weyl operator Z (A.13b), which reduces to the Pauli Z matrix for $q = 2$ (the Weyl operator basis is detailed in App. A). The local eigenstates of Z form the *computational basis*.

In the case of models with kinetic constraints but no conservation laws, we express the constraints in the computational basis (the Z eigenbasis) without loss of generality [12]. Should both symmetries and constraints be present, we require that they share a common basis—i.e., the “charge” basis should also be the computational basis. The rationale is that, if the constraint were formulated in the X basis, e.g., while charges correspond to the Z basis, then the projector onto configurations that do not satisfy the “constraint” would themselves induce dynamics on fixed-charge configurations. However, this is incompatible with the constraint, which dictates that no dynamics occur unless the constraint is satisfied. Hence, our results apply to the “natural” class of symmetry-compatible constraints—as well as to generic models with *either* Abelian symmetries or constraints [12].

The unitary gate acting on some ℓ -site cluster r can be written in the block-diagonal form

$$\mathcal{U}_r \equiv \sum_{\alpha} \mathbb{P}_r^{(\alpha)} \mathcal{U}_{r,\alpha} \mathbb{P}_r^{(\alpha)}, \quad (3.12)$$

where $\mathbb{P}_r^{(\alpha)}$ projects onto block α (which contains $n_{\alpha} \geq 1$ states of cluster r that are allowed by the symmetries and/or constraints to mix under dynamics). The unitary $\mathcal{U}_{r,\alpha}$ acts purely within block α [9–12], and is *independently* drawn for each block α from the unitary group $U(n_{\alpha})$ with uniform (Haar) measure [9–12, 54]. The blocks may correspond to configurations of cluster r with definite conserved charge $Q_r = \sum_{j \in r} \mathbf{q}_j$, configurations that satisfy the constraint, or a combination thereof. In

the case of constraints, configurations that fail to satisfy the constraint belongs to their own block (with $n_\alpha = 1$) [12]. Fig. 3 depicts the block-diagonal unitary gate for a U(1)-symmetric 1D circuit with $q = \ell = 2$; further examples appear in [12].

Unitarity of \mathcal{U}_r (3.12) requires that the projectors be complete and idempotent,

$$\sum_\alpha \mathbb{P}_r^{(\alpha)} = \mathbb{1}, \quad \mathbb{P}_r^{(\alpha)} \mathbb{P}_r^{(\alpha')} = \delta_{\alpha,\alpha'} \mathbb{P}_r^{(\alpha)}, \quad (3.13)$$

and each $\mathbb{P}_r^{(\alpha)}$ can be written as a sum over projectors onto particular ℓ -site computational-basis configurations of r that belong to the block α ,

$$\mathbb{P}_r^{(\alpha)} = \sum_{\vec{a} \in \alpha} \prod_{j \in r} |a_j\rangle\langle a_j|_j, \quad (3.14)$$

where $\vec{a} = (a_j, a_{j+1}, \dots, a_{j+\ell-1})$ labels Z -basis configurations of r . Each block α contains at least one configuration a and every configuration appears in some block.

Note that *any* combination of Abelian symmetries and (symmetry-compatible) constraints can be captured by gates of the form (3.12). Moreover, both conservation laws and constraints may be imposed either within the q -dimensional Hilbert space [9, 12] or through the introduction of ancilla degrees of freedom [10, 11]. Our only other assumption is that all blocks can be represented in a common basis—namely, the computational basis.

3.5. Floquet circuits

In calculations pertaining to dynamics, universal properties are well-captured by *noisy* quantum circuits (i.e., those that are random in space and time). However, one can also use *spectral properties* to diagnose universal quantum dynamics [8, 11, 12, 32, 33], but a spectrum only exists if evolution to arbitrary times can be captured by a single operator. In static systems, that operator is the Hamiltonian; in Floquet systems—which are periodic in time—that operator is the “Floquet unitary” (or single-period evolution operator) \mathcal{F} . Evolution by t time steps is realized by $\mathcal{W}(t) = \mathcal{F}^t$ (3.11).

It is straightforward to realize Floquet extensions of the noisy hybrid circuits described thus far. We emphasize that, while the measurement gates $\{\mathcal{V}_{\sigma,r}\}$ are periodic, their *outcomes* need not be. Because evolution is periodic, we need only determine the single-period evolution circuit \mathcal{F} —i.e., we need only specify the circuit for a single time step: Later times are reached via repeated application of the same Floquet operator. All Haar-random unitaries are independently drawn (and the sets Ω and $\{A_{\sigma,r}\}$ specified only in the first \mathcal{F} , and repeated thereafter).

The final modification is simple: We replace (3.6) with the time-independent form

$$\mathcal{V}_{\sigma,r} = \sum_{m=0}^{M-1} \mathbb{P}_{r,0}^{(m)} \otimes \tilde{X}_{M;1,r}^m, \quad (3.15)$$

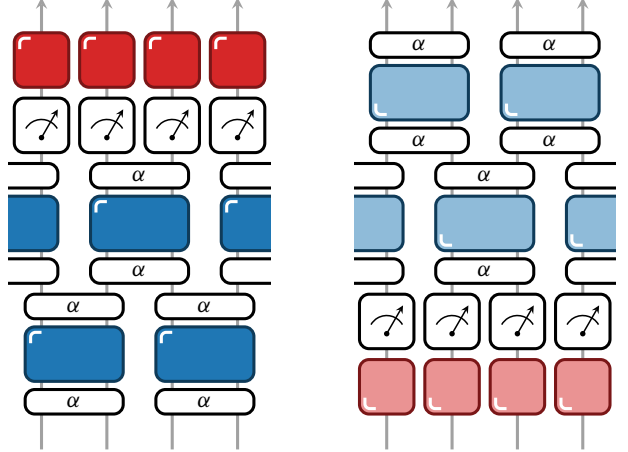


FIG. 4. Circuit diagram of a four-site cut of a 1D Floquet unitary (3.17) for $\ell = 2$, with operators multiplied from bottom to top. *Left*—Diagrammatic depiction of \mathcal{F} : The block-diagonal time-evolution gates (3.12) act first (where the blue objects are the Haar unitaries U_α and the unfilled objects labeled α are projectors onto blocks α), followed by measurement unitaries (3.6), and finally a cyclic shift (3.16) of all time slices $\tau \neq 0$ of the lattice. *Right*—Diagram for \mathcal{F}^\dagger : The alternate coloring of the gates indicates complex conjugation, while their reversed ordering and inverted marker indicate transposition. The legs correspond to all dilated sites labeled j , and the circuit continues on either side. Note that only the two α s sandwiching a given gate are related (3.12).

so that the measurement outcomes are always stored in layer $\tau = 1$, with $\tau = 0$ the physical layer.

Each time step consists of unitary evolution, followed by measurement, followed by the cyclic time translation operator \mathbf{T} , which moves the time slice $\tau > 0$ to position $\tau - 1 \bmod \mathcal{S}_{\text{tot}}$, while leaving the $\tau = 0$ slice untouched,

$$\mathbf{T} \equiv \sum_{\{n_{\tau,j}\}} \bigotimes_{j=1}^N \bigotimes_{\tau=1}^{\mathcal{S}_{\text{tot}}} |n_{j,\tau+1}\rangle\langle n_{j,\tau}|, \quad (3.16)$$

where we take Ω and $\{A_{\sigma,r}\}$ and restrict to slices $1 \leq \tau \leq \mathcal{S}_{\text{tot}}$ above. This operation is only sensible if we include N Stinespring registers with q internal state in each slice τ , as described in Secs. 3.1 and 3.2.

Thus, after the first round of measurement, the results are stored in slice $\tau = 1$, then moved to $\tau = \mathcal{S}_{\text{tot}}$, then $\mathcal{S}_{\text{tot}} - 1$, and so on. After the final measurement round is completed, the final application of \mathbf{T} moves all measurement outcomes to their expected locations—i.e., slice $\tau = t, \sigma$ (3.3) corresponds to round σ of measurements in time step t for all t, σ .

In a simple example wherein all measurement layers follow all time-evolution layers in each time step, the Floquet operator is given by the time-ordered product

$$\mathcal{F} = \mathbf{T} \bigotimes_{\sigma=1}^{\mathcal{S}} \bigotimes_{r \in \sigma}^N \mathcal{V}_{\sigma,r} \bigotimes_{\lambda=1}^{\ell} \bigotimes_{r \in \lambda}^N \mathcal{U}_{\lambda,r}, \quad (3.17)$$

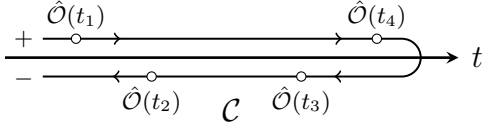


FIG. 5. Schematic depiction of the Keldysh contour \mathcal{C} . While the time arguments do not satisfy $t_n > t_{n-1}$, they are nevertheless orderable on the Keldysh contour, which contains just one forward and one backward time evolution.

with $\mathcal{V}_{\sigma,r}$ defined in (3.15). In general, the measurement layers will be interspersed with the time-evolution layers. Note that a cluster r can always be uniquely assigned to a site j in the Stinespring slice t, σ .

Once \mathcal{F} is determined, we simply apply this operator repeatedly to reach later times. Importantly, the measurement protocol (locations and observables) are the same in each time step; however, the outcomes need not be the same. This is transparent in the Stinespring formalism (2.10), as all outcomes occur. In the noisy case (as opposed to Floquet), we simply omit \mathbf{T} , take $\mathcal{V}_{t,j}$ as defined in (3.6), and draw all gates randomly and independently in both space and time. A diagrammatic depiction of the Floquet operator (3.17) appears in Fig. 4.

4. OBSERVABLES AND CORRELATIONS

We now consider expectation values and correlations of generic observables, which can diagnose dynamical behavior and phase structure of an individual sample in an experiment. This may require multiple independent “shots” to evaluate (i.e., to recover full statistics), where only the initial state ρ_0 (2.8) need be the same in each shot. That state is evolved under the hybrid circuit, and the outcomes of various “probe” measurements \mathcal{O} (as distinct from the observables A measured as part of the circuit) are recorded and averaged. Mathematically, such quantities involve only a *single copy* of the dilated density matrix ϱ (2.8), and are the most straightforward to measure in both condensed matter and AMO experiments. Importantly, they do not require postselection and are insensitive to sample-to-sample variations (e.g., gate errors). As a reminder, we only consider *nonadaptive* circuits, which are not conditioned on prior outcomes.

4.1. Quantities of interest

We first discuss the “simple” quantities that can be extracted from a *single* sample using independent experimental shots involving a small number of measurements (at most $\mathcal{O}(N)$). All phases of matter of which we are aware can be defined using quantities of this type.

The relevant quantities are of the general form

$$\langle \mathcal{O}_1(t_1) \cdots \mathcal{O}_n(t_n) \rangle_{\varrho}, \quad (4.1)$$

where the time arguments $\{t_i\}$ can be ordered on a closed time (Keldysh) contour, as shown schematically for $n = 4$ in Fig. 5 [55]. Such quantities correspond, e.g., to the time-dependent expectation value of a local observable ($n = 1$), linear response correlation functions ($n = 2$), and time-ordered nonlinear response functions (or n -point correlators) [55]. We note that out-of-time-ordered correlators (OTOCs) [6, 7] cannot be evaluated experimentally for $\gamma > 0$: While the Hermitian conjugate \mathcal{U}^\dagger of some time-evolution gate \mathcal{U} can generally be implemented, there is no experimental control over the measurement unitary \mathcal{V} (3.6), which merely represents the measurement channel—it is not possible to apply \mathcal{V}^\dagger .

The probe observables $\{\mathcal{O}_i\}$ may be treated separately from the circuit observables $\{A_{t,\sigma,r}\}$, in either the Schrödinger or Heisenberg picture. The probe observables’ evolution in the Heisenberg picture, e.g., is given by

$$\begin{aligned} & (\mathcal{W}_1^\dagger \mathcal{O}_1 \mathcal{W}_1) (\mathcal{W}_{2,1}^\dagger \mathcal{O}_2 \mathcal{W}_{2,1}) \cdots (\mathcal{W}_{n,\dots,2,1}^\dagger \mathcal{O}_n \mathcal{W}_{n,\dots,2,1}) \\ &= \mathcal{W}_1^\dagger \mathcal{O}_1 \mathcal{W}_2^\dagger \mathcal{O}_2 \cdots \mathcal{W}_n^\dagger \mathcal{O}_n \mathcal{W}_n \cdots \mathcal{W}_2 \mathcal{W}_1, \end{aligned} \quad (4.2)$$

meaning that every unitary gate U and its conjugate U^\dagger appears exactly once in any such expression. Thus, the Haar-averaged time evolution updates are given by the onefold channel (B.1) described in App. B [12, 54].

The n -point expectation values of the form (4.1) are computed by evolving a single copy of the density matrix ϱ in the Schrödinger picture under the hybrid quantum circuit and applying n additional “probe” measurement unitaries (3.6) at the corresponding times $\{t_i\}$. Finally, (4.1) is constructed from the n auxiliary outcome registers as prescribed in Sec. 2.3. Remarkably, we find that none of these particulars affect the conclusion: No evidence of a transition (or sharp feature) as a function of the measurement rate γ is witnessed by any quantity of the form (4.1). We investigate the γ dependence of generic quantities (4.1) that can be constructed in a real experiment using *independent* shots on some initial state ρ_0 . As first reported in [13] in the context of generic circuits (i.e., not enriched with block structure), quantities of this type are blind to the effects of measurement. In other words, not only is there no sharp “transition”, but, *on average, measurements have no effect* whatsoever (i.e., γ does not appear in the final result).

4.2. Transfer matrix formulation

We now evaluate (4.1) in the dilated Hilbert space, allowing for block structure. We use auxiliary Stinespring registers for the n probe observables in (4.1), which can then be determined via hybrid evolution of the dilated density matrix ϱ . We isolate the effect of measurements (parametrized by the measurement rate γ) by comparing to the same result under time evolution alone. We make this comparison for individual time steps of the circuit; this is not possible in *adaptive* circuits (conditioned on

the outcomes of prior measurements) [21, 44–46], which are instead treated in Sec. 7

As noted in Sec. 2.4, there is no reason to consider particular outcome trajectories. Essentially, because any mixed state can be realized using targeted measurements and time evolution, there are no useful predictions to be made about individual trajectories. This would also be peculiar given that we average over an ensemble of unitary gates. Additionally, since one cannot choose the outcomes of the measurements, to realize the physics of particular outcomes would require exponentially many experimental trials, and is therefore not viable as a probe of phase structure in the thermodynamic limit ($N, T \rightarrow \infty$). We therefore restrict to quantities (4.1) averaged over the outcomes of all measurements.

Essentially, prior to time step t (i.e., the t th layer of the hybrid circuit), the state of the Stinespring registers on the slice $\tau = t$ is $|\mathbf{0}\rangle\langle\mathbf{0}|$ (2.8). Those registers are affected only by the measurement gates in the t th time step (time evolution acts only on the physical slice $\tau = 0$), and we can average over outcomes immediately after all of the measurement gates in \mathcal{V}_t have been applied by taking the trace over all Stinespring registers in the slice $\tau = t$. This is only possible in nonadaptive circuits. Hence, at time t , we assume that all Stinespring registers for $\tau < t$ have been traced out (to average over outcomes), while all Stinespring registers with $\tau > t$ are in the state $|\mathbf{0}\rangle\langle\mathbf{0}|$ (2.8), and are unaffected by the application of the t th time step of the hybrid circuit.

Thus, at time t we define the outcome-averaged reduced density matrix for the *physical* system as

$$\rho_{\text{ph}}(t) \equiv \mathbb{E}[\varrho(t)]_{\tau < t} = \underset{\tau \neq 0}{\text{tr}} [\varrho(t)] \quad (4.3)$$

where the trace trivially removes Stinespring registers with $\tau > t$ (since $\text{tr}[|\mathbf{0}\rangle\langle\mathbf{0}|] = \langle\mathbf{0}|\mathbf{0}\rangle = 1$), and averages over the outcomes of all prior measurements $\tau < t$.

In order to apply both the time-evolution and measurement gates (\mathcal{W}_t and \mathcal{V}_t , respectively), we next reinstate the outcome registers for the time slice t in the state $|\mathbf{0}\rangle\langle\mathbf{0}|$. The density matrix to which we apply the t th time step of the hybrid circuit can be expanded as

$$\varrho(t) = \sum_{\vec{m}, \vec{n}} C_{\vec{m}, \vec{n}}^{(t)} \bigotimes_{j=1}^N X_{j,0}^{m_j} Z_{j,0}^{n_j} \otimes |\mathbf{0}\rangle\langle\mathbf{0}|_{j,t}, \quad (4.4)$$

where the coefficients C satisfy

$$C_{\vec{m}, \vec{n}}(t) = \frac{1}{q^N} \text{tr} \left[\rho_{\text{ph}}(t) \bigotimes_{j=1}^N Z_{j,0}^{-n_j} X_{j,0}^{-m_j} \right], \quad (4.5)$$

which follows from completeness of the unitary basis (A.17), with $\rho_{\text{ph}}(t)$ defined in (4.3).

We now introduce the *transfer matrix* (see App. C for further details). For both measurement and time-evolution layers, the transfer matrix acts on the physical part of the density matrix only—the Stinespring part

is trivially $|\mathbf{0}\rangle\langle\mathbf{0}|$ immediately prior to the measurement layer, and may be traced over immediately after.

The transfer matrix \mathcal{T} is a superoperator: The operators that act on \mathcal{H}_{dil} are themselves elements of the Hilbert space $\mathcal{H}_{\text{op}} = \text{End}(\mathcal{H}_{\text{dil}})$ —the endomorphisms of \mathcal{H}_{dil} ; the transfer matrix is an element of $\mathcal{H}_{\text{sup}} = \text{End}(\mathcal{H}_{\text{op}}) = \text{End}(\text{End}(\mathcal{H}_{\text{dil}}))$. For a unitary circuit layer $\mathcal{W}_{t,\varsigma}$ —corresponding to time evolution or outcome-averaged measurements—the transfer matrix is defined as the superoperator that implements $\mathcal{W}_{t,\varsigma}$,

$$\overline{|\rho(t+\delta t)\rangle} = \mathcal{T}_t \overline{|\rho(t)\rangle}, \quad (4.6)$$

whose matrix elements in the Weyl basis (A.12) are

$$\begin{aligned} \mathcal{T}_{\vec{m}, \vec{n}; \vec{m}', \vec{n}'}^{(t,\varsigma)} &= \left(\Gamma_{\vec{m}, \vec{n}} \middle| \mathcal{T}_{t,\varsigma} \middle| \Gamma_{\vec{m}', \vec{n}'} \right) \\ &= \frac{1}{\mathcal{D}} \text{tr} \left[\Gamma_{\vec{m}, \vec{n}}^\dagger \mathcal{W}_{t,\varsigma} \Gamma_{\vec{m}', \vec{n}'} \mathcal{W}_{t,\varsigma}^\dagger \right], \end{aligned} \quad (4.7)$$

where the many-body Weyl basis operators (A.24) act only on physical qudits as

$$\Gamma_{\vec{m}, \vec{n}} = \bigotimes_{j=1}^N X_j^{m_j} Z_j^{n_j}, \quad (4.8)$$

as in the decomposition (4.4). The evolution of $\varrho(t)$ is then described in operator space by application of the transfer matrix circuit—whose structure mirrors that of the time-evolution circuit \mathcal{W} . In 1D, the transfer matrix can be studied numerically using tensor network methods to extract the dynamical exponent z [12].

The transfer matrix elements $\mathcal{T}_{\vec{m}, \vec{n}; \vec{m}', \vec{n}'}^{(t,\varsigma)}$ describe the update to the Weyl-basis coefficient C according to

$$\overline{C_{\vec{m}, \vec{n}}^{(t+\delta t)}} = \sum_{\vec{m}', \vec{n}'} \mathcal{T}_{\vec{m}, \vec{n}; \vec{m}', \vec{n}'}^{(t,\varsigma)} \overline{C_{\vec{m}', \vec{n}'}^{(t)}}, \quad (4.9)$$

and we now derive the transfer matrices for both time evolution and outcome-averaged measurements.

4.3. Time evolution transfer matrix

In the absence of symmetries and constraints [5, 7], generic Haar-averaged time evolution replaces ρ_{ph} with the infinite-temperature density matrix $\rho_\infty \propto \mathbb{1}$ (B.5), as derived in App. B. However, the inclusion of block structure (3.12) complicates matters, producing sums over many “block trajectories”. The transfer matrix conveniently represents this sum using a local Hermitian superoperator that acts on ρ_0 (2.8) in operator space. The generic result (B.5) recovers as a simple limit of the enriched result (with block structure).

We now derive the transfer matrix elements (4.7) corresponding to time-evolution layer t, λ (3.10). We assume without loss of generality that the unitary gates $\mathcal{U}_{t,\lambda,r}$ in $\mathcal{W}_{t,\lambda}$ are block diagonal (3.12). We further require that

the projectors onto blocks (3.13) share a common basis (3.14), and impose all requirements laid out in Sec. 3.4. Importantly, we note that the basis operators $\Gamma_{\vec{m},\vec{n}}$ (4.7) are Kronecker products of local operators, and therefore factorize over the clusters r that appear in $\mathcal{W}_{t,\lambda}$ (3.10).

The transfer matrix circuit \mathcal{T}_t (4.6) corresponding to the time-evolution circuit \mathcal{W}_t (3.8) factorizes into *layers* $\mathcal{T}_{t,\lambda}$, just as \mathcal{W}_t is a product over layers $\mathcal{W}_{t,\lambda}$ (3.9). Each layer $\mathcal{T}_{t,\lambda}$ is a product of transfer matrix *gates* $T_{t,\lambda,r}$, just as $\mathcal{W}_{t,\lambda}$ is a product over unitary gates $\mathcal{U}_{t,\lambda,r}$ (3.10). Thus, \mathcal{W}_t and \mathcal{T}_t have identical circuit structure, with the latter a superoperator given by the time-ordered product,

$$\mathcal{T}_t = \bigotimes_{\lambda=1}^{\ell} \mathcal{T}_{t,\lambda} = \bigotimes_{\lambda=1}^{\ell} \bigotimes_{r \in \lambda} T_{t,\lambda,r}, \quad (4.10)$$

where the label t allows for the possibility that the circuit geometry changes with time. If the arrangement of gates in each \mathcal{W}_t is fixed, the transfer matrix (4.10) is time independent after Haar averaging [12].

The elements of the *gate* $T_{t,\lambda,r}$ (4.10) take the form

$$T_{\vec{m},\vec{n};\vec{m}',\vec{n}'}^{(t,\lambda,r)} = \frac{1}{q^\ell} \text{tr} \left[\Gamma_{\vec{m},\vec{n}}^\dagger \overline{\mathcal{U}_{t,\lambda,r} \Gamma_{\vec{m}',\vec{n}'} \mathcal{U}_{t,\lambda,r}^\dagger} \right], \quad (4.11)$$

where the label vectors (e.g., \vec{m}) are length ℓ —corresponding to the sites in cluster r —and all operators act only on the *physical* degrees of freedom.

We now expand (4.11) according to (3.12) to facilitate Haar averaging [12, 54],

$$\begin{aligned} &= \frac{1}{q^\ell} \sum_{\alpha,\alpha'} \text{tr} \left[\Gamma_{\vec{m},\vec{n}}^\dagger \mathbb{P}_r^{(\alpha)} \overline{U_\alpha \mathbb{P}_r^{(\alpha)} \Gamma_{\vec{m}',\vec{n}'} \mathbb{P}_r^{(\alpha')} U_{\alpha'}^\dagger} \mathbb{P}_r^{(\alpha')} \right] \\ &= \frac{1}{q^\ell} \sum_{\alpha} \text{tr} \left[\Gamma_{\vec{m},\vec{n}}^\dagger \mathbb{P}_r^{(\alpha)} \Phi_{\text{Haar}}^{(1)} \left[\mathbb{P}_r^{(\alpha)} \Gamma_{\vec{m}',\vec{n}'} \mathbb{P}_r^{(\alpha)} \right] \mathbb{P}_r^{(\alpha)} \right], \end{aligned}$$

where $\Phi_{\text{Haar}}^{(1)}[A]$ is the onefold Haar channel of A given by (B.1) [54], which vanishes unless $\alpha = \alpha'$. Essentially, this channel “twirls” A over the unitary group $\mathbb{U}(q^\ell)$.

Using $\Phi_{\text{Haar}}^{(1)}[A] = \text{tr}[A] \mathbb{1} / \dim(U_\alpha)$, we next write

$$\begin{aligned} &= \frac{1}{q^\ell} \sum_{\alpha} \frac{1}{n_\alpha} \text{tr} \left[\Gamma_{\vec{m},\vec{n}}^\dagger \mathbb{P}_r^{(\alpha)} \right] \text{tr} \left[\mathbb{P}_r^{(\alpha)} \Gamma_{\vec{m}',\vec{n}'} \right] \\ &= \sum_{\alpha} \frac{q^\ell}{n_\alpha} \left(\Gamma_{\vec{m},\vec{n}} \middle| \mathbb{P}_r^{(\alpha)} \right) \left(\mathbb{P}_r^{(\alpha)} \middle| \Gamma_{\vec{m}',\vec{n}'} \right), \end{aligned} \quad (4.12)$$

and taking the projectors $\mathbb{P}_r^{(\alpha)}$ to be given by (3.14) in the Weyl Z basis, the above becomes

$$= \delta_{\vec{m},\vec{m}'} \delta_{\vec{m}',\vec{0}} \sum_{\alpha} \frac{1}{n_\alpha} \sum_{\vec{a},\vec{a}' \in \alpha} \frac{\omega^{\vec{a}' \cdot \vec{n}' - \vec{a} \cdot \vec{n}}}{q^\ell}, \quad (4.13)$$

while if we take $\mathbb{P}_r^{(\alpha)} \rightarrow \tilde{\mathbb{P}}_r^{(\alpha)}$ to be given by (3.14) in the Weyl X basis, the above is instead

$$= \delta_{\vec{n},\vec{n}'} \delta_{\vec{n}',\vec{0}} \sum_{\alpha} \frac{1}{n_\alpha} \sum_{\vec{a},\vec{a}' \in \alpha} \frac{\omega^{\vec{a}' \cdot \vec{m}' - \vec{a} \cdot \vec{m}}}{q^\ell}. \quad (4.14)$$

We recover a basis-independent expression by noting

$$T_{\vec{m},\vec{n};\vec{m}',\vec{n}'}^{(t,\lambda,r)} = \left(\Gamma_{\vec{m},\vec{n}} \middle| T^{(t,\lambda,r)} \middle| \Gamma_{\vec{m}',\vec{n}'} \right), \quad (4.15)$$

and we infer from (4.12) that

$$T_{t,\lambda,r} = \sum_{\alpha} \frac{q^\ell}{n_\alpha} \left| \mathbb{P}_r^{(\alpha)} \right\rangle \left\langle \mathbb{P}_r^{(\alpha)} \right|, \quad (4.16)$$

and finally, we express (3.14) in terms of the orthonormal *diagonal* basis operators defined in App. A.4,

$$\left| \mathbb{P}_r^{(\alpha)} \right\rangle = \sum_{\vec{a} \in \alpha} \frac{1}{q^{\ell/2}} \left| \pi_r^{(\vec{a})} \right\rangle, \quad (4.17)$$

so that (4.16) becomes

$$T_{t,\lambda,r} = \sum_{\alpha} \frac{1}{n_\alpha} \sum_{\vec{a},\vec{a}' \in \alpha} \left| \pi_r^{(\vec{a})} \right\rangle \left\langle \pi_r^{(\vec{a}')} \right|, \quad (4.18)$$

which annihilates any nondiagonal operator on the cluster r and maps the diagonal basis operator $\pi_r^{(\vec{a})}$ in block α , to every other diagonal basis operator, $\pi_r^{(\vec{a}')}$ in block α , with equal weight $1/n_\alpha$, where n_α is the number of states in block α [12]. In general, the block structure is fixed by the range ℓ of the gate, the local Hilbert space dimension q , and the choice of symmetries and/or constraints, and thus independent of t, λ, r . However, the alternative is also described by (4.18).

In the absence of block structure, the time-evolution transfer matrix is simply

$$T_{t,\lambda} = |\mathbb{1}\rangle\langle\mathbb{1}|, \quad (4.19)$$

which annihilates any nonidentity component of ρ , leading to the infinite-temperature state $\rho_\infty \propto \mathbb{1}$ after a single layer. The matrix elements are given by

$$T_{\vec{m},\vec{n};\vec{m}',\vec{n}'}^{(t,\lambda)} = \delta_{\vec{m},\vec{m}'} \delta_{\vec{n},\vec{n}'} \delta_{\vec{m}',\vec{0}} \delta_{\vec{n}',\vec{0}}. \quad (4.20)$$

4.4. Measurement transfer matrix

We now repeat the procedure of Sec. 4.3 for the *measurement* gates (3.6). As before, the transfer matrix superoperator \mathcal{T}_t (4.10) that realizes hybrid evolution of operators and density matrices to time t is a local circuit with the same structure as the hybrid channel $\mathcal{W}(t)$ (3.11). Each time-evolution layer $\mathcal{W}_{s,\lambda}$ of \mathcal{W}_t (3.9) corresponds to a time-evolution transfer matrix layer $\mathcal{T}_{s,\lambda}$ (4.10), and each gate $\mathcal{U}_{s,\lambda,r}$ in $\mathcal{W}_{s,\lambda}$ (3.10) corresponds to a time-evolution transfer matrix gate $T_{s,\lambda,r}$ (4.10).

By analogy, to each measurement gate $\mathcal{V}_{s,\sigma,r}$ in measurement layer σ at time s , we associate a *measurement* transfer matrix gate $T_{s,\sigma,r}$ (4.10). Just as the time-evolution gates codify the updates to operators under unitary time-evolution gates, the measurement transfer matrix gates

encode the outcome-averaged operator update due to unitary measurement gates. The ordering of measurement and time-evolution transfer matrix layers—as well as the composition of each layer in terms of gates—follows from the hybrid protocol $\mathcal{W}(t)$ (see Fig. 4).

In analogy to (4.10), the measurement layer $\mathcal{T}_{t,\sigma}$ of the transfer matrix is given by

$$\mathcal{T}_{t,\sigma} = \bigotimes_{r \in \sigma} T_{t,\sigma,r}, \quad (4.21)$$

where $T_{\sigma,r}$ is the transfer matrix gate that captures the outcome-averaged update due to measuring $A_{t,\sigma,r}$ on cluster r in measurement layer σ of time step t .

The matrix elements of the measurement transfer matrix gate (4.21)—corresponding to the observable $A_{t,\sigma,r}$ acting on an ℓ -site cluster r —are given by

$$T_{\vec{m},\vec{n};\vec{m}',\vec{n}'}^{(t,\sigma,r)} = \frac{1}{q^\ell} \sum_{\mu=0}^{M-1} \text{tr} \left[\Gamma_{\vec{m},\vec{n}}^\dagger \mathbb{P}_r^{(\mu)} \Gamma_{\vec{m}',\vec{n}'} \mathbb{P}_r^{(\mu)} \right], \quad (4.22)$$

in analogy to (4.11), where $\{\mathbb{P}_r^{(\mu)}\}$ project onto the $M = M_{t,\sigma,r}$ unique eigenspaces of $\{A_{t,\sigma,r}\}$ (2.2) labeled μ .

Further progress can be made from (4.22) by treating the degenerate and nondegenerate measurement outcomes separately. We split the sum over μ into sums over configurations $\vec{b} \in B_\mu$ (where B_μ is the set of configurations corresponding to outcome a_μ), and a sum over all configurations. We now rewrite (4.22) as

$$\begin{aligned} &= \frac{1}{q^\ell} \sum_{\mu=0}^{M-1} \text{tr} \left[\Gamma_{\vec{m},\vec{n}}^\dagger \mathbb{P}_r^{(\mu)} \Gamma_{\vec{m}',\vec{n}'} \mathbb{P}_r^{(\mu)} \right] \\ &= \frac{1}{q^\ell} \sum_{\vec{k}} \text{tr} \left[\Gamma_{\vec{m},\vec{n}}^\dagger \mathbb{P}_r^{(\vec{k})} \Gamma_{\vec{m}',\vec{n}'} \mathbb{P}_r^{(\vec{k})} \right] \\ &+ \frac{1}{q^\ell} \sum_B \sum_{\substack{\vec{b},\vec{b}' \in B \\ \vec{b} \neq \vec{b}'}} \text{tr} \left[\Gamma_{\vec{m},\vec{n}}^\dagger \mathbb{P}_r^{(\vec{b}')} \Gamma_{\vec{m}',\vec{n}'} \mathbb{P}_r^{(\vec{b})} \right], \end{aligned} \quad (4.23)$$

where \vec{k} runs over all q^ℓ basis states for cluster r .

The first term in (4.23) corresponds to

$$T_{t,\sigma,r} = \sum_{\vec{k}} \left| \pi_r^{(\vec{k})} \right\rangle \left\langle \pi_r^{(\vec{k})} \right| + \dots, \quad (4.24)$$

where \dots represents the other term in (4.23). The normalized projectors are defined in (A.25) in App. A.4, and project onto all ℓ -site operators on cluster r that are *diagonal* in the eigenbasis of $A_{t,\sigma,r}$. Any operator containing off-diagonal terms in this basis is annihilated by (4.24); in the case of nondegenerate observables, this is the only contribution to the measurement transfer matrix gate.

However, in the more general case in which we allow degenerate circuit observables, we must consider the second term. Without loss of generality, suppose that the observable $A_{t,\sigma,r}$ with $M_{t,\sigma,r} < q^\ell$ unique eigenvalues is diagonalized by the Weyl Z basis (A.13b).

The second term in (4.23) is given by

$$\begin{aligned} &= \frac{1}{q^\ell} \sum_B \sum_{\substack{\vec{b},\vec{b}' \in B \\ \vec{b} \neq \vec{b}'}} \text{tr} \left[\Gamma_{\vec{m},\vec{n}}^\dagger \mathbb{P}_r^{(\vec{b}')} \Gamma_{\vec{m}',\vec{n}'} \mathbb{P}_r^{(\vec{b})} \right] \\ &= \delta_{\vec{m},\vec{m}'} \sum_B \sum_{\vec{b} \neq \vec{b}' \in B} \frac{\omega^{\vec{b} \cdot (\vec{n} - \vec{n}')}}{q^\ell} \delta_{\vec{m}',\vec{b}' - \vec{b}}, \end{aligned} \quad (4.25)$$

which is zero unless \vec{m}' is compatible with the difference between the configurations \vec{b} and \vec{b}' in block B . This result is easily recovered by expanding the second term in (4.23) in the Weyl basis (detailed in App. A.3).

In summary, the measurement transfer matrix gate (4.22) for an ℓ -site observable $A_{t,\sigma,r}$ (with $M_{t,\sigma,r}$ unique outcomes) in the Z basis (A.13b) has elements

$$\begin{aligned} T_{\vec{m},\vec{n};\vec{m}',\vec{n}'}^{(t,\sigma,r)} &= \delta_{\vec{m},\vec{m}'} \delta_{\vec{n},\vec{n}'} \delta_{\vec{m}',\vec{b}} \\ &+ \delta_{\vec{m},\vec{m}'} \sum_B \sum_{\vec{b} \neq \vec{b}' \in B} \frac{\omega^{\vec{b} \cdot (\vec{n} - \vec{n}')}}{q^\ell} \delta_{\vec{m}',\vec{b}' - \vec{b}}, \end{aligned} \quad (4.26)$$

where B labels degenerate blocks, and \vec{b}, \vec{b}' are two different ℓ -site Z -basis configurations of cluster r , which must be compatible with \vec{m}' (the powers of X originally in the density matrix). The second term is reminiscent of (4.13), and vanishes for nondegenerate observables.

We now use the measurement and time-evolution transfer matrices to investigate the effect of the former on the universal properties captured by (4.1), which includes all expectation values, correlations, and response functions that can be measured using independent experimental “shots” performed on a single sample, avoiding the postselection problem [19]. We explore several cases, corresponding to various choices of hybrid protocols.

4.5. Measurements have no effect in generic circuits

As a starting point, we review the effect of measurements on “generic” circuits [13]—i.e., in which time-evolution is not enriched with block structure (i.e., neither conserved quantities nor kinetic constraints). In this case, the transfer matrix for *any* time-evolution layer λ is given by (4.19), with matrix elements given by (4.20). Essentially, these Haar-random circuits model chaotic quantum systems (i.e., those that thermally equilibrate under their own dynamics): Absent constraints or conservation laws, the only possible thermal density matrix is the featureless, maximally mixed state $\rho_{\text{therm}} = \rho_\infty \propto \mathbb{1}$. On average, each time-evolution transfer matrix layer annihilates *all* possible physical operators *except* the identity.

We now consider the combination of the transfer matrices for time-evolution layer λ (4.20) and the outcome-averaged measurement of $A_{t,\sigma,r}$ on cluster r (4.26). Noting that the time-evolution transfer matrix factorizes over

sites, the elements of the *combined* transfer matrix gate for cluster r —corresponding to time evolution and measurement in either order—are given by

$$\begin{aligned}\tilde{T}_{\vec{m},\vec{n};\vec{m}'',\vec{n}''}^{(t,\sigma,r)} &\equiv \left(\Gamma_{\vec{m},\vec{n}} \middle| T_{t,\lambda,r} T_{t,\sigma,r} \middle| \Gamma_{\vec{m}'',\vec{n}''} \right) \\ &= \sum_{\vec{m}',\vec{n}'} T_{\vec{m},\vec{n};\vec{m}',\vec{n}'}^{(t,\lambda,r)} T_{\vec{m}',\vec{n}';\vec{m}'',\vec{n}''}^{(t,\sigma,r)} \\ &= \delta_{\vec{m},\vec{m}''} \delta_{\vec{n},\vec{n}''} \delta_{\vec{m}'',\vec{0}} \delta_{\vec{n}'',\vec{0}} \\ &= T_{\vec{m},\vec{n};\vec{m}'',\vec{n}''}^{(t,\lambda,r)},\end{aligned}\quad (4.27)$$

meaning that, on average, the combination of measurement layer σ and time-evolution layer λ (in either order) is identical to time evolution alone. In fact, *any* number of measurement layers are trivialized by a *single* layer of generic time-evolution acting on all physical sites in the system (in either the Schrödinger or Heisenberg picture, for arbitrary circuit geometry and choice of $\{A_{t,\sigma,r}\}$).

The blindness of (4.1) to projective measurements in generic hybrid circuits was first reported in [13]. However, it is not the case that projective measurements do nothing in such systems. Rather, the combination of generic, Haar-averaged time evolution and arbitrary measurement gates (applied in either order) annihilates the second term in the outcome-averaged measurement transfer matrix gate (4.26), which would otherwise admit nontrivial dynamics due to measurements with degenerate outcomes. The first term in the transfer matrix transfer matrix gate (4.26) acts as $\sum_{n=1}^{q-1} |Z^n\rangle\langle Z^n|$ for Z -basis measurements, on average. However, this differs from the generic time-evolution transfer matrix gate $|\mathbb{1}\rangle\langle\mathbb{1}| = |Z^0\rangle\langle Z^0|$ (4.19) only in the inclusion of the $n \neq 0$ terms, which are annihilated upon contraction with (4.19) (in either order). Hence, the combined transfer matrix (4.27) for time-evolution layer λ and any number of measurement layers before or after acts on the entire physical system as $\mathcal{T}_{t,\lambda} = |\mathbb{1}\rangle\langle\mathbb{1}|$ (4.19), which is equivalent to $\mathcal{T}_{t,\lambda}$ alone.

This appears to be a generic feature of unitary-projective dynamics when the measurement outcomes are not utilized later in the circuit [21]. Because the measurement outcomes are effectively discarded, their outcome-averaged effect is equivalent to allowing the “environment” to measure the system instead. This is most transparent in the context of quantum error correction represented in the Stinespring picture: As shown in [21], unless and until an error-correction operation is performed (using the outcomes of the measurements), the state of the measured degrees of freedom is always the maximally mixed state $\rho_\infty \propto \mathbb{1}$, which is simply a random classical bit (or dit for $q > 2$), with all measurement outcomes equiprobable (for arbitrary measurements).

The combination of generic, chaotic time-evolution and projective measurements (in any basis) maps any density matrix (or operator) to the featureless state $\rho_\infty \propto \mathbb{1}$. Consequently, projective measurements in generic non-adaptive circuits hybrid quantum circuits are entirely trivial. In Sec. 7, we consider adaptive protocols (which

utilize the measurement outcomes later in the circuit) [21, 44–46] to realize effects due to measurements [13, 21].

4.6. Measuring charge operators has no effect

Having ruled out detectable effects due to measurements in *generic* hybrid circuits, we now investigate the fate of (4.1) in nonadaptive hybrid circuits with block structure. When the dynamics are “enriched” with symmetries and/or constraints, late-time steady states other than $\rho \rightarrow \rho_\infty \propto \mathbb{1}$ can realize. Because systems retain information about conserved charges, enriched hybrid circuits admit thermal density matrices of the form $\rho_{\text{sym}} \propto e^{-\mu Q}$, compatible with nontrivial phase structure. This also distinguishes charge operators as special, as their expectation values generally remain nontrivial—even at late times—when evaluated in ρ_{sym} (but not in the maximally mixed state ρ_∞).

We now consider measuring charge operators in circuits with an Abelian symmetry [23]. All circuit observables $A_{t,\sigma,r}$ act diagonally in the charge basis, and thus commute with each other and the projectors onto dynamical blocks (3.12). Without loss of generality, we take this to be the Weyl Z basis (A.13b), so that the block projectors $\mathbb{P}_r^{(\alpha)}$ are sums over Z -basis states (3.14) and the circuit observables $\{A_{t,\sigma,r}\}$ involve sums of Z^n (A.25).

In general, the blocks may correspond to any commuting combination of symmetries and kinetic constraints [12]. In the case of symmetries, the Z -basis circuit observables $A_{t,\sigma,r}$ correspond to “charge” operators (e.g., as in [23]); in the case of kinetic constraints, the Z -basis observables $A_{t,\sigma,r}$ project onto computational basis states (e.g., “occupation numbers”). We now show that nonadaptive measurement of such operators has no effect on any quantity of the form (4.1) on average.

The transfer matrix gates for enriched time evolution and projective measurements (both in the Z basis) are given in (4.13) and (4.26), respectively. Because all $A_{t,\sigma,r}$ commute, including consecutive measurement layers either does nothing whatsoever or lifts some of the degeneracies that of a single layer. Hence, we need only consider the effect of applying one round of measurement transfer matrix gates (4.26), either before or after a layer of time-evolution transfer matrix gates (4.13).

Note that the time-evolution layer λ covers all sites, enforcing the condition $m_j = m'_j = 0$ for *every* site j (4.13). Because the measurement gate (4.26) preserves \vec{m} for all sites $j \in r$, we have $\vec{m}' = \vec{m}'' = \vec{0}$ for every measurement transfer matrix gate in every layer t, σ that appears directly before or after a layer t, λ of time-evolution.

Consequently, the term in (4.26), corresponding to degenerate blocks is trivial (since time evolution ensures that $\vec{m}' = \vec{m}'' = \vec{0}$). Only the first term in (4.26) survives, and acts trivially on any Weyl Z -basis operator. Because Weyl X operators are annihilated by time evolution (4.13), *any* Z -basis measurements applied before or after a layer of block-diagonal time evolution has no

discernible effect (on average); any subsequent Z -basis measurements does are similarly trivialized. Thus, we conclude that projective measurements that commute with the generator(s) of the symmetry (and/or the projectors encoding kinetic constraints) have no detectable effect—on average—compared to time evolution alone in *nonadaptive* protocols. In Sec. 7, we recover nontrivial results for adaptive circuits with charge measurements.

4.7. Measuring other operators only “undoes” symmetries

The scenarios considered thus far are the two most relevant to experiment [13, 23, 41]. We first ruled out the possibility that measurements of *any type* have an observable effect compared to generic chaotic time evolution alone [6, 7]. We then ruled out the possibility of “steering” toward symmetry sectors in chaotic quantum systems with Abelian conservation laws using measurements of charge operators. The results apply to all quantities of the form (4.1) in nonadaptive circuits upon averaging over measurements. As far as we are aware, there have been no attempts to investigate the measurement of “charge-changing” operators in chaotic quantum circuits with conserved quantities—most likely, this is because one naïvely expects that measuring such operators simply spoils the symmetry of the time-evolution gates, leading to featureless chaotic dynamics [6, 7] with $\rho \rightarrow \rho_\infty \propto \mathbb{1}$.

We now confirm that this is, indeed, the case for hybrid circuits acting on qubits ($q = 2$), where the Weyl X and Z operators reduce to the familiar Pauli matrices X and Z , with $Y = iXZ$. For concreteness, time evolution is generated by two-site, block-diagonal gates of the form (3.12), with symmetry blocks generated by Z , and we consider projective measurements of X and Z operators.

Setup.— The unitary gates (3.6) corresponding to measuring Pauli operators are also Hermitian (see the Supplementary Material of [21]). Consider the single- and two-site physical density matrices ρ_i and ρ_{ij} ,

$$\rho_i(t) = \sum_{\mu=0}^3 C_\mu^{(t)} \sigma_i^\mu \quad (4.28a)$$

$$\rho_{ij}(t) = \sum_{\mu,\nu=0}^3 C_{\mu,\nu}^{(t)} \sigma_i^\mu \sigma_j^\nu, \quad (4.28b)$$

and measuring X_i and $X_i X_j$, respectively, gives

$$\rho_i(t') = C_0^{(t)} \mathbb{1}_i + C_1^{(t)} X_i \quad (4.29a)$$

$$\rho_{ij}(t') = C_{0,0}^{(t)} \mathbb{1}_{ij} + C_{1,0}^{(t)} X_i + C_{0,1}^{(t)} X_j + C_{1,1}^{(t)} X_i X_j, \quad (4.29b)$$

and taking $X_{i,j} \rightarrow Z_{i,j}$ in the expressions above gives the updates corresponding to measuring Z_i and $Z_i Z_j$.

However, such Z measurements can generically and trivially be absorbed into the Z -basis time-evolution gates,

as established in Sec. 4.6. As a result, any measurements of Z have no effect on the density matrix, unless they appear between two layers of X measurements. However, we do not consider this case as it is physically equivalent to measuring X alone.

Ising symmetry.— Now suppose that the two-site time-evolution gates (3.12) conserve the \mathbb{Z}_2 Ising parity $\mathcal{G}_{i,j} = Z_i Z_j$. The unitary gate $\mathcal{U}_{i,j}$ contains two symmetry blocks, each with two states, corresponding to $\mathcal{G}_{i,j} = \pm 1$, with associated projectors $(\mathbb{1} \pm Z_i Z_j) / 2$. The Haar-averaged update to (4.28b) is then

$$\overline{\rho_{i,j}(t')} = \overline{C_{0,0}^{(t)}} \mathbb{1}_{i,j} + \overline{C_{3,3}^{(t)}} Z_i Z_j, \quad (4.30)$$

and taking (4.29) with $X \rightarrow Z$ is consistent with the claim in Sec. 4.6 that measuring any number of Z operators before or after applying such a time-evolution gate has no effect compared to time evolution alone.

According to (4.29), measuring X_i or X_j (4.29) before or after time evolving (4.30) gives

$$\overline{\rho_{i,j}(t'')} = \overline{C_{0,0}^{(t)}} \mathbb{1}_{i,j}, \quad (4.31)$$

which is equivalent to generic Haar-averaged time evolution (4.19) with neither conservation laws nor constraints. From (4.31), we conclude that measuring $X_i X_j$ gives the same result; it is also straightforward to verify that measuring $X_i X_j$ before or after applying the time-evolution gates $\mathcal{U}_{i,k}$ and $\mathcal{U}_{j,\ell}$ also leads to the maximally mixed state $\rho = \rho_\infty \propto \mathbb{1}$ on all sites i, j, k, ℓ .

In other words, any measurement of symmetry-incompatible operators X_j before or after an Ising-symmetric time-evolution gate $\mathcal{U}_{i,j}$ is equivalent to replacing $\mathcal{U}_{i,j}$ with a completely random, generic unitary. Essentially, X measurements undo the Ising symmetry, replacing the nontrivial density matrix with the maximally mixed state $\rho \propto \mathbb{1}$ everywhere that measurements are made. Thus, while measurements cannot *introduce* new universal behavior compared to chaotic time evolution, it can *negate* the universal properties of time evolution, instead realizing “generic” (i.e., featureless) evolution. Importantly, this implies that the alleged “phase structure” of [24]—and [25], which is dual to [24]—is unobservable using experimentally feasible probes (4.1). We note that the analytical probes presented in [24, 25] require postselection and are therefore not possible to evaluate in any experiment (as further discussed in Sec. 6). This also conclusively rules out the possibility of realizing interesting phases in Ising-symmetric systems using nonadaptive circuits with competing X - and Z -like measurements.

Charge conservation.— For a more nuanced example, suppose the two-site time-evolution gates conserve the local $U(1)$ charge $\mathcal{G}_{i,j} = Z_i + Z_j$ (as depicted in Fig. 3). The unitary gate $\mathcal{U}_{i,j}$ contains three symmetry blocks corresponding to $\mathcal{G}_{i,j} = \pm 1, 0$, (i.e., the configurations $\uparrow\uparrow / \downarrow\downarrow, \uparrow\downarrow$ and $\downarrow\uparrow$), with associated projectors $(\mathbb{1}_i \pm Z_i)(\mathbb{1}_j \pm Z_j) / 4$ and $(\mathbb{1}_{i,j} - Z_i Z_j) / 2$. The Haar-

averaged update to (4.28b) is then

$$\overline{\rho_{i,j}(t')} = \overline{C_{0,0}^{(t)}} \mathbb{1}_{i,j} + \overline{C_{3,3}^{(t)}} Z_i Z_j + \frac{1}{2} \left(\overline{C_{0,3}^{(t)}} + \overline{C_{3,0}^{(t)}} \right) (Z_i + Z_j), \quad (4.32)$$

where the first line is equivalent to the Ising update (4.30), and the new terms in the second line correspond to the two-state block $\uparrow\downarrow, \downarrow\uparrow$. Note that $U(1)$ -symmetric evolution mixes the operators Z_i and Z_j . As in the Ising case, one can verify that measuring Z operators immediately prior or subsequent to time-evolution layer λ has no effect on average compared to time evolution alone.

Now consider measuring the symmetry-incompatible operator X_j before or after the $U(1)$ -symmetric time-evolution gate $\mathcal{U}_{i,j}$, that produces (4.32). Averaging over measurement outcomes and the Haar ensemble, the resulting density matrix for the $U(1)$ case is

$$\overline{\rho_{i,j}(t'')} = \overline{C_{0,0}^{(t)}} \mathbb{1}_{i,j} + \frac{1}{2} \left(\overline{C_{0,3}^{(t)}} + \overline{C_{3,0}^{(t)}} \right) Z_i, \quad (4.33)$$

meaning that measuring X_j kills off any Z_j content in (4.28b); however, the time-evolution gate $\mathcal{U}_{i,j}$ mixes Z_j with Z_i (with a factor of 1/2), so that the 0,3 coefficient survives. However, measuring $X_i X_j$ leaves only the trivial term ($\rho \propto \mathbb{1}$) above, as in the \mathbb{Z}_2 Ising case (4.31).

Analysis.— A crucial observation is that the part of the $\rho(t)$ proportional to $\mathbb{1}$ survives any combination of time-evolution and measurement updates without suppression. This holds for any choice of block structure, and measurements in any basis. In contrast to the \mathbb{Z}_2 -symmetric Ising case (4.31), $U(1)$ -symmetric evolution (4.33), the nonidentity content on sites where a charge-changing operator is *not* measured survives (with a factor of 1/2). Additionally, subsequent gates can repopulate site j with a Z_j operator—instead of the $\mathbb{1}_j$ required by (4.33)—at the cost of further suppression by 1/2.

We expect these two results to be generic to symmetry-incompatible measurements in models with discrete and continuous symmetries for $q \geq 2$. In the continuous case (e.g., $U(1)$), the suppression resulting from a measurement that destroys only some of the states in a block α is expected to be $1/n_\alpha$. Additionally, the states destroyed by measurements may be repopulated by later time-evolution gates, at the cost of further suppression by $1/n_{\alpha'}$ (where the blocks α' may differ in the later time-evolution gate).

This result also generalizes to $q > 2$ in the special case of *nondegenerate* symmetry-incompatible (i.e., the Weyl X -basis) measurements: The identity always survives the combined update with coefficient one and, depending on the block structure of the time-evolution gates, certain Weyl Z operators may also survive with some $O(1/q)$ suppression. Subsequent time-evolution gates may restore Weyl Z content to the previously measured sites, at the cost of further $O(1/q)$ suppression. We then find that the late-time density matrix with sufficiently high measurement rate is guaranteed to be the maximally mixed state $\rho \propto \mathbb{1}$, with all other states suppressed by $O(q^{-2N})$ where N is the number of measured sites.

In other words, we find that measuring observables that are not compatible with the block structure of the time-evolution protocol can only trivialize (i.e., “undo”) the universal features of the time evolution itself. It is not possible for measurements to introduce new terms not permitted by time evolution without an adaptive protocol. The two limiting scenarios correspond to (i) no modification to the physics corresponding to time evolution alone and (ii) trivialization of the time-evolution physics to featureless chaotic evolution. At early times, ρ may realize any state compatible with block-structured time evolution (i), while at late times, ρ reduces to the maximally mixed state, as would result from generic time evolution alone. As the measurement rate γ is increased, one can tune from case (i) to case (ii) by suppressing all states other than the maximally mixed state with each additional measurement, without ever seeing a sharp transition. We also note that neither limiting case corresponds to “new” universal physics—measurements either preserve or trivialize the physics of time evolution. The “crossover” between these two regimes is further smoothed by averaging over measurement locations, so that the weight of nonidentity terms falls off as $q^{-\gamma N t}$.

In other words, measurements can (i) do nothing at all compared to time evolution; (ii) trivialize the dynamical properties of time evolution; or (iii) anything intermediate between these limits. However, there is no sharp “transition” as one tunes between these limits, and we conclude that measurements cannot lead to new universality classes nor transitions that can be witnessed using probes of the form (4.1) without adaptive gates.

5. SPECTRAL FORM FACTORS

5.1. Chaos and spectral rigidity

Having proved dynamical signatures of quantum chaos and possible phase structure in Sec. 4, we now consider a separate signature of chaos: *level repulsion*. Essentially, due to thermal correlations in chaotic systems, the eigenvalues of the generator of dynamics (namely, the Hamiltonian or Floquet unitary) repel one another. In general, the eigenvalues of \mathcal{F} for a chaotic quantum system are expected to obey an RMT distribution [8, 11, 12, 32–34]; this is also termed “spectral rigidity” [8, 11].

A useful diagnostic of RMT spectral rigidity is the two-point spectral form factor (SFF) [8, 11, 12, 33–39]; for purely unitary Floquet dynamics the SFF is defined as

$$K(t) = \sum_{m,n=1}^{\mathcal{D}} e^{i t (\theta_m - \theta_n)} = |\text{tr} [\mathcal{F}^t]|^2, \quad (5.1)$$

which is essentially the temporal Fourier transform of two-point correlations of the *eigenvalue* density [33]. Above, $\mathcal{D} = q^N$ is the many-body Hilbert space dimension, q is the on-site Hilbert space dimension, N is the number of sites, and $\{\theta_m\}$ are the eigenphases of the Floquet unitary

\mathcal{F} . We then average (5.1) over an ensemble of statistically similar realizations of \mathcal{F} , denoted by an overline.

Chaotic many-body quantum systems are insensitive to their initial state and microscopic details; hence, one expects that $K(t)$ (5.1) in such systems is well approximated by a *random* evolution operator with the same symmetries. For fully generic models, we expect $\overline{K(t)} = K_{\text{CUE}}(t) = t$ (for $1 \leq t \leq \mathcal{D}$) corresponding to the Circular Unitary Ensemble [8, 11, 12, 56]. At $t = 0$, $K(t)$ is trivially $\mathcal{D}^2 = q^{2N}$; for $t \geq \tau_{\text{Heis}} = \mathcal{D}$, the Heisenberg time (equal to the inverse mean level spacing), $K(t) = \mathcal{D}$. For $t \geq \tau_{\text{Heis}}$, the dominant contribution is the sum over all $m = n$ terms in (5.1), and the off-diagonal contributions ($m \neq n$) are effectively random complex numbers that sum to zero when t is larger than the mean inverse level spacing.

This linear ramp for times $1 \leq t \leq \mathcal{D}$ is a fingerprint of spectral rigidity, realized by generic Floquet circuits [8]. Intuitively, in the linear ramp regime, $K(t)$ (5.1) is dominated by paired “Feynman histories” [39], where at time t there are t possible pairings, so that $K(t) \sim t(1 + \dots)$, where the \dots terms are suppressed at long wavelengths and by ensemble averaging [8, 11, 12, 39].

In practice, typical systems do not show RMT behavior starting from $t = 1$. To see this, we first note that noninteracting, integrable, and localized models do not show a linear ramp at all, because their eigenphases are *uncorrelated* and thus do not repel. We find $K(t) = \mathcal{D}$ for all times $t > 0$ for such uncorrelated phases, as can be verified for certain noninteracting disordered models [8, 11, 12]. For a typical system, at early times one expects that interactions have not yet had a chance to produce long-wavelength thermal correlations, and the system is effectively noninteracting. Modeling the dynamics via single-site Floquet circuits predicts $K(t) \sim t^N$. However, as interactions entangle the system, these effective single-site blocks grow to size $\xi(t)$, with $\xi(0) = \mathcal{O}(1)$. The SFF at time t is then expected to be $K(t) = t^{N/\xi(t)}$. From this picture, we see that the onset of the linear ramp regime—associated with thermalization—occurs at the time τ_{th} (the “Thouless time” [8, 11, 12, 34, 38], named in analogy to the quantity describing disordered wires [57, 58]), defined by $\xi(\tau_{\text{th}}) = N$, so that $K(t) \sim t$ for $t > \tau_{\text{th}}$. Here, thermalization refers to the onset of RMT behavior and the loss of information about initial conditions, captured by a thermal density matrix.

The Thouless time heralds the onset of thermalization. Maximally chaotic systems have $\tau_{\text{th}} = \mathcal{O}(1)$; nonthermal systems have $\tau_{\text{th}} > \mathcal{D}$, so that there is no linear ramp regime. In generic systems, the scaling of the Thouless time $\tau_{\text{th}} \sim N^z$ is directly associated with linear-response correlators [12], where the exponent z is the dynamical exponent (see also App. D.1). A 1D system with a U(1) conserved charge, e.g., has $z = 2$ [11, 12, 34], from which we conclude that thermalization is delayed until information about the symmetry diffuses through the system, which requires $t \gtrsim \tau_{\text{th}} \propto L^2$.

5.2. Extension to hybrid circuits

In App. D we present additional details of the SFF (5.1), including an explicit and exact connection to averages of two-point correlation functions for random circuits in App. D.1. Using this formulation of the SFF, we argue for a natural extension to hybrid quantum systems; further details supporting this derivation appear in Apps. D.2 and D.3. It is helpful to rewrite (5.1) as

$$K(t) = \sum_{a,b=1}^{\mathcal{D}_{\text{ph}}} \langle a | \mathcal{F}^t | a \rangle \langle b | \mathcal{F}^{-t} | b \rangle, \quad (5.2)$$

where a and b run over any many-body basis of the physical Hilbert space \mathcal{H}_{ph} . We can also write

$$\begin{aligned} K(t) &= \sum_{a,b=1}^{\mathcal{D}_{\text{ph}}} \text{tr} [|b\rangle\langle a| \mathcal{F}^t |a\rangle\langle b| \mathcal{F}^{-t}] \\ &= \frac{1}{\mathcal{D}_{\text{ph}}} \sum_{a,b=1}^{\mathcal{D}_{\text{ph}}} \text{tr} [\mathcal{O}_{a,b}^{\dagger}(t) \mathcal{O}_{a,b}(0)], \end{aligned} \quad (5.3)$$

i.e., a sum over infinite-temperature autocorrelation functions of all *naïve* basis operators $\mathcal{O}_{a,b} \propto |a\rangle\langle b|$ (A.7).

We now extend (5.2) to hybrid Floquet circuits \mathcal{F} (3.17) with *isometric* measurements (as described in Sec. 2.1). Then, each of the t applications of \mathcal{F} to the state $|a\rangle$ (and \mathcal{F}^{\dagger} to $|b\rangle$) in (5.2) generates $|\Omega|$ additional Stinespring qubits, where Ω is the [sub]set of sites measured in each time step, as detailed in App. D.2. However, the trace in (5.2) only runs over \mathcal{H}_{ph} , so $K_{\text{iso}}(t)$ (5.2) is instead an *operator* on \mathcal{H}_{ss} . To recover a scalar result, we project this object onto outcome trajectory \mathbf{m} , defining

$$K_{\mathbf{m}}(t) \equiv \text{tr}_{\text{ss}} [|\mathbf{m}\rangle\langle \mathbf{m}| K_{\text{iso}}(t)], \quad (5.4)$$

where $K_{\text{iso}}(t)$ is still defined by (5.2), but where \mathcal{F} contains isometric measurement gates. Using (5.3), we find

$$\begin{aligned} K_{\mathbf{m}}(t) &= \sum_{a,b=1}^{\mathcal{D}_{\text{ph}}} \langle a, \mathbf{m} | \mathcal{F}^t | a \rangle \langle b | \mathcal{F}^{-t} | b, \mathbf{m} \rangle \\ &= \sum_{a,b=1}^{\mathcal{D}_{\text{ph}}} \text{tr}_{\text{dil}} [|b, \mathbf{m}\rangle\langle a, \mathbf{m}| \mathcal{F}^t |a\rangle\langle b| \mathcal{F}^{-t}], \end{aligned} \quad (5.5)$$

which we straightforwardly extend to the unitary representation of measurement gates (discussed in Sec. 2.2) by attaching the “default” Stinespring states to the “initial”

physical operator $|a\rangle\langle b|$, i.e.,

$$\begin{aligned} K_{\mathbf{m}}(t) &= \sum_{a,b=1}^{\mathcal{D}_{\text{ph}}} \text{tr}_{\text{dil}} \left[|b, \mathbf{m}\rangle\langle a, \mathbf{m}| \mathcal{F}^t |a, \mathbf{0}\rangle\langle b, \mathbf{0}| \mathcal{F}^{-t} \right] \\ &= \frac{1}{\mathcal{D}_{\text{dil}}} \sum_{a,b=1}^{\mathcal{D}_{\text{ph}}} \text{tr}_{\text{dil}} \left[\mathcal{O}_{a, \mathbf{m}; b, \mathbf{m}}^\dagger(t) \mathcal{O}_{a, \mathbf{0}; b, \mathbf{0}}(0) \right] \\ &= \sum_{a,b=1}^{\mathcal{D}_{\text{ph}}} \langle \mathcal{O}_{a\mathbf{m}, b\mathbf{m}}^\dagger(t) \mathcal{O}_{a\mathbf{0}, b\mathbf{0}}(0) \rangle_\infty, \end{aligned} \quad (5.6)$$

where, in the last line, we represent the SFF as an equal-weight sum over infinite-temperature temporal autocorrelation functions of all unique basis operators on the physical Hilbert space, projected onto the outcome trajectory \mathbf{m} (and weighted by the probability $p_{\mathbf{m}}$ (2.18)). Here, the infinite-temperature state corresponds to the *dilated* Hilbert space $\varrho_\infty = \mathbb{1}_{\text{dil}}/\mathcal{D}_{\text{dil}}$. As an aside, we note that allowing the \mathcal{F} and \mathcal{F}^\dagger evolutions to realize different trajectories \mathbf{m} and \mathbf{n} does not affect the final result, as only terms with $\mathbf{m} = \mathbf{n}$ contribute to the SFF for the models we consider herein.

We can simplify matters by performing the trace over the Stinespring degrees of freedom, absorbing the trajectory projection into \mathcal{F} and \mathcal{F}^\dagger directly via

$$\mathcal{V}_{\sigma, r}, \mathcal{V}_{\sigma, r}^\dagger \rightarrow \mathbb{P}_r^{(m_{t, \sigma, r})}, \quad (5.7)$$

which replaces all unitary measurement gates in (5.6) with projectors onto the outcome specified by the trajectory \mathbf{m} in (5.4). The resulting expression for the evolution operator is no longer periodic in time nor unitary. However, this does not complicate the evaluation of the SFF.

Finally, we note that our interest lies in the ensemble- and outcome-averaged SFF,

$$\mathbb{E} \left[\overline{K(t)} \right] = \overline{\mathbb{E} [K(t)]} = \sum_{\mathbf{m}} \overline{K_{\mathbf{m}}(t)}, \quad (5.8)$$

where the two averages can be performed in either order.

The SFF (5.6) for hybrid circuits with unitary measurement gates diagnoses the spectral rigidity of the evolution operator (3.17) along the particular measurement trajectory \mathbf{m} , weighted by the probability $p_{\mathbf{m}}$ (2.18). The outcome- and ensemble-averaged SFF (5.8) reflects spectral rigidity of the evolution averaged over both measurement trajectories and realizations of the evolution operator, which we now consider.

5.3. Ensemble averaging

The diagrammatic method for averaging over the unitary group is detailed in [56], and its application to the SFF is prescribed in [8]. This procedure also generalizes to systems with block structure [11, 12, 38], which generally leads to a finite Thouless time $\tau_{\text{th}} \sim L^z \gg 1$ [12],

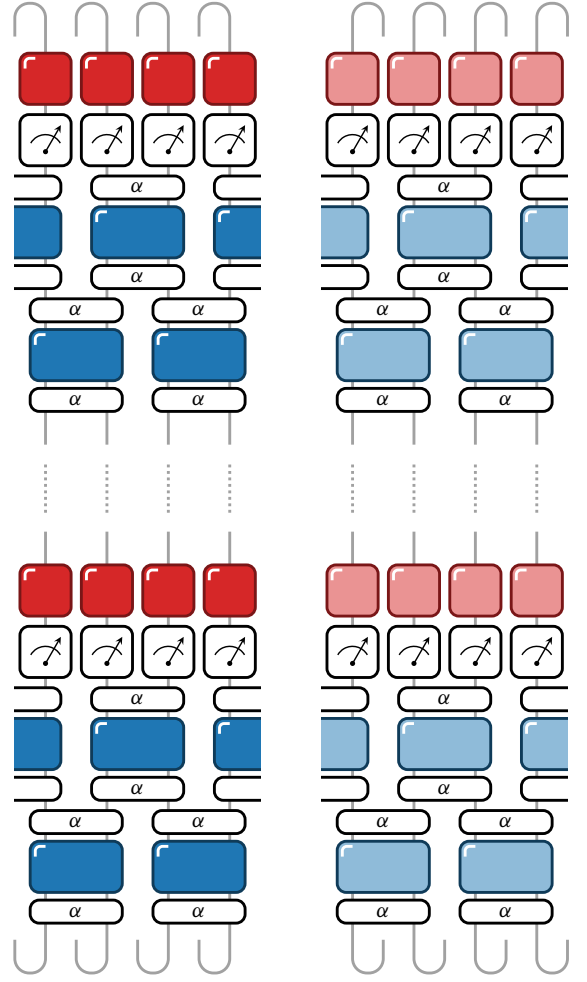


FIG. 6. Diagrammatic depiction of the spectral form factor $K(t)$ (5.1) for a simple circuit corresponding to the Floquet operator depicted in Fig. 4. The trace loop on the left involves the product of t copies of \mathcal{F} , while the trace on the right is a product of t copies of \mathcal{F}^\dagger . The loop on the right has been transposed (rotated by 180°) for convenience of pairing with the loop on the left.

where L is the linear size of the system ($N \sim L^D$). We diagrammatically average over the Haar ensemble prior to contending with the measurement gates.

The Haar-averaging procedure applies only to the unitaries U in the block-structured gates \mathcal{U} (3.12). For block α with n_α states, U is drawn from the unitary group $U(n_\alpha)$ with uniform measure. Calculations for generic circuits realize from a simple limit of the calculation enriched with block structure (there is a single block containing all q^ℓ states, and $\mathbb{P}_r^{(\alpha)} \rightarrow \mathbb{1}_r$). Regarding the various terms in (3.17), we note that the shift operator \mathbb{T} , unitary measurement gates \mathcal{V} , and projectors onto blocks $\mathbb{P}_r^{(\alpha)}$ are not modified by the Haar-averaging procedure, and so we need only introduce placeholders to account for how they are affected by Haar averaging.

In the absence of block structure, the Haar-averaging

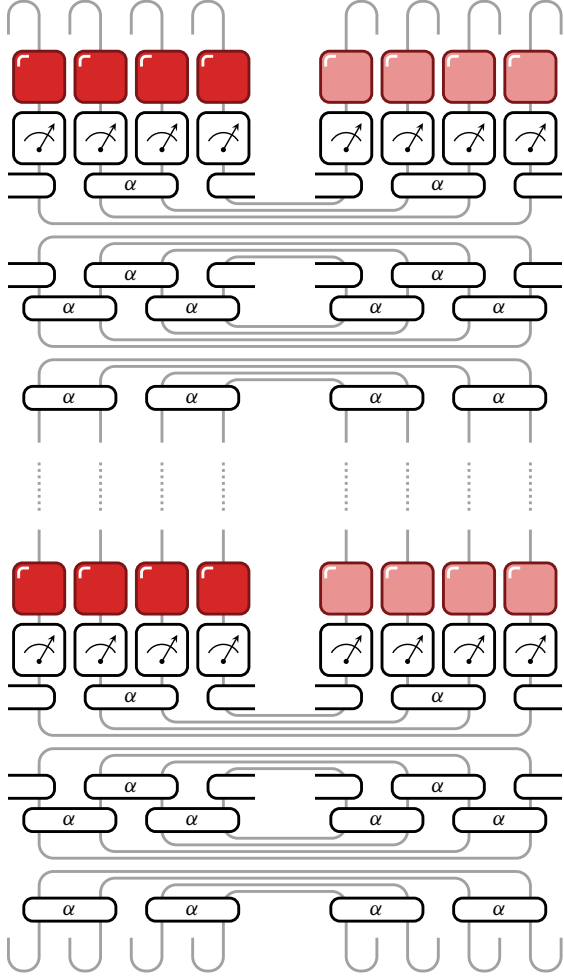


FIG. 7. The SFF circuit diagram pictured in Fig. 6 after implementing the equal-time contractions. Closed loops correspond to traces, and we note that only the physical degrees of freedom are affected by the contractions—all Stinespring registers are affected only through the entangling action of the measurement unitaries \mathcal{V}_j (3.15).

procedure for $K(t)$ involves summing over pairings of each of the t Haar-random unitary gates $U_{s,\lambda,r}$ that appear in \mathcal{F}^t with their counterparts $U_{s,\lambda,r}^*$ in $(\mathcal{F}^*)^t$, for $1 \leq s \leq t$. In practice, we replace $\langle b, \mathbf{0} | \mathcal{F}^{-t} | b, \mathbf{m} \rangle$ with $\langle b, \mathbf{m} | (\mathcal{F}^*)^t | b, \mathbf{0} \rangle^T$, as depicted in Fig. 6. Note that the trace on the right—corresponding to \mathcal{F}^* —has been rotated by 180° compared to the trace on the left.

The SFF is the sum of an exponential number of “diagrams” in which a given gate U in \mathcal{F}^t is contracted with one of its partners U^* in $(\mathcal{F}^*)^t$ [8, 56]. The diagrammatic method assigns weights to each contraction, allowing for a convenient approximation of $K(t)$ (5.1) by the “leading” diagrams [8, 56]. The contractions and their weights are determined by the t -fold Haar channel [54]. The leading-order diagrams are “Gaussian”—essentially, approximating the elements of each unitary gates as random numbers drawn from a Gaussian distribution leads to an

equivalent of Wick’s theorem, and the corresponding diagrams only contain 1-cycles [8, 56]. This approximation is also equivalent to taking the $q \rightarrow \infty$ limit.

Note that each non-Gaussian diagram is suppressed by $q^{-2\ell}$ per “violation” of the Gaussian condition (at most t per site). In general, there are far too many non-Gaussian diagrams to enumerate, let alone evaluate. It is also known that the corrections $\propto q^{-2}$ to the Gaussian approximation do not explain the SFF’s plateau for $t \geq \mathcal{D}$, nor do they predict a nontrivial Thouless time $t_{\text{th}} > 1$ (in the absence of symmetries) [8]. It also appears that the subleading corrections in q^{-2} do not capture any universal features, as indicated by excellent agreement between the calculation of $K(t)$ with $q, N, T \rightarrow \infty$ and numerical simulation for $q = 2, N \sim 12, T \lesssim 100$ in the presence of a U(1) conserved charge [11].

In the presence of block structure, the particular unitary $U_{\lambda,r,\alpha}$ in the gate $\mathcal{U}_{\lambda,r}$ (3.12) is determined by the state upon which $\mathcal{U}_{\lambda,r}$ acts. If the state belongs to the block α , then the unitary $U_{\lambda,r,\alpha}$ is applied. The full expression for $K(t)$ is then a sum over all possible “block trajectories” through the circuit, where a given Haar-random unitary appears at most t times. Note that the Haar average is only nonzero if there are equal numbers of a given Haar-random unitary U_α and its conjugate U_α^\dagger .

For a calculation involving $N \times N$ unitaries U_α and U_α^\dagger , each appearing n times, the diagrammatic weight for any Gaussian diagram is $V_t = N^{-n} + \mathcal{O}(N^{-n-2})$. Because the diagrammatic weights are tracked separately, this does not complicate the evaluation of $K(t)$ in the presence of block structure. The weight associated with a given Gaussian diagram is given by

$$V_{\vec{\alpha}} = \prod_{s=1}^t \prod_{\lambda=1}^{\ell} \prod_{r \in \lambda} \frac{1}{n_{s,\lambda,r}}, \quad (5.9)$$

to leading order, where

$$\vec{\alpha} = \{ \alpha_{s,\lambda,r} \mid 1 \leq s \leq t, 1 \leq \lambda \leq \ell, r \in \lambda \} \quad (5.10)$$

labels all blocks in a given block trajectory, $n_{s,r,\lambda} = \text{tr} [\mathbb{P}_r^{(\alpha_{s,r,\lambda})}]$ is the number of states in the local block labeled $\alpha_{s,r,\lambda}$, and we neglect subleading terms.

A total of t Gaussian diagrams contribute to $K(t)$, one of which is always the equal-time contraction depicted in Fig. 7. All t Gaussian diagrams have the same weight (5.9), and are all equivalent by cyclic invariance of the trace. It is sufficient to evaluate the equal-time contraction, which requires that \mathcal{F}^t and $(\mathcal{F}^*)^t$ realize *identical block trajectories* along the circuit in Fig. 6. To leading order, the SFF (5.1) is a sum over all block trajectories $\alpha = \{ \alpha_{s,\lambda,r} \}$ of t times the diagrammatic weight $V_{\{\alpha\}}$ (5.9) times the equal-time Gaussian contraction of \mathcal{F}^t and $(\mathcal{F}^*)^t$ [11, 12, 38]. The corresponding algebraic expression is a sum of traces over the remaining objects in the circuit after Haar averaging (which includes the measurement unitaries, block projectors that enforce the “block trajectory”, and the temporal shift operators).

Fig. 7 depicts the equal-time contraction for a 1D hybrid circuit with two layers of two-site time evolution gates ($\ell = 2$) followed by a single layer of single-site measurements in each time step. It is straightforward to generalize this picture to arbitrary hybrid Floquet unitaries with any ℓ , D , and number of measurement layers \mathcal{S} per time step. The projectors onto time-evolution blocks—denoted by rectangular boxes labeled α —are constrained by the Haar-averaging procedure to give the same “block trajectory” in both the \mathcal{F} and \mathcal{F}^* traces depicted in Fig. 6. Hence, the block projectors at equal times in each copy correspond to the same block. Because they are idempotent (3.13), the trace loops in Fig. 7 corresponding to consecutive layers of time-evolution gates $\lambda, \lambda + 1$ can be simplified according to $\text{tr} \left[\prod_{r,r'} P_r^2 Q_{r'}^2 \right] = \text{tr} \left[\prod_{r,r'} P_r Q_{r'} \right]$, where P_r and $Q_{r'}$ are placeholders for the projectors in the top and bottom layer of each such loop.

With ℓ time-evolution layers λ per time step s (3.8), we label the layer s, λ as $\varsigma = \ell s + \lambda$. The SFF is then

$$\overline{K_{\mathbf{m}}(t)} = t \sum_{\vec{\alpha}} V_{\vec{\alpha}} \prod_{\varsigma=1}^{\ell t} \text{tr} \left[\mathbb{P}_{\varsigma, \vec{m}_{\varsigma}}^{\dagger} \mathbb{P}_{\varsigma, \vec{m}_{\varsigma}} \right], \quad (5.11)$$

where $V_{\vec{\alpha}}$ is the diagrammatic weight (5.9), and the projectors above are defined by the time-ordered products

$$\mathbb{P}_{\varsigma; \vec{m}_{\varsigma}} = \mathbb{P}^{(\alpha_{\varsigma+1})} \left[\prod_{\sigma \in (\varsigma, \varsigma+1)} \mathbb{P}^{(m_{s, \sigma})} \right] \mathbb{P}^{(\alpha_{\varsigma})} \quad (5.12a)$$

$$\mathbb{P}_{\varsigma; \vec{m}_{\varsigma}}^{\dagger} = \mathbb{P}^{(\alpha_{\varsigma})} \left[\prod_{\sigma \in (\varsigma, \varsigma+1)} \mathbb{P}^{(m_{s, \sigma})} \right]^T \mathbb{P}^{(\alpha_{\varsigma+1})}, \quad (5.12b)$$

where the individual projectors above act on \mathcal{H}_{ph} as either

$$\mathbb{P}^{(\alpha_{\varsigma})} = \bigotimes_{r \in \lambda} \mathbb{P}_r^{(\alpha_{s, \lambda, r})} \quad (5.13a)$$

$$\mathbb{P}^{(m_{s, \sigma})} = \bigotimes_{r \in \sigma} \mathbb{P}_r^{(m_{s, \sigma, r})}. \quad (5.13b)$$

The middle term in (5.12a) results from projecting the measurement unitaries between time-evolution layers ς and $\varsigma + 1$ onto the outcomes $\vec{m}_{\varsigma} \subset \mathbf{m}$. The projector (5.12a) reflects both the block and outcome trajectories indicated in (5.11). The projector (5.12b) appears in reverse time order due to transposition. Note that if ς corresponds to the final evolution layer $\lambda = \ell$ in time step s , then $\varsigma + 1$ is the first evolution layer $\lambda = 1$ in time step $s + 1$; for the final trace loop with $\varsigma = \ell t$, $\varsigma + 1$ corresponds to the first layer $\lambda = 1$ of time step $s = 1$.

Fig. 7 depicts the trace loops arising from the equal-time contraction for a 1D hybrid circuit with $\ell = 2$ layers of two-site time-evolution gates (3.12) followed by a round of single-site measurements in each time step. There are two types of trace loops corresponding to $\varsigma = s, 1$ and $\varsigma = s, 2$. In the former case, the trace loop in (5.11) involves the time-evolution layers $s, 1$ and $s, 2$ in the same

time step s , with no intervening measurements; in the latter case, the trace loop contains the measurements that occur between time-evolution layers $s, 2$ and $s + 1, 1$. In general, we allow for arbitrary numbers of measurement rounds between time-evolution layers λ .

We now evaluate the Haar-averaged spectral form factor $\overline{K_{\mathbf{m}}(t)}$ (5.11) for the measurement trajectory \mathbf{m} for physically relevant implementations of the hybrid circuit.

5.4. Generic circuits

The evaluation of (5.11) for hybrid circuits with generic time evolution (i.e., no block structure) is straightforward. The important simplifications to the equations in Sec. 5.3 follow from replacing the block projectors (3.12) according to $\mathbb{P}_r^{(\alpha)} \rightarrow \mathbb{1}_r$, so that the single “block” contains all q^{ℓ} states. There is only one “block trajectory” in (5.11), with weight $V = q^{-\ell N t}$ (5.9). We have

$$\overline{K_{\mathbf{m}}(t)} = t \prod_{\varsigma=1}^{\ell t} \frac{1}{q^N} \text{tr} \left[\mathbb{P}_{\varsigma, \vec{m}_{\varsigma}}^{\dagger} \mathbb{P}_{\varsigma, \vec{m}_{\varsigma}} \right], \quad (5.14)$$

where the projectors in (5.12) simplify to

$$\mathbb{P}_{\varsigma, \vec{m}_{\varsigma}}^{\dagger} \mathbb{P}_{\varsigma, \vec{m}_{\varsigma}} = \prod_{\sigma=\sigma_{\varsigma}}^{\sigma_1} \mathbb{P}^{(m_{s, \sigma})} \prod_{\sigma'=\sigma_1}^{\sigma_{\mathcal{S}}} \mathbb{P}^{(m_{s, \sigma'})}, \quad (5.15)$$

and using idempotency (2.3), the middle two copies of $\mathbb{P}^{(m_{s, \sigma})}$ become a single $\mathbb{P}^{(m_{s, \sigma})}$. Summing $\mathbb{P}^{(m_{s, \sigma})}$ over outcomes m_{s, σ_1} resolves the identity by completeness (2.4), removing this measurement layer from (5.15). We then repeat this procedure for the two copies of $\mathbb{P}^{(m_{s, \sigma+1})}$ in the middle of the product (5.15), and so on. Summing (5.15) over all measurement trajectories resolves the identity, so that (5.14) becomes

$$\begin{aligned} \mathbb{E} \left[\overline{K(t)} \right] &= \sum_{\mathbf{m}} \overline{K_{\mathbf{m}}(t)} = t \prod_{\varsigma=1}^{\ell t} \frac{1}{q^N} \sum_{\vec{m}_{\varsigma}} \text{tr} \left[\mathbb{P}_{\varsigma, \vec{m}_{\varsigma}} \right] \\ &= t \prod_{\varsigma=1}^{\ell t} \frac{1}{q^N} \text{tr} [\mathbb{1}] = K_{\text{CUE}}(t) = t, \end{aligned} \quad (5.16)$$

which is identical to the SFF for time evolution alone [8], which corresponds to the RMT prediction for unitary gates of any size drawn from the CUE [8, 56]. Therefore, on average, measurements have no effect on spectral properties in generic chaotic models.

5.5. Charge measurements

We now evaluate (5.11) for hybrid circuits in which the projectors onto dynamical blocks (3.12) and measurement outcomes (2.2) commute. This corresponds to measuring operators in the charge (or computational) basis, which we

take to be the Weyl Z basis, without loss of generality. We again consider the projectors in (5.11), which correspond to closed loops in the diagram in Fig. 7.

Importantly, because the projectors in (5.12) mutually commute, we can write them in any order. Using idempotency of the projectors, we then write

$$\mathbb{P}_{\varsigma, \vec{m}_\varsigma}^\dagger \mathbb{P}_{\varsigma, \vec{m}_\varsigma} = \mathbb{P}^{(\alpha_{\varsigma+1})} \left[\prod_{\sigma=\sigma_1}^{\sigma_S} \mathbb{P}^{(m_{s,\sigma})} \right] \mathbb{P}^{(\alpha_\varsigma)}, \quad (5.17)$$

and the trace of this quantity can be written as

$$\langle a'_{\varsigma+1} | m_{s,\sigma_S} \rangle \langle m_{s,\sigma_S} | \cdots | m_{s,\sigma_1} \rangle \langle m_{s,\sigma_1} | a_\varsigma \rangle, \quad (5.18)$$

so that each $|m\rangle\langle m|$ term appears exactly once in the SFF (5.11). Summing over measurement outcomes gives $\sum_m |m\rangle\langle m| = \mathbb{1}$ by completeness of the measurement projectors (2.4). Averaged over outcomes, (5.18) reduces to $\langle a'_{\varsigma+1} | a_\varsigma \rangle$, which is exactly the same result that obtains in the absence of measurements [11, 12].

For concreteness, the above allows us to write

$$\mathbb{E} \left[\overline{K(t)} \right] = t \text{tr} [\mathcal{T}^t], \quad (5.19)$$

i.e., t times the [physical] trace of the t th power of the time-evolution *transfer matrix* for a single period,

$$\mathcal{T} \equiv \prod_{\lambda=1}^{\ell} \mathcal{T}_\lambda = \prod_{\lambda=1}^{\ell} \bigotimes_{r \in \lambda} T_{\lambda,r}, \quad (5.20)$$

where the individual gates are given by

$$T_{\lambda,r} \equiv \sum_{\alpha} \frac{1}{n_\alpha} \sum_{a,b \in \alpha} |a\rangle\langle b|_r, \quad (5.21)$$

which is identical to the superoperator gate T responsible for the time evolution of operators (4.18), where the q^ℓ diagonal operators $\pi^{a/b}$ have been replaced by the q^ℓ states $|a/b\rangle$ in (5.21) [11, 12].

Along some measurement trajectory \mathbf{m} we have

$$\overline{K_{\mathbf{m}}(t)} = t \text{tr} \left[\prod_{\varsigma} \prod_{r \in \varsigma} T_{\varsigma,r,\mathbf{m}} \right], \quad (5.22)$$

where $T_{\varsigma,r,\mathbf{m}}$ is simply the time-evolution gate (5.21) if ς corresponds to the time-evolution layer s, λ , and $T_{\varsigma,r,\mathbf{m}} = \mathbb{P}_r^{(m_{\varsigma,r})}$ if the layer ς corresponds to the measurement layer s, σ (where s indexes the time step). However, summing over measurement outcomes replaces the latter with the identity. Hence, we conclude that measuring charge-basis operators has no effect on spectral rigidity, on average, as probed by the spectral form factor (5.1).

6. WHAT IS A PHASE OF MATTER?

In Sec. 4 we considered probes of phase structure and universality of the generic form (4.1), including all “standard” probes of condensed matter, AMO, and other many-body quantum systems. These quantities have the specific

property that they require only one copy of the system (or density matrix ρ) and are immune to shot-to-shot variations in the fidelity of the time-evolution gates and outcomes of circuit measurements. In Sec. 5 we considered the spectral form factor $K(t)$ (5.6)—a standard analytical probe of spectral rigidity commonly used to identify quantum chaos [8, 11, 12, 32–35]. While not experimentally viable as a probe, the SFF has a close relation to two-point correlation functions of the form (4.1) as noted in [12, 34] and made explicit in App. D.1.

None of these “standard” probes show a *transition* as a function of measurement rate γ (e.g., no discontinuity or other “sharp” feature as γ is tuned through a critical value γ_c). Far from showing any such feature, the hybrid protocols relevant to the literature are independent of γ , on average. In fact, the blindness of the aforementioned quantities to the effects of measurement was reported in [13] for generic circuits without block structure. This point was also claimed but not proven in [23] in the context of charge-conserving circuits. Additionally, while the effects of measurements may be observed along particular trajectories \mathbf{n} , there are no meaningful predictions to be made, as discussed in Sec. 2.4.

However, two classes of quantities have been reported in the literature to show a sharp transition at some critical γ_c [19]: measures of entanglement [13–18, 23–25, 40–42] and variances of two-point functions [23–25]. We refer the reader to the literature for further details of these quantities, as we do not consider their technical details. Instead, we now explain why these probes cannot differentiate distinct phases of matter in any conventional sense of the term. This follows from the need for postselection in evaluating these quantities experimentally, which is incompatible with the notion of phase structure for separate practical and conceptual reasons, which we now discuss.

The first, *practical* issue is widely known [19]: These quantities are impossible to measure using independent experimental “shots” performed on an individual sample. Instead, one must coherently interfere the outcomes of multiple independent experiments, or else prepare multiple, identical copies of the system, subject them to identical hybrid-circuit protocols, and ensure that they realize identical outcomes for *all* measurements in the protocol. This requires (i) an unknown level of precision in the application of time-evolution gates and (ii) postselection of measurement outcomes. The second of these requires a number of experimental shots that is exponential in the spacetime volume; in the thermodynamic limit where $N, T \rightarrow \infty$, the number of shots diverges rapidly. This is the well known “postselection problem” [19].

Consider a D -dimensional system with $N \sim L^D$ q -state qudits, measurement rate γ , and maximum circuit depth T per shot. In the thermodynamic limit—the only regime in which phases of matter are well defined—both N and T diverge. Evaluation of a postselected quantity in the thermodynamic limit would require $q^{\gamma N T}$ shots, on average, and is thus experimentally impossible. We also rule out quantum state tomography as a viable practical

probe for the same reasons [19].

We now point out a *conceptual* problem, which does not appear to be widely recognized in the literature, and which persists *even if the practical postselection issue is remedied*, as far as we are aware. To illustrate this, suppose that we knew the “entanglement phase” of a particular sample (i.e., a particular hybrid circuit protocol and many-body state of the system whose entanglement entropy has known area- or volume-law scaling). Is this sufficient to consider the measurement-induced area-law entangled phase a genuine phase of matter?

By definition, knowing the phase to which a sample belongs must furnish predictions about its observable properties. Moreover, this behavior must be detectable (i) using experimentally measurable quantities, (ii) in finite time, (iii) by performing experiments on that sample alone, and (iv) in a manner that is insensitive to microscopic detail and certain classes of perturbations. The quantities (4.1) considered in Sec. 4 all satisfy these conditions, as do all phases of matter of which we are aware. The first condition (i) ensures that the phase is actually detectable; the second (ii) ensures that it is detectable in practice; the third (iii) stems from the requirement that the definition of a phase of matter be *useful* (in that it offers predictions for individual samples); and the fourth (iv) ensures that the phase is robust to fine-tuning and microscopic details of the sample.

A key distinction between genuine phases of matter (as constrained above) and properties of particular quantum states follows from the notion of dynamical stability. While numerous phases of matter can be distinguished using a single measurement (e.g., a ferromagnet can be detected by measuring the magnetization, a spin liquid is diagnosed via nonlinear spectroscopy [59], and numerous electronic phases are characterized via resistivity), other conventional phases may require multiple measurements (and statistics) to distinguish. A useful example is the *spin glass* phase [60, 61], whose long-range order is diagnosed, e.g., by measuring autocorrelation functions. Importantly, this long-range order is a property of the entire spin glass *phase*, and is not sensitive to the exact microscopic state of the system (i.e., generic states within the phase give equivalent predictions). Thus, it is possible to perform the multiple measurements required to diagnose spin-glass order on a single sample using independent shots, without worrying whether disturbances to the state due to measurements spoil the order. In contrast, properties of particular states of the system are highly sensitive to such disturbances, and do not admit robust diagnostics as described above. For example, in diagnosing the entanglement of a quantum state—even using ancilla probes—after making the first probe measurement, one must then prepare an *identical* many-body quantum state before performing the next one. Hence, the need for multiple measurements on a *single* sample is acceptable in a diagnostic of phase structure; the need for a large number of macroscopic samples in identical quantum many-body states is not.

We now briefly remark on several proposals for mitigating the postselection problem. For example, the ancilla probe of [40] parametrically reduces the number of measurements that require postselection; however, the measurement outcomes within the light cone emanating from the ancilla qubit must be postselected, meaning that the number of shots remains exponentially divergent in the thermodynamic limit. Likewise, the ancilla probe of [23] only reduces the measurement overhead per shot, which was hardly the limiting practical issue to begin with. The dual-unitary protocol of [62] is fine tuned, purely theoretical, and still requires postselection of measurements on the spacetime boundary—it is not clear to what extent any advantage could be realized in an experiment [19]. Additionally, proposals that require concurrent classical simulations with the same measurement outcomes also fail to remedy the practical and conceptual issues (e.g., the recent experiment [41] using the ancilla probe of [40]).

However, a recent cross-entropy diagnostic [42] using concurrent classical simulations successfully resolves the practical issue—and partially remedies the conceptual issues—that afflict other measures of entanglement entropy. Importantly, the cross-entropy probe [42] does *not* require postselection: the classical Clifford simulation uses a different initial state and allows for arbitrary measurement outcomes. Accordingly, the computational cost scales polynomially—rather than exponentially—in N , which can, in principle, be scaled to the thermodynamic limit. However, the cross-entropy protocol only works for Clifford circuits, and to the best of our knowledge does not survive generic perturbations, so fails our criterion (iv) for a genuine phase of matter.

We also distinguish between phases of matter and, e.g., computational complexity classes [63]. Knowledge of a system’s phase of matter allows for predictions about observable outcomes of experiments on that system; knowledge of a problem’s computational complexity class allows for predictions about whether a given instantiation of the problem can be solved in a certain amount of time. The “learnability transition” of [43] is of the latter type. In particular, knowledge of the learnability class of the problem predicts *whether* a classifier external to the system can determine the system’s total charge after some number of measurements. Thus, “learnability” is a property of the classifier that reflects computational complexity; *a priori*, it does not afford any predictions about the observable properties of the system accessible using a single sample. Although the learnability probe does not require postselection—and thereby avoids any practical issue—the learnability transition [43] does not imply a transition between distinct phases of matter.

7. ADAPTIVE PROTOCOLS

Having ruled out genuine measurement-induced phases of matter in large swaths of systems, we now consider the remaining class of candidates. Essentially, the n -point

functions (4.1) considered in Sec. 4 and the SFF (5.1) considered in Sec. 5 fail to show nontrivial effects due to measurements because the outcomes are discarded. As discussed, such protocols are tantamount to allowing the bath to “measure” the system, giving the same result as ensemble-averaged chaotic time evolution alone—the maximally mixed state. Introducing block structure does not modify this picture, but merely introduces the possibility of using measurements to undo the block structure itself. We then ruled out postselected probes and the possibility of genuine, measurement-induced phases of matter in random nonadaptive hybrid circuits.

The leading—and ostensibly *only*—possibility remaining is the use of *adaptive* hybrid protocols (see, e.g., [44–46]), which utilize the outcomes of circuit measurements in the *same* experimental shot via active feedback, avoiding the issues associated with postselection while also potentially realizing nontrivial effects due to measurements. The key feature of adaptive circuits is that the gates at time t may be conditioned on the outcomes of measurements made at prior times $s < t$. It is known from [21] that such adaptive gates are crucial to quantum error correction: In the context of quantum teleportation, e.g., the state is only transferred once the error-correction gate is applied; prior to that, the target qubit’s state is simply the maximally mixed state [21].

We now consider quantities of the form (4.1) evaluated in hybrid circuits with adaptive gates (i.e., the error-correction gates in various measurement-based quantum codes [21]). An adaptive gate at time t is defined in terms of the outcomes \vec{n} of measurements made at time t_m as

$$\mathcal{R}_{t;t_m} = \sum_{\vec{n}} U_{t;t_m,\vec{n}} \otimes \tilde{\mathbb{P}}_{ss,s,\sigma}^{(\vec{n})}, \quad (7.1)$$

where t_m encodes the time step (and layer) of the corresponding measurement gate, U is some unitary gate acting on the physical system, and $\tilde{\mathbb{P}}_{ss,t_m}^{(\vec{n})}$ projects onto outcomes \vec{n} in the Stinespring slice t_m of the spacetime lattice. Note that the adaptive gates cannot change the measurement’s outcome (precluding \tilde{X} operators); this leaves linear combinations of projectors, generically captured by (7.1). We then consider order parameters

$$\begin{aligned} \langle \mathcal{O}(t) \rangle &\equiv \mathbb{E} \left[\overline{\langle \psi(t) | \mathcal{O} | \psi(t) \rangle} \right] \\ &= \mathbb{E} \left[\langle \psi_0 | \overline{\mathcal{W}^\dagger(t,0) \mathcal{O} \mathcal{W}(t,0)} | \psi_0 \rangle \right], \end{aligned} \quad (7.2)$$

that vanish under time-evolution alone and in nonadaptive hybrid circuits (as demonstrated in Sec. 4). Thus, $\langle \mathcal{O}(t) \rangle \neq 0$ probes order that is unique to adaptive protocols under maximally chaotic time evolution.

7.1. Generic adaptive protocols

We first consider the evaluation of generic quantities of the form (4.1) in hybrid circuits not enriched with block

structure. It is sufficient to consider either the evolution of states in the Schrödinger picture or operators in the Heisenberg picture. We assume that the time-evolution operator in (7.2) is of the form

$$\mathcal{W}(t,0) = \mathcal{R}_{t;t_m} \mathcal{W}(t,t_m) \mathcal{V}_{[t_m]} \mathcal{W}(t_m,0), \quad (7.3)$$

where t_m is the time at which the measurement layer \mathcal{V} is applied, the $\mathcal{W}(\cdot)$ operators denote an arbitrary combination of time-evolution and measurement gates, both represented unitarily on \mathcal{H}_{dil} . Note that other measurement layers in the \mathcal{W} channels do not affect the adaptive aspect of the protocol above.

We now consider evolving a physical observable \mathcal{O} in the Heisenberg picture under (7.3), where \mathcal{O} acts as $\mathbb{1}$ on all Stinespring registers. Essentially, we absorb the time evolution of the state $|\psi(t)\rangle$ in (7.2) into the observable \mathcal{O} step by step (in reverse order), starting with

$$\begin{aligned} \mathcal{O}' &= \mathcal{R}_{t;t_m}^\dagger \mathcal{O} \mathcal{R}_{t;t_m} \\ &= \sum_{\vec{n}} U_{t,t_m,\vec{n}}^\dagger \mathcal{O} U_{t,t_m,\vec{n}} \otimes \tilde{\mathbb{P}}_{ss,t_m}^{(\vec{n})}, \end{aligned} \quad (7.4)$$

where \vec{n} gives the outcomes of all measurements performed at time t_m , which act on the subsystem Ω of physical sites.

We next conjugate by $\mathcal{W}(t,t_m)$. However, averaging the gates in $\mathcal{W}(t,t_m)$ over the Haar ensemble (assuming that the first layer corresponds to time evolution) gives

$$\begin{aligned} \mathcal{O}'' &= \overline{\mathcal{W}^\dagger(t,t_m) \mathcal{R}_{t;t_m}^\dagger \mathcal{O} \mathcal{R}_{t;t_m} \mathcal{W}(t,t_m)} \\ &= \frac{1}{\mathcal{D}_{\text{ph}}} \sum_{\vec{n}} \text{tr} \left[U_{\vec{n}}^\dagger \mathcal{O} U_{\vec{n}} \right] \mathbb{1}_{\text{ph}} \otimes \tilde{\mathbb{P}}_{ss,t_m}^{(\vec{n})} \\ &= \frac{1}{\mathcal{D}_{\text{ph}}} \text{tr} [\mathcal{O}] \mathbb{1}_{\text{dil}}, \end{aligned} \quad (7.5)$$

which is identical to the expression that recovers under $\mathcal{W}(t,t_m)$ alone (without the adaptive gate $\mathcal{R}_{t;t_m}$). We refer to protocols in which generic time evolution occurs between a circuit measurement and the adaptive gate using that outcome as *trivially adaptive*, as they are indistinguishable from nonadaptive protocols.

The triviality of (7.5) is transparent in the Schrödinger picture for $\varrho(t)$. Because $\mathcal{W}(t,t_m) \varrho(t_m) \mathcal{W}^\dagger(t,t_m)$ produces the maximally mixed state $\rho_{\text{ph}}(t) = \rho_\infty \propto \mathbb{1}_{\text{ph}}$ upon averaging, the unitary gate U in \mathcal{R} (7.1) acts trivially on ρ_∞ . Hence, all quantities (4.1) are trivial even in *adaptive* hybrid protocols, when *any amount* of generic time evolution [5–7, 13] is permitted between the circuit measurement gate \mathcal{V} , associated adaptive gate \mathcal{R} , and probe measurement \mathcal{O} .

Now, suppose that the adaptive gate \mathcal{R} (7.1) is applied *immediately* following the corresponding measurement gate \mathcal{V} , so that (7.3) instead takes the form

$$\mathcal{W}(t,0) = \mathcal{R}_{t;t_m} \mathcal{V}_{[t_m]} \mathcal{W}(t_m,0), \quad (7.6)$$

and the observable \mathcal{O} is measured immediately after application of $\mathcal{W}(t, 0)$ (7.6), all without intervening time-evolution gates. In this case, (7.5) becomes

$$\begin{aligned}\mathcal{O}'' &= \mathcal{V}_{[t_m]}^\dagger \mathcal{R}_{t;t_m}^\dagger \mathcal{O} \mathcal{R}_{t;t_m} \mathcal{V}_{[t_m]} \\ &= \sum_{\vec{\ell}, \vec{m}, \vec{n}} \mathbb{P}_\Omega^{(\vec{\ell})} U_{t_m, \vec{m}}^\dagger \mathcal{O} U_{t_m, \vec{m}} \mathbb{P}_\Omega^{(\vec{n})} \otimes X_{t_m}^{-\vec{\ell}} \tilde{\mathbb{P}}_{t_m}^{(\vec{n})} X_{t_m}^{\vec{n}},\end{aligned}$$

and we note that no gates prior to the time t_m when \mathcal{V} is applied⁴ can alter the Stinespring register t_m , as this would violate causality (the measurement has not occurred prior to time t_m). Hence, we simply evaluate the Stinespring operator in the initial state $|0\rangle$, so that

$$\mathcal{O}'' = \sum_{\vec{n}} \mathbb{P}_\Omega^{(\vec{n})} U_{t_m, \vec{n}}^\dagger \mathcal{O} U_{t_m, \vec{n}} \mathbb{P}_\Omega^{(\vec{n})}, \quad (7.7)$$

and lastly, we apply the remaining channel $\mathcal{W}(t_m, 0)$ (7.6) (which contains generic time-evolution and nonadaptive or trivially adaptive measurements, and is equivalent to Haar-random time evolution alone as seen in Sec. 4).

Hence, the order parameter (7.2) can be expressed in terms of \mathcal{O}'' (7.7) according to

$$\begin{aligned}\langle \mathcal{O}(t) \rangle &= \mathbb{E} \left[\text{tr}_{\text{ph}} \left[\rho_0 \overline{\mathcal{W}^\dagger(t, 0) \mathcal{O} \mathcal{W}(t, 0)} \right] \right] \\ &= \text{tr}_{\text{ph}} \left[\rho_0 \overline{\mathcal{W}^\dagger(t_m, 0) \mathcal{O}'' \mathcal{W}(t_m, 0)} \right],\end{aligned} \quad (7.8)$$

and because $\mathcal{W}(t_m, 0)$ is equivalent, on average, to Haar-averaged time evolution alone, we find that

$$\begin{aligned}\langle \mathcal{O}(t) \rangle &= \frac{1}{q^N} \text{tr} \left[\rho_0 \mathbb{1}_{\text{ph}} \right] \text{tr} [\mathcal{O}'''] \\ &= \frac{1}{q^N} \sum_{\vec{n}} \text{tr}_{\text{ph}} \left[\mathbb{P}_\Omega^{(\vec{n})} U_{t_m, \vec{n}}^\dagger \mathcal{O} U_{t_m, \vec{n}} \right],\end{aligned} \quad (7.9)$$

which vanishes—as it would in *any* generic, nonadaptive (or trivially adaptive) protocol—unless the operator inside the trace has nonzero overlap with $\mathbb{1}_{\text{ph}}$.

For concreteness, consider a system of qubits (i.e., $q = 2$), and take the $\mathcal{O} = Z_j$ in (7.2) for some site j . Ordinarily, the Haar-averaged expectation value is $\langle Z_j(t) \rangle = \text{tr}[Z_j] = 0$, and likewise for any nontrivial correlation functions (4.1). Suppose that the adaptive gate (7.1) is conditioned on the measurement of Z_j in layer t_m , and the adaptive unitary U_m acts at time $t > t_m$ as $\mathbb{1}_j$ if the outcome was $m = 0$ (the default) and as X_j if the outcome was $m = 1$. Then (7.7) becomes

$$\begin{aligned}Z_j'' &= \mathbb{P}_j^{(+)} \mathbb{1}_j Z_j \mathbb{1}_j \mathbb{P}_j^{(+)} + \mathbb{P}_j^{(-)} X_j Z_j X_j \mathbb{P}_j^{(-)} \\ &= \sum_{\pm} \pm \mathbb{P}_j^{(\pm)} Z_j \mathbb{P}_j^{(\pm)} = \mathbb{1}_j,\end{aligned} \quad (7.10)$$

⁴ The gates “prior to time t_m ” act at times $t < t_m$ in the Schrödinger picture, and act “later” in the Heisenberg picture.

so that $\langle Z_j(t) \rangle = \langle Z_j'' \rangle_\infty = 1$ is nontrivial. This follows straightforwardly from the adaptive protocol: We measure Z_j and if the outcome is 1, we apply X_j to flip the spin to 0, so that the expectation value of Z_j following the adaptive gate is always +1. However, we note that *any* generic chaotic time evolution between the circuit measurements, adaptive gates based on their outcomes, or evaluation of the probe observable Z_j trivializes the order parameter.

For generic $q \geq 2$ and allowing for arbitrary order parameters \mathcal{O} (7.2), the possible adaptive protocols with nontrivial order parameters are similar in spirit to the qubit example above. We require that $\text{tr}[\mathcal{O}] = 0$, so that the order parameter vanishes in all nonadaptive protocols. We also note that (7.9) vanishes if the unitary gates in (7.1) for a given outcome set \vec{n} commute with *either* the order parameter \mathcal{O} or the projectors onto \vec{n} for all \vec{n} (otherwise the adaptive gates are trivial). However, further restriction is not possible in generality. In fact, allowing the circuit observables, adaptive gates, and probe observable \mathcal{O} to realize arbitrary superpositions of mutually noncommuting operators is still compatible with nonzero (7.9). On the other hand, for a given choice of bases for these three components, one can always deform (7.9) smoothly to zero by rotating the basis of any one of these terms. Although there exist many “order parameters” (7.2) for which $\langle \mathcal{O}(t) \rangle = 0$ in the absence (nontrivial) adaptive gates, while $\langle \mathcal{O}(t) \rangle \neq 0$ (7.9) in adaptive protocols, their lack of robustness to intervening chaotic time evolution or smooth changes of basis preclude any such \mathcal{O} from distinguishing genuine phases of matter.

7.2. Enriched adaptive protocols

We now consider adaptive protocols in circuits enriched with block structure. In contrast to generic circuits, the Haar-averaged dynamics of enriched circuits preserve operators other than the identity. Although we focus on symmetries, the same principles apply to models enriched by kinetic constraints or topology by identifying the nontrivial operators preserved by chaotic dynamics. We allow for enriched time evolution between the circuit measurements, adaptive gates, and order parameter measurement (otherwise, the result of Sec. 7.1 applies, ruling out a genuine measurement-induced phase of matter).

We consider examples that conserve (*i*) a discrete \mathbb{Z}_2 Ising symmetry corresponding to charge conjugation, (*ii*) a discrete, twofold $\mathbb{Z}_2 \times \mathbb{Z}_2$ symmetry corresponding to the Affleck-Kennedy-Lieb-Tasaki (AKLT) state [64] in the Haldane phase [65–67], and (*iii*) a continuous $U(1)$ symmetry corresponding to charge conservation. For convenience, we restrict to 1D chains of qubits ($q = 2$) with symmetries represented in the Pauli Z basis.

We investigate order parameters given by (7.2), where

\mathcal{O} can always be written as a sum of Pauli strings,

$$\mathcal{O} \equiv \sum_{\vec{\mu}} C_{\vec{\mu}} \bigotimes_{j=1}^N \sigma_j^{\mu_j}, \quad (7.11)$$

where $\sigma_j^0 = \mathbb{1}_j$, and we proceed in analogy to Sec. 4.7.

Evolution to time t in (7.2) is realized by the channel

$$\mathcal{W}(t, 0) = \mathcal{W}(t, t') \mathcal{R}_{t'; t_m} \mathcal{W}(t', t_m) \mathcal{V}_{[t_m]} \mathcal{W}(t_m, 0), \quad (7.12)$$

acting on \mathcal{H}_{dil} , in analogy to (7.3). We assume that each \mathcal{W} channel contains at least one full time step of enriched Haar-random evolution (i.e., that the layers tile the system), and allow for nonadaptive (or trivially adaptive) measurements as in Sec. 7.1 (shown in Sec. 4 to have no effect). As before, we absorb the dilated channels into $\mathcal{O}(t) = \mathcal{W}^\dagger(t, 0) \mathcal{O} \mathcal{W}(t, 0)$ layer by layer, averaging the gates in all blocks over the Haar ensemble.

\mathbb{Z}_2 Ising symmetry.— Suppose that the system has a \mathbb{Z}_2 Ising symmetry given by

$$\mathcal{G} \equiv \prod_j Z_j, \quad (7.13)$$

which corresponds to charge conjugation or fermion parity. Starting from an observable of the form (7.11), we now conjugate by the channel $\mathcal{W}(t, t')$ (7.12).

Following Sec. 4.7, the update rule for operators is

$$\overline{\mathcal{O}_{i,j}(t')} = \overline{C_{0,0}^{(t)}} \mathbb{1}_{i,j} + \overline{C_{3,3}^{(t)}} Z_i Z_j, \quad (7.14)$$

so that only the trivial operator $\mathbb{1}_{i,j}$ and local symmetry generator $\mathcal{G}_{i,j} = Z_i Z_j$ survive the Haar-averaged, \mathbb{Z}_2 -symmetric evolution of sites i and j . The equivalent Schrödinger update for ρ_{ij} is given by (4.30).

Importantly, we demand that $\mathcal{W}(t, t')$ contain a full time step of Haar-averaged time evolution, so that each site j is the left and right site of at least one two-site gate (see Fig. 2). However, as a consequence, the only terms in \mathcal{O} (7.11) that survive a full time step correspond to the global identity and global symmetry generator (7.13). Hence, the only meaningful terms in the observable \mathcal{O} are

$$\mathcal{O} = \overline{\mathcal{O}'} = C_{\vec{0}} \mathbb{1}_{\text{ph}} + C_{\vec{3}} \mathcal{G}, \quad (7.15)$$

where $\mathcal{G} = \prod_j Z_j$ (7.13). Any other terms in (7.11) are trivialized by ensemble-averaged time evolution.

The next step involves conjugating \mathcal{O}' (7.15) by the adaptive layer \mathcal{R} in (7.12). This term acts trivially on the $C_{\vec{0}}$ term in \mathcal{O}' (7.15), and the result is

$$\begin{aligned} \mathcal{O}'' &\equiv \mathcal{R}_{t;t_m}^\dagger \overline{\mathcal{W}^\dagger(t, t') \mathcal{O} \otimes \widetilde{\mathbb{1}} \mathcal{W}(t, t')} \mathcal{R}_{t;t_m} \\ &= C_{\vec{0}} \mathbb{1} \otimes \widetilde{\mathbb{1}} + C_{\vec{3}} \sum_{\vec{n}} U_{\vec{n}}^\dagger \mathcal{G} U_{\vec{n}} \otimes \widetilde{\mathbb{P}}_{t_m}^{(\vec{n})}, \end{aligned} \quad (7.16)$$

and we note that (i) the order parameter (7.2) cannot depend only on $C_{\vec{0}}$, which trivially corresponds to $\mathcal{O} = \mathbb{1}$

(7.11)), so we set $C_{\vec{0}} = 0$ without loss of generality; (ii) the next step $\mathcal{W}(t', t_m)$ in the evolution (7.12) consists of a full step of time evolution, so that only $\mathbb{1}$ and \mathcal{G} (7.13) survive; and (iii) the gates $U_{\vec{n}}$ cannot convert \mathcal{G} to $\mathbb{1}$, so they must leave \mathcal{G} intact, up to some factor. Without further loss of generality, we assume that

$$\mathcal{G} U_{\vec{n}} = \eta_{\vec{n}} U_{\vec{n}} \mathcal{G} + \dots, \quad (7.17)$$

where the \dots terms are all annihilated by averaging $\mathcal{W}(t', t_m)$ over the Haar ensemble. We next have

$$\begin{aligned} \mathcal{O}''' &\equiv \overline{\mathcal{W}^\dagger(t', t_m) \mathcal{O}'' \mathcal{W}(t', t_m)} \\ &= C_{\vec{0}} \mathbb{1} \otimes \widetilde{\mathbb{1}} + C_{\vec{3}} \sum_{\vec{n}} \eta_{\vec{n}} \mathcal{G} \otimes \widetilde{\mathbb{P}}_{\text{ss}}^{(\vec{n})} \\ &\rightarrow C_{\vec{3}} \mathcal{G} \otimes \sum_{\vec{n}} \eta_{\vec{n}} \widetilde{\mathbb{P}}_{\text{ss}}^{(\vec{n})}, \end{aligned} \quad (7.18)$$

and now apply the measurement channel in (7.12),

$$\begin{aligned} \mathcal{O}'''' &\equiv \mathcal{V}_{[t_m]}^\dagger \mathcal{O}''' \mathcal{V}_{[t_m]} \\ &= C_{\vec{3}} \sum_{\vec{k}, \vec{m}, \vec{n}} \eta_{\vec{n}} \mathbb{P}_\Omega^{(\vec{k})} \mathcal{G} \mathbb{P}_\Omega^{(\vec{m})} \otimes |\vec{n} - \vec{k}\rangle \langle \vec{n} - \vec{m}|_{\text{ss}}, \end{aligned}$$

where Ω is the subset of sites measured at time t_m . Since the next channel $\mathcal{W}(t_m, 0)$ cannot act on the outcome registers above due to causality, we evaluate the Stinespring content in the default state $|0\rangle$ to find

$$\mathcal{O}'''' = C_{\vec{3}} \sum_{\vec{n}} \eta_{\vec{n}} \mathbb{P}_\Omega^{(\vec{n})} \mathcal{G} \mathbb{P}_\Omega^{(\vec{n})}, \quad (7.19)$$

and finally, we have

$$\mathcal{O}(t) \equiv \overline{\mathcal{W}^\dagger(t_m, 0) \mathcal{O}'''' \mathcal{W}(t_m, 0)}, \quad (7.20)$$

which vanishes unless \mathcal{O}'''' (7.19) overlaps with $\mathbb{1}$ and/or \mathcal{G} (7.13). The states with definite fermion parity s have $\rho_0 = (\mathbb{1} + s\mathcal{G})/q^N$, corresponding to the configuration $\vec{0}$ (for $s = 1$) and $\vec{1}$ (for $s = -1$). If $\mathcal{G}(t) = \mathcal{G}$ under (7.12), then $\langle \mathcal{G}(t) \rangle = s$ overall. However, for this to happen, we must have $\eta_{\pm} \propto 1$ in (7.17) and the circuit observables must correspond to Z_r . In other words, the protocol is either nonadaptive or trivially adaptive, with \mathcal{O} , the adaptive gate U , and the circuit observables A_r , all proportional to Z , which is both fine tuned and trivial.

Generic initial states ρ_0 need only contain the term $\rho_\infty = 1/q^N$ (this term is solely responsible for the unit trace of ρ_0). Hence, for the order parameter (7.2) to be nonzero in generic initial states, \mathcal{O}'''' must contain a term proportional to the identity (on all sites). The channel $\mathcal{W}(t_m, 0)$ in (7.12) acts trivially on that term, giving

$$\langle \mathcal{O}(t) \rangle = \frac{1}{q^N} C_{\vec{3}} \sum_{\vec{n}} \eta_{\vec{n}} \text{tr} \left[\mathcal{G} \mathbb{P}_\Omega^{(\vec{n})} \right], \quad (7.21)$$

which vanishes unless the set Ω of measured sites is the entire system. If the projectors do not act on some site j ,

then the summand of (7.21) includes a factor of $\text{tr}[\mathcal{G}_j] = \text{tr}[Z_j] = 0$ for all \vec{n} , so that $\langle \mathcal{O}(t) \rangle \rightarrow 0$.

We imagine grouping the measurements at time t_m into clusters r of arbitrarily many sites (which may vary in size), where the measured observables are the Pauli-string operators A_r . We then write (7.21) as

$$\begin{aligned} \langle \mathcal{O}(t) \rangle &= \frac{1}{q^N} C_{\vec{3}} \prod_r \sum_{\pm} \eta_{r,\pm} \text{tr} \left[\frac{1}{2} (\mathbb{1}_r \pm A_r) Z_r \right] \\ &= \frac{1}{q^N} C_{\vec{3}} \prod_{j=1}^N \sum_{\pm} \pm \frac{1}{2} \eta_{r,\pm} \text{tr} [Z_r A_r], \end{aligned} \quad (7.22)$$

which vanishes unless $A_r = Z_r$ and $\eta_{\pm} \propto \pm 1$, meaning that $U_{r,0} = \mathbb{1}_r$ and $U_{r,1} = X_r$ in (7.1). No other option generically gives a nonzero order parameter (7.2).

Essentially, in adaptive protocols with a \mathbb{Z}_2 Ising symmetry generated by \mathcal{G} (7.13), the only observable \mathcal{O} that is suitable as an order parameter is $\mathcal{O} = \mathcal{G}$. In the measurement round at time t_m , we measure Z on *every* site (without intervening time evolution), where the sites may be divvied into clusters r of arbitrarily many spins apiece. The subsequent adaptive gate based on the measurement of Z_r at time t_m also occurs without intervening time evolution, and applies $\mathbb{1}_r$ if the outcome was 0 (+) and X_r if the outcome was 1 (-). In this case, (7.22) becomes

$$\mathbb{E} [\langle \overline{\mathcal{O}(t)} \rangle] = C_{\vec{3}} = 1, \quad (7.23)$$

for all times t and any initial state ρ_0 .

The findings above suggest that *only* nonlocal string order parameters [47]—often associated with symmetry-protected topological orders⁵ (SPTs) [49]—survive in systems with global discrete symmetries \mathcal{G} . Generic states can be steered toward a state with definite charge ± 1 under \mathcal{G} (7.13). However, the measurements in such a protocol are highly fragile: One must measure Z_j on *every* site in the *same* time step, and subsequently implement all adaptive gates in the same time step (meaning that the measurement layer \mathcal{V} and adaptive layer \mathcal{R} must both occur without intervening time evolution). This lack of robustness to measurement errors suggests that a *measurement-induced* phase of matter is not realizable.

Now, suppose that we take $\gamma = 1$, so that all qubits are measured as required. While this precludes a transition as a function of γ , it admits a nonzero string order parameter $\langle \mathcal{G}(t) \rangle \neq 0$. Such a protocol is robust to perturbations that preserve the symmetry (7.13), and the resulting phase may be amenable to SPT order [47, 49]. Moreover, such 1D SPTs are known to be useful for measurement-based quantum computation [21, 52, 53]: The adaptive protocol above can teleport a Majorana mode from one edge of the chain to the other by measuring sites in the bulk. We now consider a related model often used for measurement-based quantum computing (e.g., teleportation).

⁵ Although the SPT string order parameters are slightly different.

$\mathbb{Z}_2 \times \mathbb{Z}_2$ Cluster states.— An extension of Ising symmetric models is the XZX “cluster” model—or equivalently, the AKLT model [64]—which both realize an SPT in the Haldane phase [65–67] and can be used, e.g., for state transfer [21, 52, 53]. The model’s $\mathbb{Z}_2 \times \mathbb{Z}_2$ symmetry is generated by the operators

$$\mathcal{G}_A = \prod_{j \text{ odd}} Z_j, \quad \mathcal{G}_B = \prod_{j \text{ even}} Z_j, \quad (7.24)$$

in the XZX representation [53]. In the AKLT formulation [64–67], the two operators in (7.24) are replaced by product over sites of Z and X ⁶.

A minimal AKLT circuit comprises two layers of three-site gates, which acting on qubits $j-1, j, j+1$, preserve both Z_j and $Z_{j-1}Z_{j+1}$ (giving four distinct, two-state symmetry blocks). Only two layers of gates are needed per time step to tile the chain, corresponding to even versus odd j (though sites $j=1, N$ are excluded to avoid “partial” gates). Both the order parameter \mathcal{O} and the circuit observables A must act trivially or as Z_j on all j .

As in the Ising case, the only operators \mathcal{O} that survive a full round of Haar-averaged time evolution are the four operators spanned by $\mathcal{G}_{A,B}$ (7.24). This also requires that Z_j be measured on *every* site, or else $\langle \mathcal{O}(t) \rangle = 0$. Note that the independent measurements of Z_j and Z_{j+1} in the XZX language correspond to measurements of $Z_j Z_{j+1}$ and $X_j X_{j+1}$ in the AKLT language [21, 64]; the change of basis corresponds to Bell decoding [21].

Once again, all *local* order parameters (7.11) are blind to measurements in Haar-averaged AKLT dynamics with the discrete symmetry (7.24). However, the *nonlocal* string order parameters (7.24) may realize $\langle \mathcal{G}_{A,B}(t) \rangle \neq 0$ in adaptive circuits. However, Z_j must be measured on all A sites without intervening time evolution (and likewise for the B measurements, and the corresponding adaptive gates for each). The adaptive gate on site j applies X_j if the outcome of measuring Z_j was “1”, and does nothing if the outcome was “0”. This scenario is consistent with the fact that one can perform measurement-based quantum computation (e.g. teleportation) using 1D states in the Haldane phase [21, 52, 53]. The protocols that transfer a qubit from one edge of the chain to the other also require that the underlying dynamics preserve a pair of string-like operators (7.24), the use of adaptive gates (albeit of a different type), and measuring *every* site in the bulk.

As before, Haar-averaged time evolution apparently precludes a transition as a function of measurement rate γ , and missing even a single measurement trivializes the order parameter. However, as in the Ising case, if $\gamma = 1$, the adaptive AKLT protocol is amenable to MBQC in a manner that is robust to perturbations that preserve the symmetry (7.24). We relegate a more detailed consideration of the relation between adaptive protocols, SPT order, and MBQC to future work [68].

⁶ An even number of qubits is required to ensure commutation of the two symmetry generators.

U(1) Charge conservation.— Suppose that the system instead has a *continuous* U(1) symmetry corresponding to conservation of the total charge

$$Q = \sum_j Z_j, \quad (7.25)$$

and following Sec. 4.7, the update rule for operators is

$$\begin{aligned} \overline{\mathcal{O}_{i,j}(t')} &= \overline{C_{0,0}^{(t)}} \mathbb{1}_{i,j} + \overline{C_{3,3}^{(t)}} Z_i Z_j \\ &+ \frac{1}{2} \left(\overline{C_{0,3}^{(t)}} + \overline{C_{3,0}^{(t)}} \right) (Z_i + Z_j), \end{aligned} \quad (7.26)$$

for standard two-site gates [9–12]. Under such gates, the identity $\mathbb{1}_{ij}$ and parity operator $Z_i Z_j$ remain fixed, while either Z_i or Z_j maps to the average of both.

Note that the Pauli strings $\sigma^{\vec{U}}$ that comprise \mathcal{O} (7.11) act nontrivially on site j only as Z_j , or fail to contribute to $\langle \mathcal{O}(t) \rangle \neq 0$ (7.2). We can map these Pauli strings to computational-basis *states* of the system, where site j is *empty* (0) if $\mu_j = 0$ (so that $\mathcal{O}_j = \mathbb{1}_j$) and *occupied* (1) if $\mu_j = 3$ (so that $\mathcal{O}_j = Z_j$). The observable \mathcal{O} is then a superposition over such configurations, and the time-evolution transfer matrix \mathcal{T} realizes a Trotterized symmetric simple exclusion process (SSEP) thereupon [69]. The Z_j operators are like the hard-core particles of the SSEP; if $\mathcal{O} = Z_j$, then Z_j executes a random walk. More generally, the Z_j “particles” near the edges of strings of Z_r diffuse outward under dynamics, while the interior Z operators spread more slowly (at first).

The only operators that are fully invariant under a full time step of Haar-averaged U(1) dynamics are spanned by $\mathbb{1}$ and Q (7.25). However, generic operators that act nontrivially only as Z are also conserved under dynamics, at the cost of being “spread out” across many sites in the system, with only the total weight over all sites conserved. Hence, any choice of \mathcal{O} (7.11) that acts as Z or $\mathbb{1}$ on each site is viable as an adaptive order parameter, at the cost of (7.2) potentially decaying with time t . To draw contrast with the behavior of systems with discrete global symmetries, we consider the maximally local order parameter $\mathcal{O} = Z_j$ for an arbitrary site j . The sum of this quantity over sites is conserved exactly under the Haar-random dynamics (its behavior is identical to the order parameters for the \mathbb{Z}_2 and $\mathbb{Z}_2 \times \mathbb{Z}_2$ cases). After τ rounds of alternating two-site time-evolution gates (as in Fig. 2), Z_j has spread across the light-cone interval $[j - 2\tau, j + 2\tau]$, and the weight on site j is given by

$$f(\tau) \equiv (Z_j | \mathcal{T}^\tau | Z_j) = \frac{1}{4^\tau} \binom{2\tau - 1}{\tau}, \quad (7.27)$$

which is identical to the ZZ autocorrelation function in nonadaptive U(1)-symmetric dynamics. We then have

$$\mathcal{O}'_j = f(t - t') Z_j + \dots, \quad (7.28)$$

where the \dots terms act on other sites $i \neq j$. We next

conjugate by the adaptive gate (7.1), giving

$$\begin{aligned} \mathcal{O}_j'' &\equiv \mathcal{R}_{t;t_m}^\dagger \overline{\mathcal{W}^\dagger(t, t') \mathcal{O} \otimes \tilde{\mathbb{1}} \mathcal{W}(t, t')} \mathcal{R}_{t;t_m} \\ &= f(t - t') \sum_{\vec{n}} U_{\vec{n}}^\dagger Z_j U_{\vec{n}} \otimes \tilde{\mathbb{P}}_{ss}^{(\vec{n})}, \end{aligned} \quad (7.29)$$

where some U must act as X_j for $\mathcal{O}(t)$ to be nontrivial.

The next step in (7.12) corresponds to Haar-averaged U(1)-symmetric time evolution from time t_m to time t' . Note that only the parts of \mathcal{O}_j'' that overlap with strings of Z and $\mathbb{1}$ survive the averaged evolution. While there are numerous symmetry-compatible operators to which U could map Z_j (e.g., $Z_j Z_{j+1}$), for concreteness, we choose gates U in (7.1) such that (7.17) holds (with \mathcal{G} replaced by Z_j). Conjugating \mathcal{O}_j'' (7.29) by $\mathcal{W}(t', t_m)$ gives

$$\begin{aligned} \mathcal{O}_j''' &\equiv \overline{\mathcal{W}^\dagger(t', t_m) \mathcal{O}_j'' \mathcal{W}(t', t_m)} \\ &= f(t - t') f(t' - t_m) \sum_{\vec{n}} \eta_{\vec{n}} Z_j \otimes \tilde{\mathbb{P}}_{ss}^{(\vec{n})}, \end{aligned} \quad (7.30)$$

and for convenience, we define

$$F(t, t', t_m) \equiv f(t - t') f(t' - t_m), \quad (7.31)$$

where $f()$ is defined in (7.27).

We next conjugate \mathcal{O}_j''' (7.30) by the measurement layer \mathcal{V} for time t_m . For convenience, we immediately project onto the default state of the Stinespring qubits, finding

$$\begin{aligned} \mathcal{O}_j'''' &\equiv \mathcal{V}_{[t_m]}^\dagger \overline{\mathcal{W}^\dagger(t', t_m) \mathcal{O}_j'' \mathcal{W}(t', t_m)} \mathcal{V}_{[t_m]} \\ &= F(t, t', t_m) \sum_{\vec{n}} \eta_{\vec{n}} \mathbb{P}_\Omega^{(\vec{n})} Z_j \mathbb{P}_\Omega^{(\vec{n})}, \end{aligned} \quad (7.32)$$

which vanishes if the observable measured on site j anticommutes with Z_j . For this \mathcal{O} , measurements on sites $i \neq j$ do not help (even with subsequent adaptive gates), so we take the measurement layer at time t_m to contain a single measurement of an observable A_r acting on a cluster r that includes site j . However, (7.32) is trivial if $\{A_r, Z_j\} = 0$; the only nontrivial possibility is that $A_r = Z_j \otimes A_{r \setminus \{j\}}$. In this case, (7.32) becomes

$$\mathcal{O}_j'''' = \frac{1}{2} F(t, t', t_m) \sum_{\pm} \eta_{\pm} (Z_j \pm A_{r \setminus \{j\}}), \quad (7.33)$$

and we note that the remaining channel $\mathcal{W}(t_m, 0)$ in (7.12) can only move Z_j around, but not eliminate it. As in the \mathbb{Z}_2 case, we wish to identify order parameters that do not depend on the initial state, so we only assume that ρ_0 contains the term $\rho_\infty = 1/q^N$. This requires that (7.33) contain a term that is traceless, which obtains upon taking $\eta_{\pm} = \pm 1$ in (7.30) and $A_{r \setminus \{j\}} = \mathbb{1}$.

This choice corresponds to the local order parameter $\mathcal{O} \rightarrow \mathcal{O}_j = Z_j$, where we measure $A_j = Z_j$ at time t_m , and apply an adaptive gate at time t' that acts as $\mathbb{1}$ if the outcome was 0 and X_j if the outcome was 1. This is

a natural choice designed to steer site j into the $|0\rangle$ state. The order parameter for this protocol is

$$\mathbb{E} \left[\overline{\langle \mathcal{O}(t) \rangle} \right] = F(t, t', t_m), \quad (7.34)$$

where F is defined in (7.31), t_m is the time step in which A_j is measured, t' is the time step in which the adaptive gate is applied, and t corresponds to the order parameter.

We note that this adaptive protocol does not seem to admit a transition as a function of measurement rate γ . In general, if the adaptive gate is applied some fixed number of time steps τ after the measurement, then either site j undergoes adaptive measurement and the result (7.34) applies, or no measurement is made and the result is zero. The expectation value is simply γ times the result (7.34). If, instead, we demand that the adaptive gate be applied prior to measurement of the probe observable Z_j , conditioned on the *most recent* circuit measurement of Z_j at time t_* , then on average $t_\gamma \sim 1/\gamma$ is the expected number of time steps that enters into (7.34). However, because $f(t)$ is a smooth function (7.27), $f(1/\gamma)$ is also smooth on the interval $\gamma \in (0, 1)$.

A phase transition is identified by a discontinuity in the order parameter (7.34) at some critical γ_c . However, it is unclear whether such a sharp feature as a function of γ is possible using adaptive protocols and probes of the form considered. In the protocol with the least trivial dependence on γ , the order parameter (7.27) varies smoothly with γ , suggesting that genuine phase transitions between distinct phases of matter as a function of measurement rate γ may not be detectable even in enriched, adaptive, Haar-random circuits with measurements. However, the robustness of this adaptive protocol to perturbations that respect the $U(1)$ symmetry (7.25) is clear, given the use of Haar-random gates; however, by considering *deterministic* protocols (i.e., in which gates are not drawn from a chaotic ensemble), it may be possible to engineer a phase transition between distinct phases of matter as a function of some other parameter. We relegate further study of the landscape of adaptive $U(1)$ charge-conserving hybrid protocols to future work.

8. CONCLUSION

We have explored the effect of projective measurements on chaotic quantum dynamics in generic models, both with and without symmetries (and/or constraints). We find no possibility of new phases of matter in nonadaptive hybrid dynamics (compared to time evolution alone), as diagnosed by all typical and experimentally tractable probes of condensed matter and AMO systems. The intuition is that, if the outcomes of measurements are not utilized, their average effect on the system is indistinguishable from an interaction with a thermal bath, generically resulting in the maximally mixed state ρ_∞ [21]. However, this is precisely the result of the underlying chaotic quantum dynamics alone, and hence measurements have no

observable effect in the cases of interest. At most, one can trivialize a symmetry of the dynamics by performing measurements in a noncommuting basis. This blindness to measurements on average is a generic feature of probes evaluated in nonadaptive protocols [13, 21].

However, by considering *adaptive* protocols, which utilize the outcomes of prior measurements, it is possible to realize nontrivial phases of matter. In particular, adaptive protocols with symmetries admit nontrivial “order parameters” of the form $\langle \mathcal{O}(t) \rangle \neq 0$ that vanish in the absence of *either* measurements or the adaptive gates. This is consistent with the recent findings of [44–46]; however, there are several important caveats.

We first note that such order parameters are trivial in the canonical model of [13], unless we demand that the measurement gate, adaptive gate based on its outcome, and measurement of the order parameter occur successively, without intervening, ensemble-averaged time evolution. Such fine tuning is incompatible with robust phases of matter and with transitions as a function of γ : Either one succeeds, and $\langle \mathcal{O}(t) \rangle = O(1)$, or one fails, and $\langle \mathcal{O}(t) \rangle = 0$, independent of γ . Absent enrichments, the only workaround is to use a gate ensemble (or deterministic time-evolution protocol) that does not immediately trivialize the physics of measurements.

On the other hand, enriched hybrid models (with symmetries and/or constraints) are not instantly trivialized by the appearance of ensemble-averaged time-evolution gates between circuit measurements, adaptive gates, and/or probe measurements. Systems with continuous symmetries—such as $U(1)$ charge conservation—are compatible with a nonvanishing *local* order parameter $\langle Z_j(t) \rangle \neq 0$, indicating the ability to “steer” the system toward particular configurations. Essentially, systems with continuous symmetries trivialize far fewer operators under Haar-averaged time evolution, making the constraints on measurements and adaptive gates far less severe. While it is possible to concoct protocols such that $\langle \mathcal{O}(t) \rangle = c(\gamma, t)$ depends nontrivially on the measurement rate γ , this dependence seems to be continuous in general.

However, this does not preclude a stable phase of matter. On the contrary, the order parameter $\langle Z_j(t) \rangle$ is robust to symmetry-respecting perturbations, and it may be possible to engineer phase transitions as a function of γ (as has been done in [44–46]), or some other parameter (e.g., by considering other time-evolution protocols). In particular, considering time-evolution gates that do not instantly scramble the entire system may be more amenable to measurement-induced *transitions* as a function of γ .

Another important class of enriched hybrid protocols features global *discrete* symmetries (e.g., the \mathbb{Z}_2 Ising model and the $\mathbb{Z}_2 \times \mathbb{Z}_2$ AKLT (or cluster) model). Because the symmetry is not locally generated, only the nonlocal string order parameters \mathcal{G} (the generators of the symmetry) survive ensemble-averaged evolution. Provided that every site of the system is measured and the adaptive gates are applied correctly, one has $\langle \mathcal{G}(t) \rangle = O(1)$; if not, $\langle \mathcal{G}(t) \rangle = 0$, independent of γ . However, as in the $U(1)$ case,

the order parameter is robust to symmetry-respecting perturbations; moreover, a deterministic protocol may yield a phase transition as a function of some parameter defining the protocol. However, it is unclear whether a transition as a function of γ is possible.

We also note an important connection between adaptive protocols enriched with discrete symmetries and both measurement-based quantum computation (MBQC) [51, 52] and fault-tolerant quantum computation (FTQC) [70–73]. In general, the former relate to symmetry-protected topological orders (SPTs) [47–50], and the latter to symmetry-enriched topological orders (SETs) [74–78]. Both are associated with sets of nonlocal string operators (or order parameters) that are protected under dynamics, and thus suitable order parameters for adaptive hybrid protocols. Additionally, the relationship between SPTs and MBQC is well known [51, 52, 68], and the SPT states that one can prepare using adaptive protocols can be used to teleport information across the $1D$ chain by measuring all sites in the bulk. While SET states can also be used for MBQC tasks such as teleportation, they are better suited to *storage* (i.e., use as quantum memories). These phases are robust to generic, local perturbations, and their various protected nonlocal operators (e.g., Wilson loops) are valid order parameters [74–78]. This robustness of the SPT and SET and order parameters is compatible with the conventional notion of a phase of matter (see Sec. 6). These states are also known to be *useful*, especially to quantum computing. Moreover, by considering deterministic time-evolution protocols, it may be possible to engineer topological phase transitions in these adaptive circuits, although it is unclear whether a transition as a function of γ is possible.

To summarize, future efforts exploring phases of matter in quantum dynamics with measurement should focus on adaptive hybrid protocols [21, 44–46]. In particular, our investigation of adaptive dynamics shows that they admit both local and string-like order parameters that are (*i*) trivial in the absence of either measurements or adaptive circuitry, (*ii*) nontrivial in adaptive protocols, and (*iii*) robust to perturbations (possibly subject to symmetry constraints). While the accessible phases may not be unique to hybrid dynamics, the first point (*i*) implies that these orders are special to adaptive dynamics with measurement, as they vanish in the absence of either.

Additionally, we suggest that future work look beyond ensemble-averaged time evolution. Realizing interesting phases of matter in adaptive hybrid dynamics likely requires the use of deterministic time-evolution gates or Hamiltonian dynamics, as opposed to those drawn from a chaotic ensemble. In particular, this could avoid having the combined effects of measurement and adaptive gates be “washed out” by averaging over some chaotic ensemble. Such protocols are also more relevant to experiment; indeed, the primary utility of the Haar ensemble used herein is (*i*) as a computational tool for analytical convenience and (*ii*) to establish robustness to perturbations and sample-to-sample variations. We stress that

all phases of matter require robustness to *some* class of perturbations. Future works that consider measurement-induced transitions in more fine-tuned protocols must establish some robustness of this type, and particularly, to the most common sources of errors (namely, errors in the application of unitary gates [41]).

ACKNOWLEDGEMENTS

We thank Andy Lucas for useful discussions, and thank Andrew Potter and M.P.A. Fisher for feedback on this manuscript. AJF is supported in part by a Simons Investigator Award via Leo Radzhivsky. OH and RN are supported by the Air Force Office of Scientific Research under award number FA9550-20-1-0222. RN acknowledges the support of the Simons Foundation through a Simons Fellowship in Theoretical Physics. OH and RN acknowledge the hospitality of Stanford University, and RN further acknowledges the hospitality of the KITP during the completion of this work. The KITP is supported in part by the National Science Foundation under Grant No. NSF PHY-1748958.

Appendix A: Operator gymnastics

Here we provide some supporting details regarding operator spaces and bases relevant to the main text.

A.1. Operator space

A quantum “state” is realized by an appropriately normalized element of the physical Hilbert space \mathcal{H} with dimension \mathcal{D} —i.e., a vector space defined over the complex field \mathbb{C} with \mathcal{D} linearly independent basis vectors $\{|n\rangle\}$, imbued with an inner product satisfying $\langle a|b\rangle = \langle b|a\rangle^*$ and $\langle m|n\rangle = \delta_{m,n}$ for the basis vectors.

The operators $|\mathcal{O}\rangle$ that act on the state space \mathcal{H} are elements of the *operator space* $\text{End}(\mathcal{H})$. The set $\text{End}(\mathcal{H})$ of linear maps on \mathcal{H} is itself a Hilbert space with dimension \mathcal{D}^2 and an inner product satisfying $\langle A|B\rangle = \langle B|A\rangle^*$.

By convention, the operator inner product is given by the standard (Frobenius) norm

$$\langle A|B\rangle = \frac{1}{\mathcal{D}} \text{tr} [A^\dagger B] , \quad (\text{A.1})$$

which manifestly obeys $\langle A|B\rangle = \langle B|A\rangle^*$, where $\mathcal{D} = \text{tr}[\mathbb{1}]$ is the dimension of the underlying state space. Given this norm, the \mathcal{D}^2 basis operators satisfy

$$(\sigma^\mu|\sigma^\nu) = \delta_{\mu,\nu} , \quad (\text{A.2})$$

where $\mu, \nu \in [0, \mathcal{D}^2 - 1]$ label the \mathcal{D}^2 many-body basis operators, where $\mu = 0$ corresponds to the identity.

This basis is both orthonormal and complete, i.e.,

$$\widehat{\mathbb{1}} = \sum_{\mu=0}^{D^2-1} |\sigma^\mu\rangle\langle\sigma^\mu|, \quad (\text{A.3})$$

realizes the superidentity $\widehat{\mathbb{1}} |A\rangle = |A\rangle$, which maps any operator onto itself. Using these relations, any operator can be written in the basis-dependent form

$$A = \sum_{\mu=1}^{D^2} A_\mu \sigma^\mu, \quad (\text{A.4})$$

where the coefficients are given by

$$A_\mu = (\sigma^\mu |A\rangle) = \frac{1}{D} \text{tr} [(\sigma^\mu)^\dagger A], \quad (\text{A.5})$$

much as a vector can be decomposed in a given basis according to $|v\rangle = \sum_n v_n |n\rangle$ with $v_n = \langle n|v\rangle$. In the case of time-dependent operators, all time dependence is carried by the coefficients (A.5), as the basis is static.

In general, our interest lies in local lattice models, in which the physical Hilbert space factorizes over a collection of sites as $\mathcal{H} = \mathcal{H}_1^{\otimes N}$, where $\mathcal{H}_1 = \mathbb{C}^q$ is the on-site Hilbert space. We then form a *many-body* operator basis as the set of Kronecker products over sites of the single-site basis operators. In other words, (A.4) becomes

$$A = \sum_{\mu} a_{\mu} \sigma^{\mu} \equiv \sum_{\mu} A_{\mu} \bigotimes_{j=1}^N \sigma_j^{\mu_j}, \quad (\text{A.6})$$

where the length- N vector $\mu = (\mu_1, \dots, \mu_N)$ stores which basis operator acts on each site, with $\mu_j \in [0, q^2 - 1]$. For a system of qubits ($q = 2$), the on-site operator space is spanned by the Pauli matrices $\mathbb{1}$, X , Y , and Z ; the many-body operator basis is then the set of all possible Pauli string operators σ^{μ} .

A.2. The naïve basis

A simple choice of operator basis—which we term the “naïve basis”—is specified straightforwardly by the matrix elements of operators as realized by a particular basis for the underlying Hilbert space \mathcal{H} for *states*.

We define the on-site orthonormal basis operators

$$\mathcal{O}_{mn} = q^{1/2} |m\rangle\langle n|, \quad (\text{A.7})$$

where $0 \leq m, n \leq q - 1$ (in some orthonormal basis for the single-site Hilbert space \mathcal{H}_j) label the q^2 unique basis operators for a given site. The basis operators (A.7) are orthonormal under the operator inner product (A.1), as can be verified by direct inspection:

$$\begin{aligned} (\mathcal{O}_{k\ell} | \mathcal{O}_{mn}) &= \frac{1}{q} \text{tr} [q^{1/2} |\ell\rangle\langle k| q^{1/2} |m\rangle\langle n|] \\ &= \delta_{k,m} \delta_{\ell,n}, \end{aligned} \quad (\text{A.8})$$

and completeness of the basis follows from linear independence: i.e., the only solution to

$$\sum_{m,n=0}^{q-1} a_{m,n} \mathcal{O}_{mn} = 0, \quad (\text{A.9})$$

is the trivial solution, $a_{m,n} = 0$ for all m, n .

Following (A.4), generic single-site operators can be expressed in this basis as

$$A = \sum_{m,n=0}^{q-1} A_{m,n} \mathcal{O}_{mn}, \quad (\text{A.10})$$

where the coefficient

$$A_{m,n} = \langle m|A|n\rangle, \quad (\text{A.11})$$

is simply the matrix element of the operator A in the chosen on-site state-space basis. The many-body operator basis is simply the Kronecker product over sites of the single-site operator basis (A.6).

A.3. The Weyl basis

For on-site dimension $q > 2$, it is useful to identify a unitary extension of the Pauli matrices, which provide a convenient basis for $q = 2$. That basis is realized by

$$\Gamma_{mn} = X^m Z^n, \quad (\text{A.12})$$

where the operators X and Z are defined by

$$X \equiv \sum_{k=0}^{q-1} |k+1\rangle\langle k| \quad (\text{A.13a})$$

$$Z \equiv \sum_{k=0}^{q-1} \omega^k |k\rangle\langle k|, \quad (\text{A.13b})$$

where the ket labels are defined modulo q , $|k+q\rangle \cong |k\rangle$, and ω is the q th root of unity,

$$\omega \equiv e^{2\pi i/q}, \quad (\text{A.14})$$

and we also have

$$\mathbb{1} = X^q = Z^q \quad (\text{A.15a})$$

$$0 = \text{tr}[Z] = \text{tr}[X] \quad (\text{A.15b})$$

$$X^\dagger = X^{-1} \quad (\text{A.15c})$$

$$Z^\dagger = Z^{-1}, \quad (\text{A.15d})$$

so that Z and X are both traceless and *unitary*, and reduce to the X and Z Pauli matrices for $q = 2$. These two operators obey the *multiplication rule*

$$ZX = \omega XZ, \quad (\text{A.16})$$

and corollary relations follow from $Z^m X^n = \omega^{mn} X^n Z^m$ (note that $\omega \rightarrow -1$ for $q = 2$). We verify that Γ_{mn} (A.12) forms an orthonormal basis by checking (A.2):

$$\begin{aligned} \left(\Gamma_{jk} \middle| \Gamma_{mn} \right) &= \frac{1}{q} \text{tr} [Z^{-k} X^{-j} X^m Z^n] \\ &= \frac{1}{q} \text{tr} [X^{m-j} Z^{n-k}] \\ &= \delta_{j,m} \delta_{k,n}, \end{aligned} \quad (\text{A.17})$$

and completeness follows from linear independence.

Single-site operators are decomposed in this basis via

$$A = \frac{1}{q} \sum_{m,n=0}^{q-1} \text{tr} [Z^{-n} X^{-m} A] X^m Z^n, \quad (\text{A.18})$$

from which we derive

$$|m\rangle\langle m| = \frac{1}{q} \sum_{k=0}^{q-1} \omega^{-mk} Z^k, \quad (\text{A.19})$$

where $|m\rangle$ satisfies $Z|m\rangle = \omega^m|m\rangle$. By convention, the Z eigenbasis is the default basis for single-qudit states.

Owing to self duality of the clock operators, we can express projectors onto eigenstates of X as

$$|\tilde{m}\rangle\langle\tilde{m}| = \frac{1}{q} \sum_{\tilde{k}=0}^{q-1} \omega^{-\tilde{m}\tilde{k}} X^{\tilde{k}}, \quad (\text{A.20})$$

from which it is straightforward to verify that

$$X|\tilde{m}\rangle\langle\tilde{m}| = \omega^{\tilde{m}}|\tilde{m}\rangle\langle\tilde{m}|, \quad (\text{A.21})$$

meaning $|\tilde{m}\rangle$ is an eigenstate of X with eigenvalue $\omega^{\tilde{m}}$, as expected. Specifically,

$$|\tilde{m}\rangle \equiv \sum_{k=0}^{q-1} \omega^{-\tilde{m}k} |k\rangle, \quad (\text{A.22})$$

where $|k\rangle$ is the eigenstate of X with eigenvalue ω^k .

Generic *many-body* operators can be written as

$$A = \frac{1}{\mathcal{D}} \sum_{\mathbf{m},\mathbf{n}} \text{tr} [\Gamma_{\mathbf{m},\mathbf{n}}^\dagger A] \Gamma_{\mathbf{m},\mathbf{n}}, \quad (\text{A.23})$$

where we have implicitly defined the shorthand

$$\Gamma_{\mathbf{m},\mathbf{n}} \equiv \bigotimes_{i \in \mathcal{H}_{\text{dil}}} X_i^{m_i} Z_i^{n_i}, \quad (\text{A.24})$$

where the vectors \mathbf{m} and \mathbf{n} contain integers corresponding to the powers of X and Z that act on each degree of freedom in the dilated Hilbert space. Note that this formula is equally valid for operators supported only on some subset of the dilated Hilbert space.

A.4. Projectors and other useful relations

Using the naïve operator basis (A.7) with Weyl Z -basis states, we define the orthonormal set of *diagonal* operators (or normalized Z -state projectors) according to

$$\pi_j^{(n)} \equiv \mathcal{O}_{n,n} = \sqrt{q} |n\rangle\langle n|_j = \sum_{k=0}^{q-1} \frac{\omega^{-nk}}{\sqrt{q}} Z_j^k, \quad (\text{A.25})$$

where $Z|n\rangle = \omega^n|n\rangle$. We similarly define the set of projectors onto Weyl X states of site j via

$$\tilde{\pi}_j^{(n)} \equiv \mathcal{O}_{\tilde{n},\tilde{n}} = \sqrt{q} |\tilde{n}\rangle\langle\tilde{n}|_j = \sum_{k=0}^{q-1} \frac{\omega^{-nk}}{\sqrt{q}} X_j^k, \quad (\text{A.26})$$

where $X|\tilde{n}\rangle = \omega^{\tilde{n}}|\tilde{n}\rangle$ (A.22). The projectors (A.25) and (A.26) are orthonormal (A.2),

$$\left(\pi_j^{(n)} \middle| \pi_j^{(m)} \right) = \left(\tilde{\pi}_j^{(n)} \middle| \tilde{\pi}_j^{(m)} \right) = \delta_{n,m}, \quad (\text{A.27})$$

as can be verified from (A.1) and the definition (A.25). These operators therefore comprise a complete orthonormal basis for the *diagonal* operators acting on site j in either the Weyl Z ($\pi^{(n)}$) or X ($\tilde{\pi}^{(n)}$) eigenbases.

For reference, we also state the following relations:

$$\mathcal{O}_{ab} = \sqrt{q} |a\rangle\langle b| = \sum_{n=0}^{q-1} \frac{\omega^{-nb}}{\sqrt{q}} X^{a-b} Z^n \quad (\text{A.28a})$$

$$\mathcal{O}_{\tilde{a}\tilde{b}} = \sqrt{q} |\tilde{a}\rangle\langle\tilde{b}| = \sum_{m=0}^{q-1} \frac{\omega^{-m\tilde{a}}}{\sqrt{q}} X^m Z^{\tilde{b}-\tilde{a}}, \quad (\text{A.28b})$$

with inner products given by

$$\left(\mathcal{O}_{ab} \middle| \Gamma_{mn} \right) = q^{-1/2} \omega^{-b n} \delta_{a,m+b} \quad (\text{A.29a})$$

$$\left(\mathcal{O}_{\tilde{a}\tilde{b}} \middle| \Gamma_{mn} \right) = q^{-1/2} \omega^{-\tilde{a} m} \delta_{\tilde{b},n+\tilde{a}}. \quad (\text{A.29b})$$

Appendix B: The onefold Haar channel

We now introduce the Haar-averaging procedure in the context of generic, Haar-averaged time evolution (i.e., without conservation laws or constraints). In the Schrödinger picture, one considers the time evolution of density matrices (or similar objects like $\mathcal{W}A\rho\mathcal{W}^\dagger$), while operators remain constant in time; in the Heisenberg picture, one considers the density matrices (and states) to be independent of time, and instead evolves operators according to $\mathcal{W}^\dagger\mathcal{O}\mathcal{W}$. However, upon averaging the Haar random unitary, U , over $\mathcal{U}(q^\ell)$ we find that $\overline{U^\dagger AU} = \overline{UAU}$. In other words, Haar-averaged time evolution updates of density matrices in the Schrödinger picture and averaged evolution of operators in the Heisenberg picture are both captured by the *same* one-fold Haar channel [54],

$$\Phi[A] \equiv \overline{UAU^\dagger} = \frac{1}{\mathcal{D}} \mathbb{1} \text{tr}[A], \quad (\text{B.1})$$

where \mathcal{D} is the dimension of the underlying Hilbert space (i.e., the unitaries U are averaged over $\mathcal{U}(\mathcal{D})$ with uniform measure). The equivalence of the Heisenberg- and Schrödinger-picture update channels can be verified by noting that $\Phi[A^\dagger] = \Phi[A^*]$.

In the absence of symmetries or constraints (i.e., each unitary gate is a $q^\ell \times q^\ell$ Haar-random unitary without block structure), the Haar-averaged update rule for the time-evolution layer labeled λ is given by

$$\overline{\varrho(t + \delta t)} = \overline{\mathcal{W}_{t,\lambda} \varrho(t) \mathcal{W}_{t,\lambda}^\dagger}, \quad (\text{B.2})$$

in the Schrödinger picture, and we note that the “upper” average applies only to the unitaries in layer t, λ , and the “lower” average on the right-hand side includes averages for all prior time steps, captured by the Haar-averaged time-dependent coefficient C (4.5).

Because the unitary gates act only on the physical Hilbert space, we can replace the dilated density matrix ϱ with the physical density matrix ρ in (B.2). Using (A.23), the physical density matrix is decomposed according to

$$\overline{\rho(t)} = \sum_{\vec{m}, \vec{n}} \overline{C_{\vec{m}, \vec{n}}^{(t)}} \bigotimes_{j=1}^N Z_j^{n_j} X_j^{m_j}, \quad (\text{B.3})$$

where \vec{m}, \vec{n} are restricted to the physical slice $\tau = 0$, and the coefficient C is given by

$$\overline{C_{\vec{m}, \vec{n}}^{(t)}} \equiv \frac{1}{q^N \text{dil}} \text{tr} \left[\overline{\varrho(t)} \bigotimes_{j=1}^N X_j^{-m_j} Z_j^{-n_j} \right], \quad (\text{B.4})$$

which may be averaged over previous time-evolution gates (denoted by the overline on ϱ).

Assuming that \mathcal{W} is a circuit of the form (3.10), applying the Haar averaged time-evolution channel to ρ (B.3) at time t gives

$$\begin{aligned} \overline{\rho(t + \delta t)} &= \sum_{\vec{m}, \vec{n}} \overline{C_{\vec{m}, \vec{n}}^{(t)}} \mathcal{W}_{t,\lambda} \Gamma_{\vec{m}, \vec{n}} \mathcal{W}_{t,\lambda}^\dagger \\ &= \sum_{\vec{m}, \vec{n}} \overline{C_{\vec{m}, \vec{n}}^{(t)}} \bigotimes_{r \in \lambda} \overline{\mathcal{U}_{t,\lambda,r} \Gamma_{\vec{m}, \vec{n}}^{(r)} \mathcal{U}_{t,\lambda,r}^\dagger} \\ &= \sum_{\vec{m}, \vec{n}} \overline{C_{\vec{m}, \vec{n}}^{(t)}} \bigotimes_{r \in \lambda} \frac{1}{q^\ell} \mathbb{1}_r \text{tr} \left[\Gamma_{\vec{m}, \vec{n}}^{(r)} \right] \\ &= \sum_{\vec{m}, \vec{n}} \overline{C_{\vec{m}, \vec{n}}^{(t)}} \mathbb{1} \prod_{j=1}^N \delta_{m_j, 0} \delta_{n_j, 0} \\ &= \overline{C_{\vec{0}, \vec{0}}^{(t)}} \mathbb{1} = \frac{1}{q^N} \mathbb{1} = \rho_\infty, \end{aligned} \quad (\text{B.5})$$

which is the infinite-temperature density matrix $\rho_\infty \propto \mathbb{1}$, which is a featureless, maximally mixed state. Also note that this result does not depend on the density matrix $\overline{\rho(t)}$ at time t —rather, because $\overline{\rho(t)}$ is a valid density matrix, we have $\overline{C_{\vec{0}, \vec{0}}^{(t)}} = q^{-N} \text{tr} \left[\overline{\rho(t)} \right] = q^{-N}$.

Regarding (B.5), it is straightforward to restore the full density matrix in the dilated Hilbert space,

$$\overline{\varrho(t + \delta t)} = \frac{1}{q^N} \mathbb{1}_{\text{ph}} \text{tr}_{\text{ph}} \left[\overline{\varrho(t)} \right], \quad (\text{B.6})$$

which has a simple physical interpretation: Each Haar-averaged time-evolution layer λ acts on the dilated density matrix $\overline{\varrho(t)}$ by replacing the physical content with the infinite-temperature density matrix $\rho_\infty = q^{-N} \mathbb{1}_{\text{ph}}$, while leaving the Stinespring content unaffected.

Similarly, observables in the Heisenberg picture are updated according to

$$\overline{\mathcal{O}(t + \delta t)} = \frac{1}{q^N} \mathbb{1}_{\text{ph}} \otimes \text{tr}_{\text{ph}} \left[\overline{\mathcal{O}(t)} \right], \quad (\text{B.7})$$

where \mathcal{O} acts on \mathcal{H}_{dil} . Note that the physical part of the density matrix (or observable) is mapped to the infinite-temperature density matrix, $\rho_\infty \propto \mathbb{1}$ after a single, ensemble-averaged layer of time evolution.

Appendix C: Transfer matrices in operator space

Following [12], we find it convenient to represent updates to the density matrix $\varrho(t)$ (or observables $\mathcal{O}(t)$) in the dilated Hilbert space \mathcal{H}_{dil} using a “transfer matrix”. We denote by $|\mathcal{O}\rangle$ an element of the operator Hilbert space $\mathcal{O} \in \text{End}(\mathcal{H}_{\text{dil}})$, which acts on states in \mathcal{H}_{dil} . The operator bra-ket notation is defined in App. A.

Consider the dilated density matrix $\overline{\varrho(t)}$ averaged over some ensemble of similar circuits. We decompose $\overline{\varrho(t)}$ in the Weyl string basis (A.23) in analogy to (B.3) as

$$\overline{|\varrho(t)\rangle} \equiv \sum_{\mathbf{m}, \mathbf{n}} \overline{C_{\mathbf{m}, \mathbf{n}}^{(t)}} |\Gamma_{\mathbf{m}, \mathbf{n}}\rangle, \quad (\text{C.1})$$

where $\Gamma_{\mathbf{m}, \mathbf{n}}$ is defined in (A.24) and the coefficients \overline{C} follow from (A.3). In analogy to (B.4), we define

$$\overline{C_{\mathbf{m}, \mathbf{n}}^{(t)}} = \langle \Gamma_{\mathbf{m}, \mathbf{n}} | \overline{\varrho(t)} \rangle = \frac{1}{\mathcal{D}} \text{tr} \left[\Gamma_{\mathbf{m}, \mathbf{n}}^\dagger \overline{\varrho(t)} \right], \quad (\text{C.2})$$

where $\mathcal{D} = \text{tr}[\mathbb{1}_{\text{dil}}]$ is the dimension of the Hilbert space upon which $\Gamma_{\mathbf{m}, \mathbf{n}}$ acts, and we next apply an arbitrary update to the density matrix (C.1).

Suppose that we then evolve this state to time $t + \delta t$ under some hybrid quantum protocol \mathcal{W}_t according to

$$\overline{\varrho(t + \delta t)} = \overline{\mathcal{W}_t \varrho(t) \mathcal{W}_t^\dagger}. \quad (\text{C.3})$$

Casting this expression into the form (C.1) gives

$$\overline{|\varrho(t + \delta t)\rangle} \equiv \sum_{\mathbf{m}', \mathbf{n}'} \overline{C_{\mathbf{m}', \mathbf{n}'}^{(t + \delta t)}} |\Gamma_{\mathbf{m}', \mathbf{n}'}\rangle, \quad (\text{C.4})$$

where we expand the new coefficient \overline{C} (C.2), finding

$$\begin{aligned}\overline{C_{\Gamma_{\mathbf{m}',\mathbf{n}'}}^{(t+\delta t)}} &= \left(\Gamma_{\mathbf{m}',\mathbf{n}'} \middle| \overline{\varrho(t+\delta t)} \right) = \frac{1}{\mathcal{D}} \text{tr} \left[\Gamma_{\mathbf{m}',\mathbf{n}'}^\dagger \overline{\varrho(t+\delta t)} \right] \\ &= \frac{1}{\mathcal{D}} \text{tr} \left[\Gamma_{\mathbf{m}',\mathbf{n}'}^\dagger \overline{\mathcal{W}_t \varrho(t) \mathcal{W}_t^\dagger} \right] \\ &= \frac{1}{\mathcal{D}} \sum_{\mathbf{m},\mathbf{n}} \text{tr} \left[\Gamma_{\mathbf{m}',\mathbf{n}'}^\dagger \mathcal{W}_t \Gamma_{\mathbf{m},\mathbf{n}} \mathcal{W}_t^\dagger \right] \overline{C_{\mathbf{m},\mathbf{n}}^{(t)}},\end{aligned}$$

implicitly defining the *transfer matrix* for \mathcal{W}_t via

$$\overline{C_{\mathbf{m}',\mathbf{n}'}^{(t+\delta t)}} = \sum_{\mathbf{m},\mathbf{n}} \mathcal{T}_{\mathbf{m}',\mathbf{n}';\mathbf{m},\mathbf{n}}^{(t)} \overline{C_{\mathbf{m},\mathbf{n}}^{(t)}}, \quad (4.9)$$

where the superoperator \mathcal{T} has elements given by

$$\begin{aligned}\mathcal{T}_{\mathbf{m}',\mathbf{n}';\mathbf{m},\mathbf{n}}^{(t)} &= \left(\Gamma_{\mathbf{m}',\mathbf{n}'} \middle| \mathcal{T}_t \middle| \Gamma_{\mathbf{m},\mathbf{n}} \right) \\ &= \frac{1}{\mathcal{D}} \text{tr} \left[\Gamma_{\mathbf{m}',\mathbf{n}'}^\dagger \overline{\mathcal{W}_t \Gamma_{\mathbf{m},\mathbf{n}} \mathcal{W}_t^\dagger} \right],\end{aligned} \quad (4.7)$$

and now, working backward from (4.9), we have

$$\begin{aligned}\left(\Gamma_{\mathbf{m}',\mathbf{n}'} \middle| \overline{\varrho(t+\delta t)} \right) &= \sum_{\mathbf{m},\mathbf{n}} \left(\Gamma_{\mathbf{m}',\mathbf{n}'} \middle| \mathcal{T} \middle| \Gamma_{\mathbf{m},\mathbf{n}} \right) \left(\Gamma_{\mathbf{m},\mathbf{n}} \middle| \overline{\varrho(t)} \right) \\ \left(\Gamma_{\mathbf{m}',\mathbf{n}'} \middle| \overline{\varrho(t+\delta t)} \right) &= \left(\Gamma_{\mathbf{m}',\mathbf{n}'} \middle| \mathcal{T}_\lambda \middle| \overline{\varrho(t)} \right),\end{aligned}$$

where we used the completeness relation (A.3) above to resolve the superidentity. Since the relation above holds for *any* basis operator $\Gamma_{\mathbf{m}',\mathbf{n}'}$, we find

$$\left| \overline{\varrho(t+\delta t)} \right\rangle = \mathcal{T}_\lambda \left| \overline{\varrho(t)} \right\rangle, \quad (4.6)$$

as expected. Essentially, \mathcal{T} is the superoperator that evolves a density matrix, represented in the operator space $\text{End}(\mathcal{H}_{\text{dil}})$ by one time step. Note that no modification is required for the other $q(q-1)$ nondiagonal operators.

Appendix D: Details of the spectral form factor

Here we provide additional information related to our scrutiny of the spectral form factor (SFF) in Sec. 5 of the main text. The SFF can be defined for Hamiltonian (static) and Floquet (periodic) evolution, and we restrict our attention to the latter. In Floquet systems, time evolution is generated by repeated application of the Floquet unitary \mathcal{F} (or ‘single-period evolution operator’), so that $|\psi(t)\rangle = \mathcal{F}^t |\psi(0)\rangle$. Supposing that the system has many-body Hilbert space \mathcal{H} with dimension $\mathcal{D} = \dim(\mathcal{H})$, we denote by $\{\theta_n\}$ the \mathcal{D} eigenvalues of \mathcal{F} , which comprise the *spectrum* of the evolution operator.

The spectral form factor $K(t)$ is defined in terms of the spectrum of \mathcal{F} according to

$$K(t) = \sum_{m,n=1}^{q^N} e^{i t (\theta_m - \theta_n)} = |\text{tr} [\mathcal{F}^t]|^2, \quad (5.1)$$

which is the Fourier transform of the two-point eigenvalue density-density correlation function, where ‘density’ here refers to the density of eigenvalues of \mathcal{F} [33]. The SFF is generally only well behaved when averaged over an ensemble evolutions [8, 11, 33–35]. Thus, in practice, we only consider $\overline{K(t)}$ with unitary gates averaged over the Haar ensemble. For convenience of notation, we omit the overlines denoting the Haar average in the following.

We now rewrite (5.1) in a form that simultaneously elucidates the connection between the SFF and correlation functions (first conjectured in [34], with some formal progress made in [12]) and facilitates extensions to hybrid quantum dynamics with measurement.

D.1. Connection to correlation functions

We first consider the SFF (5.1) under time evolution alone, and make a direct connection to correlation functions. Noting that $\mathcal{F}^\dagger = \mathcal{F}^{-1}$, we write (5.1) as

$$\begin{aligned}K(t) &= \sum_{a,b=1}^{\mathcal{D}} \langle a | \mathcal{F}^{-t} | a \rangle \langle b | \mathcal{F}^t | b \rangle \\ &= \sum_{a,b=1}^{\mathcal{D}} \text{tr} [|b\rangle\langle a| \mathcal{F}^{-t} |a\rangle\langle b| \mathcal{F}^t],\end{aligned} \quad (D.1)$$

where the labels a and b correspond to any valid choice of orthonormal basis for \mathcal{H} , e.g. the Weyl Z basis (A.13b).

In the naïve operator basis of App. A.2, (D.1) becomes

$$\begin{aligned}K(t) &= \sum_{a,b=1}^{\mathcal{D}} \frac{1}{\mathcal{D}} \text{tr} \left[\mathcal{O}_{ab}^\dagger \mathcal{F}^{-t} \mathcal{O}_{ab} \mathcal{F}^t \right] \\ &= \frac{1}{\mathcal{D}} \sum_{a,b=1}^{\mathcal{D}} \text{tr} \left[\mathcal{O}_{ab}^\dagger(0) \mathcal{O}_{ab}(t) \right] \\ &= \sum_{a,b=1}^{\mathcal{D}} \langle \mathcal{O}_{ab}^\dagger(0) \mathcal{O}_{ab}(t) \rangle_{T=\infty},\end{aligned} \quad (D.2)$$

in the Heisenberg picture of Floquet operator evolution, where in the last line, the correlation functions are evaluated in the infinite-temperature state $\rho_\infty = \mathbb{1}/\mathcal{D}$.

Finally, making use of the properties of operator spaces (as discussed in App. A.1), we have

$$\begin{aligned}K(t) &= \sum_{a,b=1}^{\mathcal{D}} \left(\mathcal{O}_{ab}(0) \middle| \mathcal{O}_{ab}(t) \right) \\ &= \sum_{a,b=1}^{\mathcal{D}} \left(\mathcal{O}_{ab} \middle| \mathcal{F}^t \middle| \mathcal{O}_{ab} \right),\end{aligned} \quad (D.3)$$

where \mathcal{F} is the *transfer matrix* corresponding to Haar-averaged time evolution by one period (or time step). Transfer matrices are superoperators that act on elements of the operator space as discussed in App. C. Because

the unitary gates repeat in time, Haar averaging (D.3) involves the t -fold Haar channel [8, 11, 12, 54, 56].

Importantly, (D.3) is an equal-weight sum over the temporal autocorrelation functions of all basis operators at infinite temperature—where (5.1) defines the SFF at infinite temperature (this is most natural given that Floquet evolution does not conserve energy and generically heats up to $T = \infty$, although it is possible to define the SFF at finite temperature as well). Note that the connection between the SFF and correlation functions was first conjectured in [34], and similar connections—between the SFF and both correlation functions and transfer matrices—were first reported in [12].

D.2. Extension to isometric measurements

Using the expressions of App. D.1, we now extend the SFF to hybrid Floquet dynamics including both time evolution and unitary measurement, as outlined in Sec. 2.2. The starting point for this derivation is (D.1), with the two terms in the summand in the reverse order,

$$K(t) = \sum_{a,b=1}^D \langle a | \mathcal{F}^t | a \rangle \langle b | \mathcal{F}^{-t} | b \rangle, \quad (\text{D.4})$$

and we now extend the above definition of the SFF to circuits with *isometric* measurement gates, as described in Sec. 2.1. We also consider this extension for the original ordering (D.1) momentarily.

In isometric hybrid circuits, each measurement layer in each \mathcal{F} generates additional Stinespring qudits, i.e., where one such layer (labeled t, σ) acts as

$$\begin{aligned} |a\rangle\langle b|_{\text{ph}}(t) &\rightarrow |a\rangle\langle b|_{\text{ph}}(t+1) \\ &= \mathbb{V}_{t,\sigma} |a\rangle\langle b|_{\text{ph}}(t) \mathbb{V}_{t,\sigma}^\dagger \\ &= \sum_{\vec{m}, \vec{n}} \mathbb{P}_{\text{ph}}^{(\vec{m})} |a\rangle\langle b|(t) \mathbb{P}_{\text{ph}}^{(\vec{n})} \otimes |\vec{m}\rangle\langle \vec{n}|_{\text{ss}}, \end{aligned} \quad (\text{D.5})$$

where the isometric measurement layer t, σ spawns a new temporal slice of Stinespring qubits, where we have omitted the label t, σ for convenience.

It is then natural to extend (D.4) to hybrid circuits with isometric measurement channels by defining the SFF (5.1) for the particular trajectory \mathbf{m} as

$$K_{\mathbf{m}}(t) \equiv \sum_{a,b=1}^D \langle a, \mathbf{m} | \mathcal{F}^t | a \rangle \langle b | \mathcal{F}^{-t} | b, \mathbf{m} \rangle, \quad (\text{D.6})$$

which projects onto the particular outcome trajectory \mathbf{m} (2.9) for *both* \mathcal{F} and \mathcal{F}^\dagger . We note that allowing different trajectories \mathbf{m} and \mathbf{n} for \mathcal{F} and \mathcal{F}^\dagger has no effect, since the contribution to $K(t)$ vanishes *unless* $\mathbf{m} = \mathbf{n}$. The above expression (D.6) can also be written as

$$K_{\mathbf{m}}(t) = \text{tr}_{\text{ss}} [|\mathbf{m}\rangle\langle \mathbf{m}|_{\text{ss}} K_{\text{iso}}(t)], \quad (\text{D.7})$$

where $K_{\text{iso}}(t)$ is given by (D.4), but where the Floquet operators \mathcal{F} and \mathcal{F}^\dagger contain isometries. In contrast to the measurement-free SFF (D.1), $K_{\text{iso}}(t)$ is no longer simply a number; instead, it is the outer product of vectors (i.e., an operator) acting on the Stinespring degrees of freedom. This operator is captured by the Stinespring part of (D.5) is not eliminated by the physical trace in (D.2), e.g., so that the SFF is generically a sum over terms

$$K_{\text{iso}}(t) = \sum_{\mathbf{m}, \mathbf{n}} k_{\mathbf{m}, \mathbf{n}}(t) |\mathbf{m}\rangle\langle \mathbf{n}|_{\text{ss}}, \quad (\text{D.8})$$

where the coefficients $k_{\mathbf{m}, \mathbf{n}}$ are captured by the physical trace, and (D.7) implies that $k_{\mathbf{m}, \mathbf{m}}(t) = K_{\mathbf{m}}(t)$. For the hybrid circuits we consider in the main text,

$$k_{\mathbf{m}, \mathbf{n}}(t) = \delta_{\mathbf{m}, \mathbf{n}} K_{\mathbf{m}}(t). \quad (\text{D.9})$$

We also comment that (D.6) implicitly encodes the probability for trajectory \mathbf{m} , and there is no obvious and “natural” means by which to normalize this quantity to remove the implicit $p_{\mathbf{m}}$ (2.18). However, one generally only considers the SFF averaged over a statistical ensemble of unitary evolutions, and in keeping with that spirit, our interest lies in the SFF averaged over measurement outcomes. The outcome-averaged spectral form factor is given by

$$\mathbb{E}[K(t)] = \sum_{\mathbf{m}} K_{\mathbf{m}}(t) = \text{tr}_{\text{ss}} [K_{\text{iso}}(t)], \quad (\text{D.10})$$

and we also average this quantity over realizations of \mathcal{F} ,

$$\mathbb{E} [\overline{K(t)}] = \overline{\mathbb{E}[K(t)]} = \overline{\text{tr}_{\text{ss}} [K_{\text{iso}}(t)]}, \quad (\text{D.11})$$

which is the quantity we wish to probe.

Note that we could have equally well have arranged the terms in the summand of (D.4) in the other order—corresponding to (D.1). Then, the extension to isometries requires no explicit modification, and is immediately equivalent to (D.11). Essentially, instead of (D.5), the isometric measurement updates act as

$$\begin{aligned} |a\rangle\langle b|_{\text{ph}}(t) &\rightarrow \mathbb{V}_{t,\sigma}^\dagger |a\rangle\langle b|_{\text{ph}}(t) \mathbb{V}_{t,\sigma} \\ &= \sum_{\vec{m}, \vec{n}} \mathbb{P}_{\text{ph}}^{(\vec{m})} |a\rangle\langle b|(t) \mathbb{P}_{\text{ph}}^{(\vec{n})} \otimes \langle \vec{m} | \vec{n} \rangle_{\text{ss}} \\ &= \sum_{\vec{m}} \mathbb{P}_{\text{ph}}^{(\vec{m})} |a\rangle\langle b|(t) \mathbb{P}_{\text{ph}}^{(\vec{m})}, \end{aligned} \quad (\text{D.12})$$

which naturally sums over all possible outcomes with no additional Stinespring operator content over which to trace, reproducing (D.11). Because these two equivalent orderings—(D.1) and (D.4)—only produce equivalent results in the presence of isometric measurement gates when averaged over all outcomes, we only consider the outcome-averaged SFF (D.11) to be physical.

D.3. Extension to unitary measurements

The extension of (D.6) to unitary measurements (2.10) is straightforward. We note that the Stinespring qudits are always initialized in the “default” state $|0\rangle$; including the Stinespring $|\mathbf{0}\rangle$ state in the middle term $|a\rangle\langle b|$ in (D.6) is then consistent with \mathcal{F} being a time-evolution operator. The SFF for unitary measurement is given by

$$\begin{aligned} K_{\mathbf{m}}(t) &\equiv \sum_{a,b=1}^{\mathcal{D}} \langle a, \mathbf{m} | \mathcal{F}^t | a, \mathbf{0} \rangle \langle b, \mathbf{0} | \mathcal{F}^{-t} | b, \mathbf{m} \rangle \\ &= \frac{1}{\mathcal{D}_{\text{dil}}} \sum_{a,b=1}^{\mathcal{D}_{\text{ph}}} \text{tr}_{\text{dil}} \left[\mathcal{F}^{-t} \mathcal{O}_{a\mathbf{m},b\mathbf{m}}^{\dagger} \mathcal{F}^t \mathcal{O}_{a\mathbf{0},b\mathbf{0}}^{\dagger} \right] \\ &= \sum_{a,b=1}^{\mathcal{D}_{\text{ph}}} \langle \mathcal{O}_{a\mathbf{m},b\mathbf{m}}^{\dagger}(t) \mathcal{O}_{a\mathbf{0},b\mathbf{0}}(0) \rangle_{\infty}, \end{aligned} \quad (\text{D.13})$$

where we have extended the naïve basis operators to the *dilated* Hilbert space, and the last line reflects an infinite-temperature average in the *dilated* Hilbert space.

Note that the expression above can be recast as a sum over eigenvalues $\{\Theta_{\mu}\}$ of the *dilated* Floquet unitary (5.1) by writing

$$\mathcal{F} = \sum_{\mu=1}^{\mathcal{D}_{\text{dil}}} e^{i\Theta_{\mu}} |\mu\rangle\langle\mu|, \quad (\text{D.14})$$

so that $K_{\mathbf{m}}(t)$ (D.13) can be rewritten

$$\begin{aligned} &= \sum_{\mu,\nu=1}^{\mathcal{D}_{\text{dil}}} e^{i t (\Theta_{\mu} - \Theta_{\nu})} \sum_{a,b=1}^{\mathcal{D}_{\text{ph}}} \langle a, \mathbf{m} | \mu \rangle \langle \mu | a, \mathbf{0} \rangle \langle b, \mathbf{0} | \nu \rangle \langle \nu | b, \mathbf{m} \rangle \\ &= \sum_{\mu,\nu=1}^{\mathcal{D}_{\text{dil}}} e^{i t (\Theta_{\mu} - \Theta_{\nu})} \sum_{a=1}^{\mathcal{D}_{\text{ph}}} \langle \mu | |a\rangle\langle a| \otimes |\mathbf{m}\rangle\langle\mathbf{0}| | \mu \rangle \\ &\quad \times \sum_{b=1}^{\mathcal{D}_{\text{ph}}} \langle \nu | |b\rangle\langle b| \otimes |\mathbf{0}\rangle\langle\mathbf{m}| | \nu \rangle, \end{aligned}$$

which we massage into a form that resembles (5.1),

$$K_{\mathbf{m}}(t) = \sum_{\mu,\nu=1}^{\mathcal{D}_{\text{dil}}} \mathcal{C}_{\mathbf{m}}^{\mu,\nu} e^{i t (\Theta_{\mu} - \Theta_{\nu})}, \quad (\text{D.15})$$

where the coefficients

$$\mathcal{C}_{\mathbf{m}}^{\mu,\nu} = \langle \mu | \mathbb{1}_{\text{ph}} \otimes |\mathbf{m}\rangle\langle\mathbf{0}| | \mu \rangle \langle \nu | \mathbb{1}_{\text{ph}} \otimes |\mathbf{0}\rangle\langle\mathbf{m}| | \nu \rangle, \quad (\text{D.16})$$

reflect the overlap of the eigenstates $|\mu\rangle$ and $|\nu\rangle$ of \mathcal{F} (3.17) with the trajectory $|\mathbf{0}\rangle \rightarrow |\mathbf{m}\rangle$. In the limit that no measurements are performed, the overlaps vanish *unless* $\mathbf{m} = \mathbf{0}$ so that $\mathcal{C}_{\mathbf{m}}^{\mu,\nu} \rightarrow \delta_{\mathbf{m},\mathbf{0}}$, reproducing (5.1).

Note that hybrid Floquet circuits include the temporal shift operator \mathbb{T} (3.16) after each measurement layer σ of the Floquet unitary. Additionally, the Stinespring content has no effect on the physical unitaries in \mathcal{F} , and so we can trace over the Stinespring Hilbert space in (D.13) without any knowledge of the particular models. Essentially, for each measurement gate in the t th copy of both \mathcal{F} and \mathcal{F}^{\dagger} , we can impose the Stinespring projection

$$\mathcal{V}_{\sigma,r} \rightarrow \text{tr}_{\text{ss}} \left[|\mathbf{0}\rangle\langle m_{t,\sigma,r}|_{\text{ss},\sigma,r} \mathcal{V}_{\sigma,r} \right] = \mathbb{P}_r^{(m_{t,\sigma,r})}, \quad (\text{D.17})$$

and likewise for each gate $\mathcal{V}_{\sigma,r}^{\dagger}$ in the t th copy of \mathcal{F}^{\dagger} . Thus, we replace the measurement unitaries \mathcal{V} and \mathcal{V}^{\dagger} corresponding to cluster r in layer σ in the t th layer of \mathcal{F} and \mathcal{F}^{\dagger} with $\mathbb{P}_r^{(m_{t,\sigma,r})}$ (D.17).

[1] J. M. Deutsch, Quantum statistical mechanics in a closed system, *Phys. Rev. A* **43**, 2046 (1991).

[2] M. Srednicki, Chaos and quantum thermalization, *Phys. Rev. E* **50**, 888 (1994).

[3] R. Nandkishore and D. A. Huse, Many-body localization and thermalization in quantum statistical mechanics, *Annu. Rev. Condens. Matter Phys.* **6**, 15 (2015).

[4] D. A. Abanin, E. Altman, I. Bloch, and M. Serbyn, Colloquium: Many-body localization, thermalization, and entanglement, *Rev. Mod. Phys.* **91**, 021001 (2019).

[5] A. Nahum, J. Ruhman, S. Vijay, and J. Haah, Quantum entanglement growth under random unitary dynamics, *Phys. Rev. X* **7**, 031016 (2017).

[6] A. Nahum, S. Vijay, and J. Haah, Operator spreading in random unitary circuits, *Phys. Rev. X* **8**, 021014 (2018).

[7] C. W. von Keyserlingk, T. Rakovszky, F. Pollmann, and S. L. Sondhi, Operator hydrodynamics, OTOCs, and entanglement growth in systems without conservation laws, *Phys. Rev. X* **8**, 021013 (2018).

[8] A. Chan, A. De Luca, and J. T. Chalker, Solution of a minimal model for many-body quantum chaos, *Phys. Rev. X* **8**, 041019 (2018).

[9] T. Rakovszky, F. Pollmann, and C. W. von Keyserlingk, Diffusive hydrodynamics of out-of-time-ordered correlators with charge conservation, *Phys. Rev. X* **8**, 031058 (2018).

[10] V. Khemani, A. Vishwanath, and D. A. Huse, Operator spreading and the emergence of dissipative hydrodynamics under unitary evolution with conservation laws, *Phys. Rev. X* **8**, 031057 (2018).

[11] A. J. Friedman, A. Chan, A. De Luca, and J. T. Chalker, Spectral statistics and many-body quantum chaos with conserved charge, *Phys. Rev. Lett.* **123**, 210603 (2019).

[12] H. Singh, B. A. Ware, R. Vasseur, and A. J. Friedman, Subdiffusion and many-body quantum chaos with kinetic constraints, *Phys. Rev. Lett.* **127**, 230602 (2021).

[13] B. Skinner, J. Ruhman, and A. Nahum, Measurement-induced phase transitions in the dynamics of entanglement, *Phys. Rev. X* **9**, 031009 (2019).

[14] Y. Li, X. Chen, and M. P. A. Fisher, Quantum Zeno effect and the many-body entanglement transition, *Phys. Rev. B* **98**, 205136 (2018).

[15] A. Chan, R. M. Nandkishore, M. Pretko, and G. Smith, Unitary-projective entanglement dynamics, *Phys. Rev. B* **99**, 224307 (2019).

[16] Y. Li, X. Chen, and M. P. A. Fisher, Measurement-driven entanglement transition in hybrid quantum circuits, *Phys. Rev. B* **100**, 134306 (2019).

[17] S. Choi, Y. Bao, X.-L. Qi, and E. Altman, Quantum error correction in scrambling dynamics and measurement-induced phase transition, *Phys. Rev. Lett.* **125**, 030505 (2020).

[18] C.-M. Jian, Y.-Z. You, R. Vasseur, and A. W. W. Ludwig, Measurement-induced criticality in random quantum circuits, *Phys. Rev. B* **101**, 104302 (2020).

[19] M. P. A. Fisher, V. Khemani, A. Nahum, and S. Vijay, Random quantum circuits, *arXiv* (2022), arXiv:2207.14280 [quant-ph].

[20] W. F. Stinespring, Positive functions on C^* -algebras, *Proc. Amer. Math. Soc.* **6**, 211 (1955).

[21] A. J. Friedman, C. Yin, Y. Hong, and A. Lucas, Locality and error correction in quantum dynamics with measurement, *arXiv* (2022), arXiv:2206.09929 [quant-ph].

[22] M.-D. Choi, Completely positive linear maps on complex matrices, *Linear Algebra and its Applications* **10**, 285 (1975).

[23] U. Agrawal, A. Zabalo, K. Chen, J. H. Wilson, A. C. Potter, J. H. Pixley, S. Gopalakrishnan, and R. Vasseur, Entanglement and charge-sharpening transitions in U(1) symmetric monitored quantum circuits, *arXiv* (2021), arXiv:2107.10279 [cond-mat.dis-nn].

[24] S. Sang and T. H. Hsieh, Measurement-protected quantum phases, *Phys. Rev. Research* **3**, 023200 (2021).

[25] A. Lavasani, Y. Alavirad, and M. Barkeshli, Measurement-induced topological entanglement transitions in symmetric random quantum circuits, *Nature Physics* **17**, 342 (2021).

[26] F. Ritort and P. Sollich, Glassy dynamics of kinetically constrained models, *Advances in Physics* **52**, 219 (2003).

[27] J. P. Garrahan, P. Sollich, and C. Toninelli, Kinetically constrained models, *arXiv* (2010), arXiv:1009.6113 [cond-mat.stat-mech].

[28] I. Lesanovsky and J. P. Garrahan, Kinetic constraints, hierarchical relaxation, and onset of glassiness in strongly interacting and dissipative Rydberg gases, *Phys. Rev. Lett.* **111**, 215305 (2013).

[29] M. M. Valado, C. Simonelli, M. D. Hoogerland, I. Lesanovsky, J. P. Garrahan, E. Arimondo, D. Ciampini, and O. Morsch, Experimental observation of controllable kinetic constraints in a cold atomic gas, *Phys. Rev. A* **93**, 040701 (2016).

[30] J. P. Garrahan, Aspects of nonequilibrium in classical and quantum systems: Slow relaxation and glasses, dynamical large deviations, quantum nonergodicity, and open quantum dynamics, *Physica A* **504**, 130 (2018).

[31] N. Pancotti, G. Giudice, J. I. Cirac, J. P. Garrahan, and M. C. Bañuls, Quantum East model: Localization, nonthermal eigenstates, and slow dynamics, *Phys. Rev. X* **10**, 021051 (2020).

[32] O. Bohigas, M. J. Giannoni, and C. Schmit, Characterization of chaotic quantum spectra and universality of level fluctuation laws, *Phys. Rev. Lett.* **52**, 1 (1984).

[33] E. Brézin and S. Hikami, Spectral form factor in a random matrix theory, *Phys. Rev. E* **55**, 4067 (1997).

[34] H. Gharibyan, M. Hanada, S. H. Shenker, and M. Tezuka, Onset of random-matrix behavior in scrambling systems, *JHEP* **2018** (7).

[35] P. Kos, M. Ljubotina, and T. Prosen, Many-body quantum chaos: Analytic connection to random matrix theory, *Phys. Rev. X* **8**, 021062 (2018).

[36] B. Bertini, P. Kos, and T. c. v. Prosen, Exact spectral form factor in a minimal model of many-body quantum chaos, *Phys. Rev. Lett.* **121**, 264101 (2018).

[37] A. Chan, A. De Luca, and J. T. Chalker, Spectral statistics in spatially extended chaotic quantum many-body systems, *Phys. Rev. Lett.* **121**, 060601 (2018).

[38] S. Moudgalya, A. Prem, D. A. Huse, and A. Chan, Spectral statistics in constrained many-body quantum chaotic systems, *Phys. Rev. Research* **3**, 023176 (2021).

[39] S. Garratt and J. Chalker, Local pairing of Feynman histories in many-body Floquet models, *Phys. Rev. X* **11** (2021).

[40] M. J. Gullans and D. A. Huse, Scalable probes of measurement-induced criticality, *Phys. Rev. Lett.* **125**, 070606 (2020).

[41] C. Noel, P. Niroula, D. Zhu, A. Risinger, L. Egan, D. Biswas, M. Cetina, A. V. Gorshkov, M. J. Gullans, D. A. Huse, and C. Monroe, Measurement-induced quantum phases realized in a trapped-ion quantum computer, *Nature Physics* **18**, 760 (2022).

[42] Y. Li, Y. Zou, P. Glorioso, E. Altman, and M. P. A. Fisher, Cross entropy benchmark for measurement-induced phase transitions, *arXiv* (2022), arXiv:2209.00609 [quant-ph].

[43] F. Barratt, U. Agrawal, A. C. Potter, S. Gopalakrishnan, and R. Vasseur, Transitions in the learnability of global charges from local measurements, *arXiv* (2022), arXiv:2206.12429 [quant-ph].

[44] T. Iadecola, S. Ganeshan, J. H. Pixley, and J. H. Wilson, Dynamical entanglement transition in the probabilistic control of chaos, *arXiv* (2022), arXiv:2207.12415 [cond-mat.dis-nn].

[45] M. Buchhold, T. Müller, and S. Diehl, Revealing measurement-induced phase transitions by pre-selection, *arXiv* (2022), arXiv:2208.10506 [cond-mat.dis-nn].

[46] A. Milekhin and F. K. Popov, Measurement-induced phase transition in teleportation and wormholes, *arXiv* (2022), arXiv:2210.03083 [hep-th].

[47] D. Pérez-García, M. M. Wolf, M. Sanz, F. Verstraete, and J. I. Cirac, String order and symmetries in quantum spin lattices, *Phys. Rev. Lett.* **100**, 10.1103/PhysRevLett.100.167202 (2008).

[48] F. Pollmann, A. M. Turner, E. Berg, and M. Oshikawa, Entanglement spectrum of a topological phase in one dimension, *Phys. Rev. B* **81**, 10.1103/PhysRevB.81.064439 (2010).

[49] F. Pollmann, E. Berg, A. M. Turner, and M. Oshikawa, Symmetry protection of topological phases in one-dimensional quantum spin systems, *Phys. Rev. B* **85**, 075125 (2012).

[50] F. Pollmann and A. M. Turner, Detection of symmetry-protected topological phases in one dimension, *Phys. Rev. B* **86**, 125441 (2012).

[51] R. Jozsa, An introduction to measurement-based quantum computation, *arXiv* (2005), arXiv:quant-ph/0508124 [quant-ph].

[52] D. V. Else, I. Schwarz, S. D. Bartlett, and A. C. Doherty, Symmetry-protected phases for measurement-based quantum computation, *Phys. Rev. Lett.* **108** (2012).

[53] R. Verresen, R. Moessner, and F. Pollmann, One-dimensional symmetry protected topological phases and their transitions, *Phys. Rev. B* **96** (2017).

[54] D. A. Roberts and B. Yoshida, Chaos and complexity by design, *JHEP* **2017** (4).

[55] O. Hart and R. Nandkishore, Extracting spinon self-energies from two-dimensional coherent spectroscopy, *arXiv* (2022), arXiv:2208.12817 [cond-mat.str-el].

[56] P. W. Brouwer and C. W. J. Beenakker, Diagrammatic method of integration over the unitary group, with applications to quantum transport in mesoscopic systems, *J. Math. Phys.* **37**, 4904 (1996).

[57] D. Thouless, Electrons in disordered systems and the theory of localization, *Physics Reports* **13**, 93 (1974).

[58] D. Thouless, Maximum metallic resistance in thin wires, *Phys. Rev. Lett.* **39**, 1167 (1977).

[59] R. M. Nandkishore, W. Choi, and Y. B. Kim, Spectroscopic fingerprints of gapped quantum spin liquids, both conventional and fractonic, *Phys. Rev. Research* **3**, 013254 (2021).

[60] K. Binder and A. P. Young, Spin glasses: Experimental facts, theoretical concepts, and open questions, *Rev. Mod. Phys.* **58**, 801 (1986).

[61] E. Vincent and V. Dupuis, Spin glasses: Experimental signatures and salient outcomes, in *Frustrated Materials and Ferroic Glasses* (Springer International Publishing, 2018) pp. 31–56.

[62] M. Ippoliti and V. Khemani, Postselection-free entanglement dynamics via spacetime duality, *Phys. Rev. Lett.* **126**, 060501 (2021).

[63] U. Vazirani, A survey of quantum complexity theory, in *Proceedings of Symposia in Applied Mathematics*, Vol. 58 (2002) pp. 193–220.

[64] I. Affleck, T. Kennedy, E. H. Lieb, and H. Tasaki, Rigorous results on valence-bond ground states in antiferromagnets, *Phys. Rev. Lett.* **59**, 799 (1987).

[65] F. Haldane, Continuum dynamics of the 1D Heisenberg antiferromagnet: Identification with the O(3) nonlinear sigma model, *Phys. Lett. A* **93**, 464 (1983).

[66] F. D. M. Haldane, Nonlinear field theory of large-spin Heisenberg antiferromagnets: Semiclassically quantized solitons of the one-dimensional easy-axis Néel state, *Phys. Rev. Lett.* **50**, 1153 (1983).

[67] I. Affleck and F. D. M. Haldane, Critical theory of quantum spin chains, *Phys. Rev. B* **36**, 5291 (1987).

[68] A. J. Friedman, D. T. Stephen, C. Stahl, and Y. Hong, Measurement-based quantum computing and symmetry-protected topology, *arXiv* , to appear (2022).

[69] G. Schütz, Exactly solvable models for many-body systems far from equilibrium, in *Phase Transitions and Critical Phenomena*, Vol. 19, edited by C. Domb and J. Lebowitz (Academic Press, 2001) pp. 1–251.

[70] P. Shor, Fault-tolerant quantum computation, in *Proceedings of 37th Conference on Foundations of Computer Science* (1996) pp. 56–65.

[71] J. Preskill, Fault-tolerant quantum computation, in *Introduction to Quantum Computation and Information* (World Scientific, 1998) pp. 213–269.

[72] D. Gottesman, Theory of fault-tolerant quantum computation, *Phys. Rev. A* **57**, 127 (1998).

[73] A. Kitaev, Fault-tolerant quantum computation by anyons, *Annals of Physics* **303**, 2 (2003).

[74] M. Levin and X.-G. Wen, Detecting topological order in a ground state wave function, *Phys. Rev. Lett.* **96**, 110405 (2006).

[75] C.-Y. Huang, X. Chen, and F. Pollmann, Detection of symmetry-enriched topological phases, *Phys. Rev. B* **90**, 045142 (2014).

[76] Z.-C. Gu, Z. Wang, and X.-G. Wen, Classification of two-dimensional fermionic and bosonic topological orders, *Phys. Rev. B* **91**, 125149 (2015).

[77] X. Chen, F. J. Burnell, A. Vishwanath, and L. Fidkowski, Anomalous symmetry fractionalization and surface topological order, *Phys. Rev. X* **5**, 041013 (2015).

[78] D. J. Williamson, N. Bultinck, and F. Verstraete, Symmetry-enriched topological order in tensor networks: Defects, gauging and anyon condensation, *arXiv* (2017), arXiv:1711.07982 [quant-ph].